Adsorption Kinetics of Alkane-thiol Capped Gold Nanoparticles at Liquid-Liquid Interfaces

by

Sultana Ferdous

A thesis
presented to the University of Waterloo
in fulfillment of the
thesis requirement for the degree of
Doctor of Philosophy
in
Chemical Engineering

Waterloo, Ontario, Canada, 2012

I hereby declare that I am the sole author of this thesis. This is a true copy of the thesis, including any required final revisions, as accepted by my examiners.

I understand that my thesis may be made electronically available to the public.

Abstract

The pendant drop technique was used to characterize the adsorption behavior of *n*-dodecane-1-thiol and *n*-hexane-1-thiol capped gold nanoparticles at the hexane–water interface. The adsorption process was studied by analyzing the dynamic interfacial tension versus nanoparticle concentration, both at early times and at later stages (i.e., immediately after the interface between the fluids is made and once equilibrium has been established). Following free diffusion of nanoparticles from the bulk hexane phase, adsorption leads to ordering and rearrangement of the nanoparticles at the interface and formation of a dense layer. With increasing interfacial coverage, the diffusion-controlled adsorption for the nanoparticles at the interface was found to change to an interaction-controlled assembly and the presence of an adsorption barrier was experimentally verified. At the same bulk concentration, different sizes of *n*-dodecane-1-thiol nanoparticles showed different absorption behavior at the interface, in agreement with the findings of *Kutuzov et al.*[1]. The experiments additionally demonstrated the important role played by the capping agent. At the same concentration, gold nanoparticles stabilized by *n*-hexane-1-thiol exhibited greater surface activity than gold nanoparticles of the same size stabilized by *n*-dodecane-1-thiol. 1.6 nm, 2.8 nm, and 4.4 nm nanoparticles capped with *n*-dodecane-1-thiol, and 2.9 nm, and 4.3 nm particles capped with *n*-hexane-1-thiol were used in this study. The physical size of the gold nanoparticles was determined by TEM image analysis. The pendant drop technique was also used to study the adsorption properties of mixtures of gold nanoparticles at the hexane–water interface; and also investigate the effects of different factors (i.e., temperature, pH or ionic strength) on interfacial tension (IFT). The interfacial properties of mixtures of these nanoparticles, having different sizes and capping agents, were then studied. No interaction was found between the unmixed studied nanoparticles. Using the theory of non-ideal interactions for binary mixtures, the interaction parameters for mixtures of nanoparticles at the interface were determined. The results indicate that nanoparticle concentration of the mixtures has a profound effect on the interfacial nanoparticle composition. A repulsive interaction between nanoparticles of different size and cap was found in the mixtures at the interface layer. The interfacial tension for mixtures was found to be higher than the interfacial tension for non-mixed nanoparticle suspensions. The nanoparticle composition at the interface was found to differ from the composition of nanoparticles in the bulk liquid phase. The activity of unmixed nanoparticles proved to be a poor predictor of the activity of mixtures. It was observed that the most active nanopar-

ticles concentrated at the interface. The effects of temperature, pH and ionic strength concentration on the equilibrium and dynamic IFT of 4.4 nm gold nanoparticles capped with *n*-dodecane-1-thiol at the hydrocarbon–water interface was studied. The pendant drop technique was also used to study the adsorption properties of these nanoparticles at the hexane–water and nonane–water interface. The addition of NaCl was found to cause a decrease of the equilibrium and dynamic IFT greater than that which accompanies the adsorption of nanoparticles at the interface in the absence of NaCl. Although IFT values for acidic and neutral conditions were found to be similar, a noticeable decrease in the IFT was found for more basic conditions. Increasing the temperature of the system was found to cause an increase in both dynamic and equilibrium IFT values. The adsorption of functionalized gold nanoparticles at liquid–liquid interfaces is a promising method for self-assembly and the creation of useful nanostructures. These findings contribute to the design of useful supra-colloidal structures by the self-assembly of alkane-thiol capped gold nanoparticles at liquid-liquid interfaces.

Acknowledgements

I want to express my sincere gratitude to my PhD supervisors, Dr. Dale Henneke and Dr. Marios. A. Ioannidis, for their continuous support, thoughtful guidance, encouragement and motivation throughout my PhD program. Their extensive knowledge and methodical way of thinking about nano-research make my PhD program more productive and fascinating. I am very lucky to have them as my supervisors who always gave me the freedom to study my own. I would like to thank my PhD committee members, for their encouraging comments that greatly helped me a lot to think enthusiastically about my research. I would like to thank Dr. Claude Lemarie, Dr. Robert Donkers, Dr. Nima Rezaie, Dr. Rosendo Diaz and Jasdeep Mandur for their assistance. I would also like to thank Chemical Engineering Department for giving me enormous support throughout my PhD program.

Most importantly, I would like to express my sincere gratitude to my parents and husband for their unwavering support.

Dedication

This is dedicated to my loving family and friends.

Contents

List of Tables

List of Figures

List of Abbreviations

IFT	:	Interfacial Tension
NPs	:	Nanoparticles
AuNPs	:	Gold Nanoparticles
AT-AuNPs	:	Alkhanethiol Capped Gold Nanoparticles
DT	:	Dodecanethiol
HT	:	Hexanethiol
DT-AuNPs	:	Dodecanethiol Capped Gold Nanoparticles
HT-AuNPs	:	Hexanethiol Capped Gold Nanoparticles
ADSA	:	Axisymmetric Drop Shape Analysis
HR-TEM	:	High-Resolution Transmission Electron Microscopy
EDS	:	Energy-Dispersive Spectroscopy
^{1}H-NMR	:	Proton Nuclear Magnetic Resonance Spectroscopy
UV-VIS	:	Ultraviolet Visible Spectroscopy
SAED	:	Selected-Area Electron Diffraction
MD	:	Molecular Dynamics
TOPO	:	Tri-n-octylphosphine oxide
3-MPA	:	3-Mercaptopropionic Acid
4-MBA	:	4-Mercaptobenzoic Acid
HLB	:	Hydrophilic-Liphophilic Balance
DTBE	:	$2, 2'$-dithiobis[1-(2-bromo-2-methyl-propionyloxy)ethane]

List of Symbols

k_B	:	Boltzmann constant
ΔE	:	Interfacial energy change
θ	:	Contact angle
τ	:	Line tension
$\gamma_{o/w}$	:	Interfacial tension at oil/water interface
$\gamma_{p/w}$	:	Interfacial tension at particle/water interface
$\gamma_{p/o}$	:	Interfacial tension at particle/oil interface
Γ_∞	:	Adsorption density
D_{S-E}	:	Stokes-Einstein diffusivity
D_o	:	Diffusivity at the earlier time
D_∞	:	Diffusivity at the later time
a_L	:	Langmuir parameter
A_{min}	:	Minimum area per nanoparticle
N_A	:	Avogadro's number
β	:	Interaction parameter
Γ_{hex}	:	Adsorption density for hexagonal arrangement
Γ_{squ}	:	Adsorption density for square arrangement

Chapter 1

Introduction

Although the principles of colloidal science have been known for many years, advances in nanotechnology are providing a new set of tools to analyze problems and to develop novel technologies. A wealth of knowledge already exists about the interaction of surfactants and colloidal particles at air-liquid and liquid-liquid interfaces.This knowledge has been acquired primarily from observations of natural phenomena and is owed to the importance of interfacial phenomena in industrial applications. For example, surfactants are used in chemical flooding processes for tertiary oil recovery [2]. Today, stable suspensions of particles with dimensions in the nanometer range (i.e., colloids of nanoparticles), and their interaction with fluid interfaces have become an interesting area of research. Colloidal nanoparticles may permit the development of new applications and technologies, especially those related to foams and emulsions. This promising research area has spawned a great deal of new literature; both experimental and theoretical work on these systems, are being conducted.

The study of the self-assembly of colloidal particles and their adsorption behavior at interfaces has generated much scientific interest. Colloidal particles have the tendency to adsorbed at interfaces. This allows the use of the interface as an effective and favorable platform for particle self-assembly [3]. Nanoparticles (NPs) can make significant contributions to the search for functional advanced materials. Controlled self-assembly at the liquid-liquid interface is a proposed method for constructing two-dimensional materials [4]. For future development of novel functional devices, it is necessary to understand the self-assembly of nanomaterials at the interfaces of films and to characterize their properties [5].

The controlled assembly of nanoparticles can be achieved by tuning the size and the chemical characteristics of ligands on NP surface. Uniform, and Janus-type [6], nanoparticles may be produced by controlling the ligand type at the liquid-liquid interfaces. Crosslinked sheets of nanoparticles can be produced by succeeding reactions of ligands at the interface. This technique has been used to generate encapulants, and filtration devices [7]. Although the self-assembly of colloidal particles at liquid-liquid interfaces has been studied thoroughly, the adsorption kinetics of nanoparticles has yet to be fully understood [8].

The behaviour of nanoparticles at fluid-fluid interfaces has attracted significant attention in recent years, as a result of a drive to devise strategies for producing novel functional materials or devices via size-selective particle self-assembly [9]. Binding of particles at liquid-liquid interfaces, which has been known to stabilize Pickering emulsions, has been explained in terms of a decrease in the free energy [10]. Since placement of a single spherical particle of radius r at the oil-water interface decreases the entropy by a about k_BT,the interfacial energy change, ΔE, must be negative for placement of the particle to be thermodynamically favoured. The energy change associated with placement of a single particle at the oil-water interface depends on the particle radius r and on the particle-oil ($\gamma_{p/o}$), particle-water ($\gamma_{p/w}$) and oil-water ($\gamma_{o/w}$) interfacial tensions as follows:

$$\Delta E = -\frac{\pi r^2}{\gamma_{o/w}}[\gamma_{o/w} - (\gamma_{p/w} - \gamma_{p/o})]^2 \tag{1.1}$$

An extension of this result to include the influence of line tension has been given by *Aveyard and Clint* [11]. This extension was recently tested by molecular simulation [12]. A thorough review of the thermodynamics of nanoparticle attachment at fluid-fluid interfaces has been provided by *Bresme and Oettel* [13]. Equation 1.1 highlights a key difference between μm-sized and nm-sized particles- the latter being much less stably adsorbed at liquid-liquid interfaces. For typical interfacial tension values, the magnitude of ΔE is of the order of k_BT for particles with radius of a few nm. As a result, binding of very small nanoparticles at fluid-fluid interfaces is expected to be destabilized by thermal fluctuations [14] and this expectation is confirmed by experiment [15]. On the contrary, attachment of μm-sized particles to fluid-fluid interfaces may be considered irreversible, due to the fact that ΔE exceeds k_BT by many orders of magnitude [14]. Using Young's equation, it can be also shown that the bracketed term in Equation 1.1 is a maximum when the contact angle θ of the particle with the fluid-fluid interface is 90^o and decreases rapidly as $\theta \longrightarrow 0^o$ (or

$\theta \longrightarrow 180^o$), highlighting the influence of particle wettability on the stability of particle attachment to the interface [14].

Although a large body of literature exists on the use of liquid-liquid interfaces as the locus of nanoparticle self-assembly into a variety of supra-colloidal structures with applications in sensing, encapsulation, data storage and catalysis ([15], [7], [16], [5], [17]), much less is known about the kinetics of nanoparticle adsorption at liquid-liquid interfaces. Dynamic interfacial tension measurements, made for example by pendant drop tensiometry, are well suited for this task. This technique has been used extensively for interrogating the adsorption kinetics of surfactants on liquid interfaces, but only a few applications to nanoparticle adsorption have been reported. *Glaser et al.* used pendant drop tensiometry to demonstrate the interfacial activity of Janus nanoparticles at the hexane-water interface [18] . Using the same method, *Kutuzov et al.* studied the time evolution of toluene-water interfacial tension as tri-*n*-octylphosphine oxide (TOPO)-stabilized CdSe nanoparticles, initially suspended in toluene, diffused towards and were adsorbed at the toluene-water interface [1]. Very recently, *Isa et al.* also used pendant drop tensiometry in a qualitative study of self-assembly of iron oxide poly(ethylene glycol) core-shell nanoparticles at the *n*-decane-water interface [4] .

Of the above mentioned studies, only the work of *Kutuzov et al.*[1] addressed quantitatively the kinetics of ligand-stabilized nanoparticle adsorption. These authors analyzed the time evolution of the interfacial tension using the theory of *Ward and Tordai* [19] to infer the characteristics of the adsorption process at early and late stages. For TOPO-stabilized CdSe nanoparticles in the size range 2.3-6 nm, *Kutuzov et al.* [1] found the decay of interfacial tension to be consistent with a mixed diffusion-activation adsorption mechanism. Using a model developed by *Liggieri et al.* [20] to describe the adsorption kinetics of non-ionic surfactants, they estimated a magnitude of the energy barrier to adsorption of a few k_BT, approximately equal to the desorption energy for a single particle calculated from Equation 1.1. They proposed that such an adsorption barrier originates from particle-to-particle interactions near the oil-water interface (collisions of the nanoparticles approaching the interface from the bulk with nanoparticles that are already adsorbed or that desorb from the interface due to thermal fluctuations), which become increasingly important with increasing interfacial coverage. It is worth noting that a mixed diffusion-activation adsorption mechanism has been found to apply to many different surfactants, with a small adsorption barrier always in the range 2-5 k_BT regardless of molecular weight, structure

or critical micelle concentration of the surfactant - an observation consistent with the idea that the adsorption barrier is related to the work, W_{ads}, that a molecule must do against surface pressure [21]. The latter may be estimated as , $W_{ads} = (\gamma_o - \gamma_\infty) \times A \times 10^{-23}$, where $(\gamma_o - \gamma_\infty)$ is the equilibrium surface pressure (in mN/m) and A is the area (in $\mathring{A}^2$) at the fluid-fluid interface occupied by one adsorbed molecule. For adsorbed particles, $A{=}\pi(r\sin\theta)^2$ from geometrical considerations. Insofar as nanoparticles are considered, direct evidence of an energy barrier to adsorption on liquid-liquid interfaces is, at present, too limited to establish mixed diffusion-activation as the operative adsorption mechanism, let alone elucidate the physical origin of an adsorption barrier.

Gold nanoparticles capped by alkanethiol self-assembled monolayers are easily synthesized and are known to exhibit remarkable stability and ease of functionalization. Not surprisingly, they are some of the most studied nanomaterials [22]. Yet, an investigation of the adsorption kinetics of thiol-capped gold nanoparticles at liquid-liquid interfaces is lacking, despite the fact that the adsorption process is a prerequisite for self-assembly of these nanoparticles into useful supra-colloidal structures. Such an investigation is reported in the present study. Similar to *Kutuzov et al.*[1], we also employ pendant drop tensiometry to interrogate the kinetics of alkanethiol-stabilized gold nanoparticles at the hexane-water interface. The effects of nanoparticle size, concentration in the bulk organic phase and ligand chain length (n-dodecane-1-thiol vs. n-hexane-1-thiol) on adsorption behaviour are investigated. The results corroborate the finding of *Kutuzov et al.*[1] that a mixed diffusion-activation mechanism governs nanoparticle adsorption at a liquid-liquid interface.

Despite progress recently made in understanding the adsorption kinetics of nanoparticles at the liquid-liquid interfaces [1], [18], [4], no effort has been made, either theoretically or experimentally, to understand the adsorption kinetics of mixtures of nanoparticles at these interfaces. The adsorption process for mixtures of nanoparticles is far more complex than for non-mixed nanoparticle suspensions. The adsorption process for binary mixtures of surfactants, however has been studied extensively. In binary mixtures of surfactants, very complex interactions have been found [23], [24], [25],[26],[27] and synergism between the components has been documented. It has been proposed that the interfacial properties of these surfactant mixtures are heavily influenced by molecular interactions between the surfactants molecules [28], [29], [30]. The interfacial properties of some mixtures of surfactants have been found to be radically different from those of their individual components.

Similar to mixtures of surfactants, a synergistic effect may exist for mixtures of differently sized or differently capped nanoparticles. Many factors have a pronounced effect on the adsorption of surfactants at the oil–water interface. The nature of the surfactant and oil, the ionic strength of the solution, and the temperature, all change the IFT of oil–water interfaces [31], [32], [33], [34] , [35], [36], [37], [38]. It has been surmised that the adsorption of nanoparticles at an oil–water interface might be influenced by the above mentioned factors in a similar way as for surfactant containing systems [39], [40]. The effects of temperature, pH value and ionic strength on the interfacial behavior have not been directly observed for gold nanaparticles at the liquid–liquid interface. It is important to know the temperature dependence of IFT when temperature variations exist (e.g. along an extraction column) [41]. *Miquilena et al.* [42] studied IFT between decane and aqueous solutions of Triton X-100 surfactant using the pendant-drop technique. Their results show that for surfactants the IFT increases with an increase in temperature. The authors also state that temperature has greater influence on the IFT for lower Triton X-100 concentrations than it does for higher bulk surfactant concentrations. A similar behavior was observed by *Ye et al.* [34] on the interfacial tension between crude oil and a gemini surfactant solution above a certain temperature. After reaching the temperature of 70^{o}C, the IFT for that system increased with an increase in temperature. They claimed that the increase occurs because there is diffusion of the surfactant from the interface to the oil phase. *Sottmann and Strey* [43] found that an increase in temperature causes the IFT of water-n-alkane surfactant systems to increase above a certain temperature. *Ataev* [44] determined that the IFT in water-hydrocarbon systems also increase as the temperature is raised. *Ataev* surmised that the increase may be due to an increase in the probability of impurities diffusing from the interface to the bulk phase (i.e., impurities that are present in oil phase).

The addition of sodium chloride has been shown to change the IFT of oil–water–surfactant systems. *Han et al.*[45] found that the IFT between crude oil and a gemini surfactant solution is changed as salt is added to the system. Increasing the ionic strength leads to a decrease in the IFT. According to *Han et al.*[45], adding salt may change the oil–water interface because there is a change in the hydrophilic-lipophilic balance and there is a compression of the electrical double layer at the interface. The net effect reduces the thickness and rigidity of the interface film which leads to an increase in the density of the surfactant at the interface (i.e., a decrease of the surface area occupied by one surfactant molecule). Overall, a reduction in the IFT at the oil–water interface was observed. *Gaonkar*

[46] also observed that the IFT decreases as the concentration of salt was increased in the aqueous phase for a vegetable oil–water interface [46].

Simovic and Prestidge [47] investigated how the pH and concentration of an electrolyte affected the adsorption of hydrophobic silica nanoparticles at the poly(dimethyl-siloxane) (PDMS) droplet–water interface. They found a dramatic increase in particle interfacial packing (i.e., a decrease in the adsorbed interfacial area per particle) with an increase in the salt concentration. These results showed a pH-dependent adsorption at the interface. The authors claimed that the balance of hydrophobic and electrostatic forces controls hydrophobic particle adsorption. *Simovic and Prestidge* [48] also investigated the adsorption behavior of hydrophilic silica nanoparticles at the polydimethylsiloxane (PDMS) droplet–water interface with the change of solution conditions (i.e., change of pH and electrolyte concentration of solution). Their findings showed that the surface coverage and particle packing at the interface are significantly influenced by salt addition, but pH has a very weak effect on particle adsorption. These findings indicate that the magnitude of particle-droplet and particle-to-particle interactions have an effect on particle penetration at the droplet-water interface. *Santos et al.* [49] studied the molecular behavior of ionic and non-ionic surfactant in a saline medium. They found that KCl has a weak effect on non-ionic surfactants. From experimental studies and computer simulations, *Li et al.* [50] observed a significant synergistic effect between sodium dodecylbenzene sulfonate (SDBS) and non-ionic Trion X-100 at the oil-water interface; the IFT values were lower as salt concentration increased. These authors speculated that as the salt concentration increases, a greater screening of the electrostatic repulsion between anionic surfactants. Thus, the hydrophobic interaction in the water phase increases, which in turn leads to a decrease in IFT.

1.1 Nanoparticle Stabilized Emulsions

It has been demonstrated that the presence of a nanoparticle colloid has a stabilizing effect on an emulsion, but the principles behind this effect are not clear. In an emulsion, the stability of a liquid film is increased in the presence of nanoparticles. Theoretical and experimental studies have been done in an attempt to understand these systems, but the stabilizing effect is not clearly understood. It is known that the attachment of nanoparticles

at a liquid interface directly affects the interfacial tension. A number of theoretical studies of solid nanoparticles in two phase fluid systems have been undertaken, and many of these studies focused on the partitioning of particles between aqueous bulk and fluid interfaces [51]. A schematic of nanoparticles stabilize emulsions at the oil-water interface can be seen in Figure 1.1.

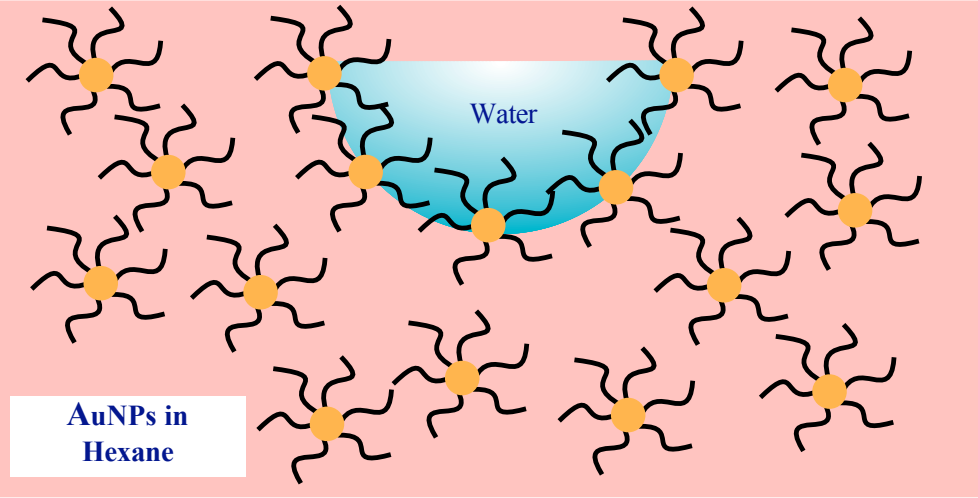

Figure 1.1: Schematic of nanoparticle stabilized emulsions at the oil-water interface.

The affinity of nanoparticles for the fluid interface depends on the hydrophilic or lipophilic character of the particles. In order to understand how a nanoparticle colloid affects the stability of an interface, the properties of the colloid must be systematically altered. By controlling the size, shape, and hydrophobicity of the nanoparticles as they are synthesized, the properties of the colloid can be changed in a methodical way.

1.2 Colloidal Particles and Self-Assembly

Colloidal particles are small objects dispersed in a continuous medium. Particles range in size from several nanometers to a few micrometers. Colloidal particles have been an important research topic for the last few decades. Currently, self assembly is the most effective method to locate NPs at the liquid-liquid interface. The self assembly of particles at the interfaces is controlled by inter-particle interactions including capillary, dipolar, and

electrostatic. Nanoparticles are attached to the interfaces by a reduction of energy (i.e., of the order of thermal energy). The self-assembly of nanoparticle is at the interface is dynamic; particles can absorb or desorb from interfaces [52]. Assembled particles form monolayers at the liquid-liquid interfaces [4]. The assembly of non-functionalized NPs and functionalized NPs at the interfaces is quite different; as the presence of ligands modifies surface activity [53]. *Isa et al.* studied the self-assembly of iron-oxide NPs stabilized by a poly (ethylene glycol) PEG shell at a water-*n*–decane interface. They observed the kinetics of NP at the liquid-liquid interface using the pendant drop tensiomentry method and concluded that particles self-assemble into monolayers at the water-decane interface [4]. The schematic of self assembly of nanoparticles without core shell, and with core shell NPs at the oil-water interfaces can be seen in Figure 1.2 and Figure 1.3.

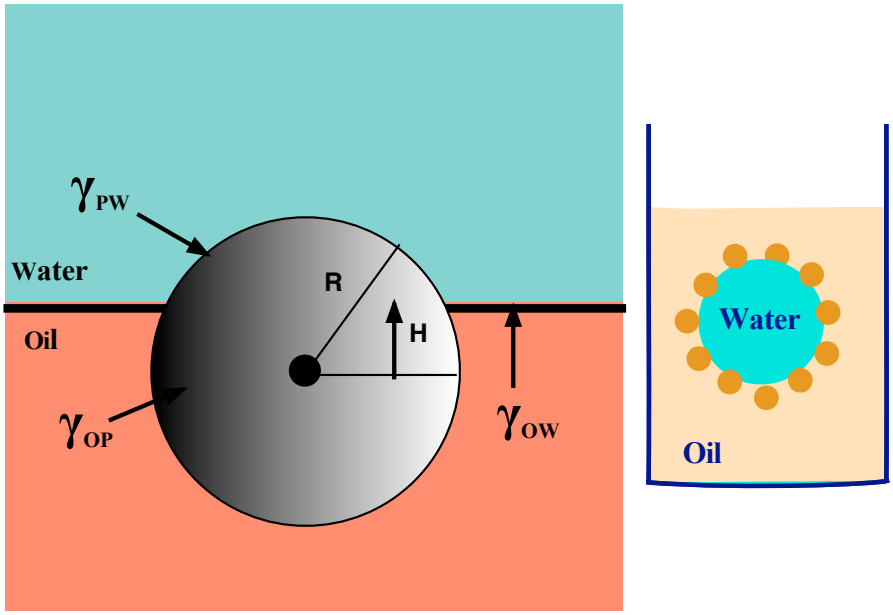

Figure 1.2: Schematic of (a) a sperical particle and (b) self-assembly of nanoparticles at the oil-water interface. [Reproduced from reference [52], [7]].

1.2.1 Colloidal Particles and Surfactants

Colloidal particles behave in similar ways to surfactant molecules. They can spontaneously gather at a two-fluid interface (either liquid-gas or liquid-liquid). At these interfaces, ad-

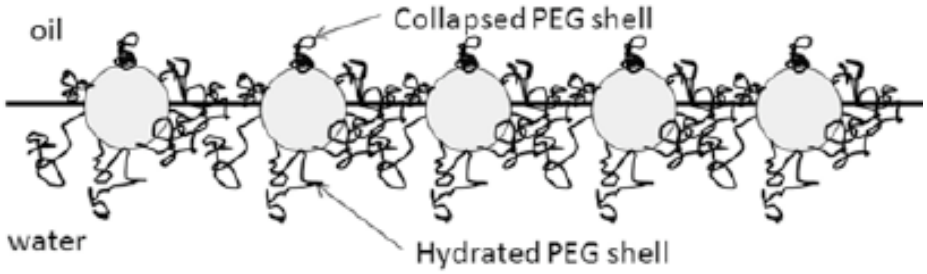

Figure 1.3: Schematics of core-shell NPs at a water–decane interface [4].

sorbed colloidal particles form monolayers. The interactions between the particles depends on the properties of the fluids, and the nature of the adsorbed particles [9].

Binks [14] compared and contrasted the behavior of surfactants and particles. Surfactant molecules are able to aggregate or self-assemble as micelles or in other liquid crystalline phases. However, this behavior has not been observed using colloidal particles. Like surfactant molecules, colloidal particles are able to stabilize emulsion droplets [54]. The systems stabilized by surfactants can either be oil-in-water (o/w) or water-in-oil (w/o) emulsions. The nature of the emulsion (either o/w or w/o) is defined by the hydrophile-lipophile balance (HLB). HLB is dependent on the surfactant packing factor p. p is defined as $p = a_e/a_h$, where a_e and a_h are the effective cross-sectional areas of the surface chain moiety and cross-sectional areas of the head group, respectively. With oil-water-surfactants, an o/w emulsion is formed if $p < 1$, whereas for $p > 1$ the emulsion is w/o [54]. Like surfactants, particles readily adsorb at the oil/water interface. The surfactants are amphiphilic in nature, but the particles are only a surface-active agent. The energy required to attach a surfactant molecule at the oil-water interface is around 10-20 k_BT. The colloidal particles are isotropically hydrophilic or hydrophobic, whereas surfactants consist of well-separated hydrophilic heads on one end, and hydrophobic tails at the other [3]. The adsorption of surfactants at the oil-water interface is reversible, while particles are adsorbed irreversibly [3].

Oil-water interfaces make a contact angle (θ) with the particle surface.Particle wettability is defined by θ which defines the emulsion type for particles. The schematic of NPs

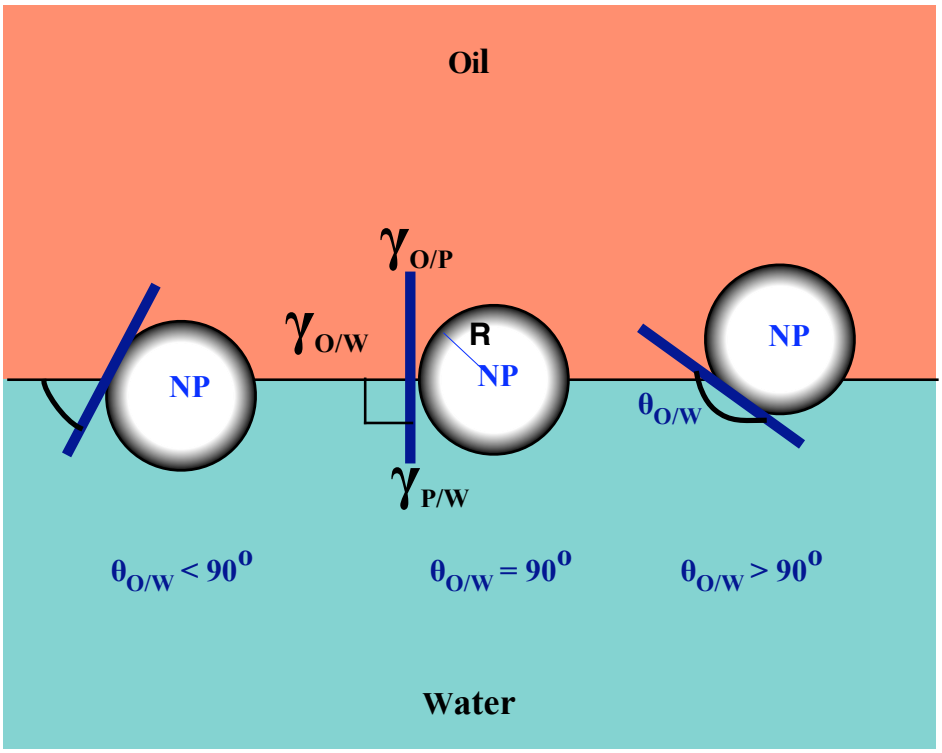

Figure 1.4: Schematic of NPs wettability at oil-water interface. Reproduced from reference [55].

wettability at oil-water interface can be seen in Figure 1.4. Like HLBs in surfactant systems, wettability for a particle is the parameter relevant to the description of its oil-liking or water-liking tendency at the interfaces. [54]. The energy required to locate a particle at the oil–water changes with the particle wettabilty.

1.3 Interfacial Phenomena and Nanoparticle Self-Assembly

Much nanoparticle research has been focused on the self-organization of particles at interfaces [55]. Uncharged dielectric and metallic nanoparticles capped with organic molecules are commonly used in nanoparticle self-assembly studies [56]. Through a deeper understanding of emulsified nanoparticle colloids, new nanostructured devices may be possible.

For example, nanoporous containers, or filtering devices, may be possible [57].

Liquid interfaces could be used as a platform for self-assembly of colloidal particles [57]. Because of their potential for large-scale production, foams and emulsions may provide an ideal means for mass-production of self-assembled nanoparticles within larger structures. Some potentially valuable applications of this technology include: thin-membrane generation, functionalization and modification of nanometer-scale objects at specific position, size selection of nanometer-sized objects, and controlled mixing of nanoparticles. Novel opto-electronic materials could also be made by self-assembling nanoparticles into two or three-dimensional superlattices. The optical, electrical, magnetic properties of nanoparticles are size-dependent, so in the search for a method to organize nanoparticles at interfaces, consideration must be given to nanoparticle size [58]. Processes with a high degree of nanoparticle organizational selectivity at the interfaces are the desired outcome.

In short, how supramolecular organization of nanoparticles, nanocrystals and other nanometer-sized objects occur at interfaces needs to be more fully understood.

1.4 The Effect of Impurities on Interfacial Tension

Due to the significance of water-oil interfaces in chemistry, biology, and their industrial importance, numerous studies have been done to characterize these interfaces. From these studies, it has become apparent that the purity of the compounds in experimental works is extremely important. Frequently, a surfactant may contain traces of other compounds. If impure surfactants are used, the surface activity of these trace compound may be much stronger than the surfactant itself; this will have a strong effect on the adsorption layer [59]. It is thus necessary to remove these trace impurities from the investigated system. However, the source of impurities may be from the solvents that is used (e.g., water). In order to investigate the interfacial properties at liquid/liquid interfaces, it is necessary to check the presence of surface-active trace impurities in both solvents [58].

1.5 Motivation & Description of Research Work

The interactions between adsorbed colloidal particles and the structure of the monolayer they form at liquid–liquid interfaces has not been well studied. Knowledge of how nanopar-

ticles behave at the liquid–vapor and liquid–liquid interfaces is necessary, especially in the areas of mineral processing, flotation and refining crude oil. Due to their outstanding optical, electronic, and magnetic properties, the controlled synthesis of the nanoparticles has also become a very promising area of research. For their potential applications in optoelectronics, catalysis and the other areas; the synthesis and physical characterization of nanometer scale metal and semiconductor colloids is an exciting area of research. In this respect, gold is one of the most widely investigated colloids. Gold nanoparticles exhibit unique robustness and high surface area. AuNPs capped with different surface functionalities can be used to provide highly selective nanoprobes for disease diagnosis [60]. They are used in clinical diagnostic methods as imaging therapeutic agents [61]. AuNPs are now recognized as a favorable platform for drug and gene delivery and function as a complement to more conventional delivery vehicles [62]. AuNPs are the best understood materials in the field of nanoscience and nanotechnology. The self-assembled monolayer-protected AuNPs can be used a a building block to design nano-devices and architecture. Due to their potential applications in biology, catalysis, and optoelectronics, many studies have been performed to synthesize and functionalize self-assembled monolayer protected AuNPs [22]. Based on this previous research, gold nanoparticles were chosen as the study material for the research presented in this thesis.

Alkanethiol gold nanocrystals were synthesized to perform the experiments. By changing the thiol to Au ratio, the reduction temperature, and the rate of reducing agent addition; different core sizes of alkanthiolate protected Au clusters can be made. Several characterization techniques such as ultraviolet visible spectroscopy (UV-Vis), high- resolution transmission electron microscopy (HRTEM), proton nuclear magnetic resonance spectroscopy (^{1}H-NMR) and Energy-dispersive spectroscopy (EDS) were performed to characterize the synthesized gold nanoparticles. IFT measurements of gold-capped nanoparticles at liquid-liquid interfaces were performed by pendant drop experiments using axisymmetric drop shape analysis methods (ADSA). Figure 1.5 illustrates the schematic of a pendant droplet of water held up by a needle in an organic suspension of alkhane-thiol capped gold nanoparticles (AT-capped AuNps).

The attached ligands or surfactants on the surface of the nanoparticles are responsible for its monodispersivity, stability, and controlled growth of each material. The surfactant chain-length also has an effect on the interfacial tension (IFT). Different capping agents (e.g., *n*-hexane-1-thiol, and *n*-dodecane-1-thiol) were used to synthesize the stabi-

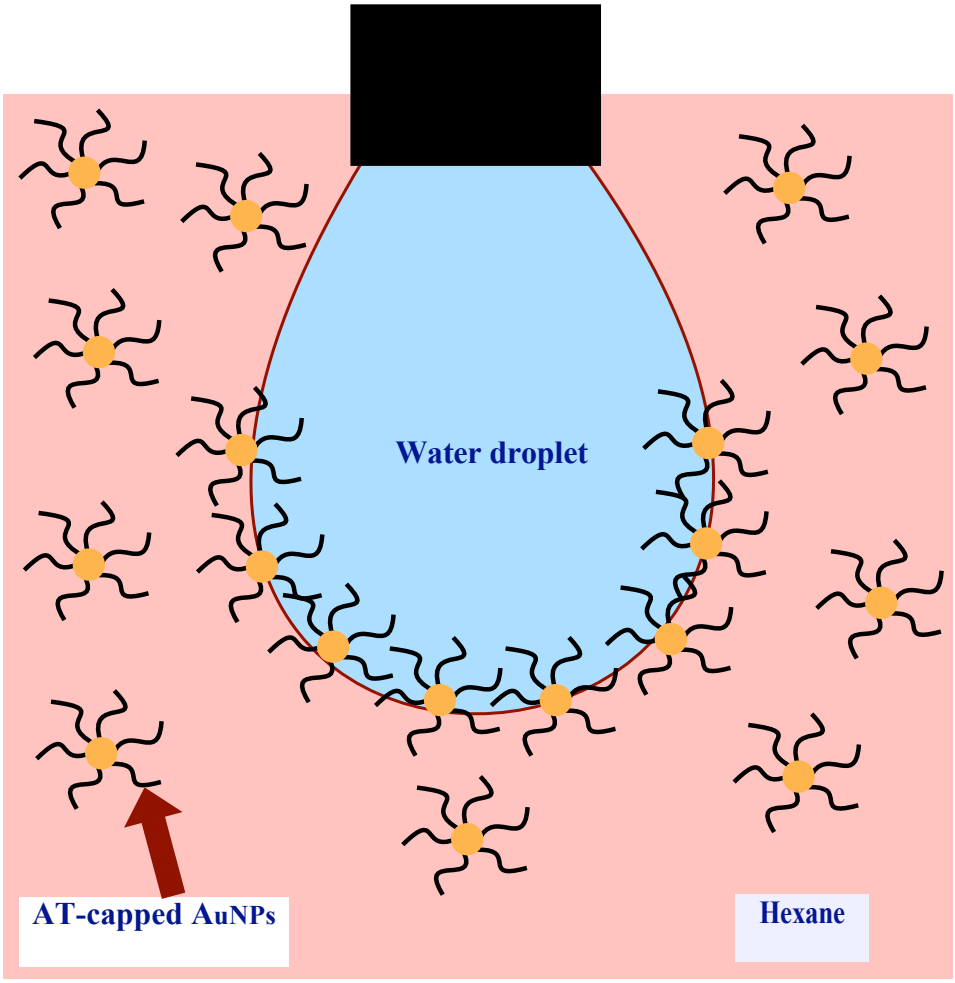

Figure 1.5: Schematic of a pendant droplet of water held up by a needle in an organic suspension of AT-capped AuNPs at the hexanel-water interface.

lized ligand-capped gold nanoparticles in oder to see their effects on the interfacial properties. It was observed that the interfacial tension changes as the bulk concentration, particle size, nature of the capping agent and temperature change. The size selective self-assembly of alkhanethiol capped gold nanoparticles (AT-capped AuNps) at the hexane–water can be schematized in Figure 1.6. Experiments were done for different bulk concentrations with different sizes of the nanoparticles by changing the temperature, ionic strength and pH of the aqueous phase. An overview of this thesis and the potential applications for this research can be seen in Figure 1.7 and Figure 1.8.

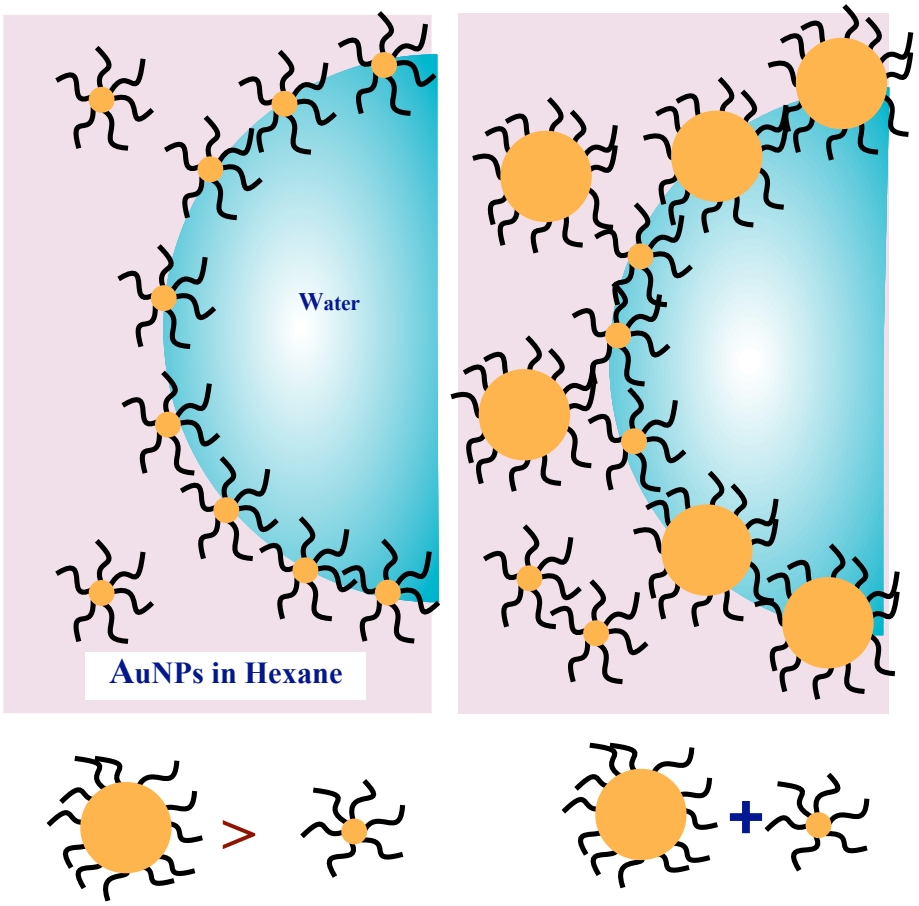

Figure 1.6: Schematic of size selective self-assembly of (a) unmixed AT-capped AuNPs and (b) mixed AT-capped AuNPs at the hexanel-water interface.

The following list summarizes the research objectives of this thesis:

Objective I: To investigate the adsorption kinetics of different sized *n*-dodecanethiol and *n*-hexanethiol capped gold nanoparticles at the liquid -liquid interface. The following factors were studied with respect to their effects on the interfacial tension at a hexane-water interface:

- The effect of NP bulk concentration.
- The effect of NP size.
- The effect of capping agent.

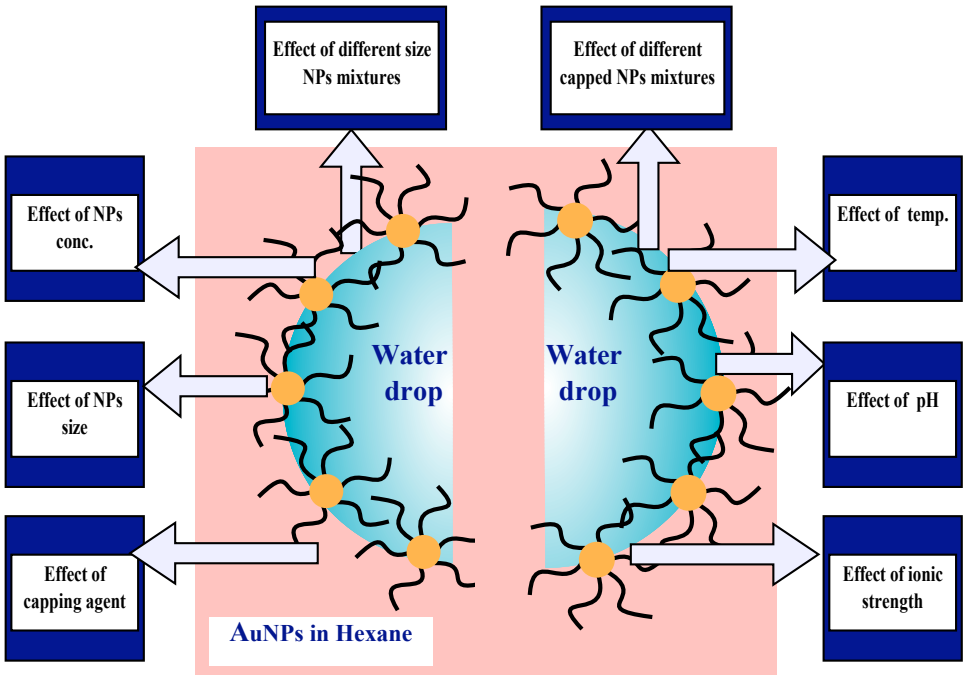

Figure 1.7: An overview of the thesis showing the different factors that have an effect on the adsorption kinetics of AT-capped AuNPs at the liquid-liquid interface.

Objective II: To determine the interaction parameter representative of the interfacial properties of mixtures of NPs. These experiments were performed by estimating the interaction parameters at hexane-water interfaces. The following variables were explored:

- mixtures of differently size NPs.
- mixtures of differently capped NPs.

Objective III: To determine the effects of temperature, ionic strength and pH on the IFT and adsorption behaviour of AuNPs at the liquid-liquid interface. The following factors were studied with respect to their effects on the interfacial tension at the nonane-water and hexane-water interface:

- The effect of temperature.
- The effect of ionic strength.
- The effect of pH.

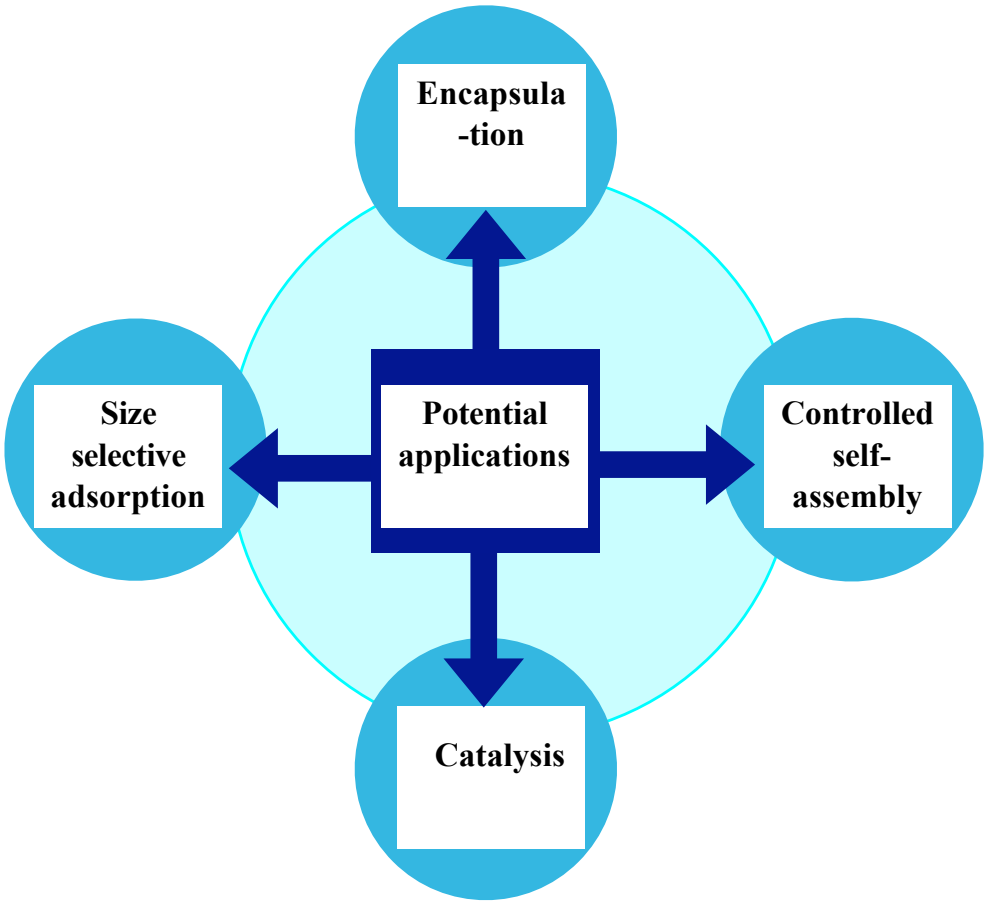

Figure 1.8: Schematic of potential applications of research work

Throughout the whole research work, the effects of these parameters were studied in order to understand the adsorption kinetics of the capped gold nanoparticles at the liquid-liquid interface. The journal articles written on the basis of data obtained during this research are listed in Appendix 8.2.

1.6 Organization of the Thesis

The rest of the thesis is organized as follows:

Chapter 2 provides an idea of the current research in the area of self-assembly of NPs at liquid-liquid interfaces. The main focus of this survey was to scrutinize

how the issues stated in Section 1.5 have been addressed in the current research on nanoparticle self-assembly. The literature review also emphasizes the factors that govern the interfacial stability of NPs.

Chapter 3 presents the experimental procedures and characterization techniques used to analyze the synthesized alkhanethiol capped gold nanoparticles. This chapter also describes the other experimental methods used in this thesis.

Chapter 4 provides the theoretical information to analyze the adsorption kinetics of alkhanethiol capped gold nanoparticles at liquid-liquid interfaces. This chapter also briefly outlines the sample preparation procedure used in this thesis.

Chapter 5 extensively describes the adsorption kinetics of different capped alkhanethiol gold nanoparticles at hexane-water interfaces. This chapter also describes the effects of bulk nanoparticle concentration, particle size, and the nature of the ligands on interfacial tension.

Chapter 6 describes the interfacial properties of both mixtures of differently sized gold nanoparticles, and different capping agents at the hexane-water interface.

Chapter 7 describes the effects of temperature, pH, and ionic strength on the adsorption behavior of nanoparticles at nonane-water and hexane-water interfaces.

Chapter 8 concludes the thesis with a summary of contributions that the research presented in this thesis accomplished and a note on the future direction of research in this field.

1.7 Summary

This chapter addresses the motivation and goals of the thesis and the contributions that the findings make to the field of nanotechnology, especially in the area of NP self-assembly. The chapter also provides a brief background on NP self-assembly at liquid-liquid interfaces. The next chapter provides a literature review on the same topic.

Chapter 2

Literature Review

This chapter provides a general view of the self-assembly of NPs at the liquid-liquid interfaces with a special focus on how these questions addressed the research issues discussed in Chapter 1.

2.1 Effect of Nanoparticle Size on the Interfacial Energy

2.1.1 Self-Assembly of Nanoparticles at Interfaces

The way in which nanoparticle self assemble depends on the particle size. According to *Lin et al.*, the fluid-fluid interfaces can be made by assembling ligand-stabilized nanoparticles without changing the properties of the nanoparticles. Also, it was found that smaller nanoparticles, ∼2 nm, have a very weak confinement at the fluid interfaces compared to larger ones. This enables one to choose the size-selective particle assembly, two-dimensional phase behavior, and functionalization [15]. Nanoparticles are easily displaced from the interface, but there is always a replacement of the particles; the replacement rate depends on the particle size. The schematic of size selective self-assembly of NPs at the oil-water interface can be seen in Figure 2.1. Due to thermal activation, smaller particles are more rapidly displaced than larger

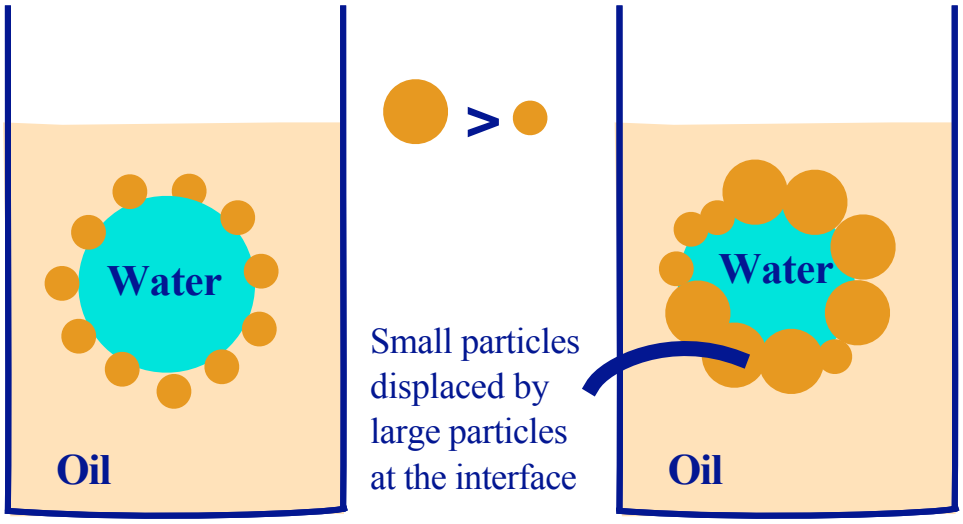

Figure 2.1: Schematic of size selective self-assembly of NPs at the oil-water interface. Reproduced from reference [63].

particles, and so, assemblies of larger nanoparticles are more stable. Also, the free energy for the smaller particles at equilibrium is less than for larger particles [57].

2.1.2 Kinetics of Nanoparticle Self-Assembly at Interfaces

Kutuzov et al. performed time-dependent interfacial tension measurements of water–toluene/CdSe nanoparticle colloidal suspensions. They found that the dynamic interfacial tension decreases with two parameters: time and particle size. For larger particles, ∼6 nm, the interfacial energy decreases very sharply and mostly occurs when the interface is initially created during droplet formation; this is the sharpest decrease in the interfacial tension. For larger particles, the tension was found to decrease very quickly in the early stages ($t \longrightarrow 0$), then decrease slowly, and finally become almost constant. For smaller particles, the interfacial tension becomes constant only at long times ($t \longrightarrow \infty$). Given enough time, the rate of adsorption and desorption of larger nanoparticles at the interface is the same, and a dynamic equilibrium state is reached. The maximum coverage of these particles occurs at equilibrium.

2.1.3 Free Energy of Nanoparticles at Interfaces

Du et al. observed the energy of adsorption of nanoparticles and microparticles at the oil-water interface, and found that the change of adsorption energy (ΔE) of citrate-stabilized gold nanoparticles is proportional to the square of the particle radius [8]. The reduction in the interfacial energy is the main driving force for the self assembly of nanoparticles at the liquid-liquid interfaces [7]. *Cheung et al.* performed molecular simulations to determine the interaction energy between a fluid interface and a nanoparticle. They found an attractive interaction between the nanoparticle and the interface. The binding energy (1-10 k_BT) increased in a quadratic relationship with the radius of the particle [12]. Due to higher attachment energy at the interface, larger particles are considered to be irreversibly absorbed, but smaller particles can be easily detached from the interface. The attachment energy of the particle at the liquid-liquid interface depends on the contact angle, and the line tension acting on the particles surface at the interfaces [11].

As soon as a droplet is formed, the nanoparticles diffuse to the water-oil interface, and the total free energy of the system decreases. The energy change for a single particle can be seen in Equation 1.1 By holding the temperature, $\gamma_{o/w}$, $\gamma_{p/w}$, and $\gamma_{p/o}$ constant, changes in the interfacial energy, ΔE, are only affected by changes in particle size. As a result, for a given constant temperature system, the stability of the nanoparticles at the interface increases with particle size. From equation 1.1, it is evident that larger particles adsorb more strongly than smaller particles because the change in interfacial energy depends on the particle size.

Investigations of the assembly of tri-*n*-octylphoshpine oxde (TOPO) stabilized CdSe nanoparticles with size of 2.8 nm and 4.6 nm have been done [15]. In these investigations, where a confocal fluorescence microscope was used, the adsorption of larger nanoparticles was found to be greater. Figure 2.2 shows the size selective self-assembly of different sizes of CdSe nanoparticles in toluene [15].

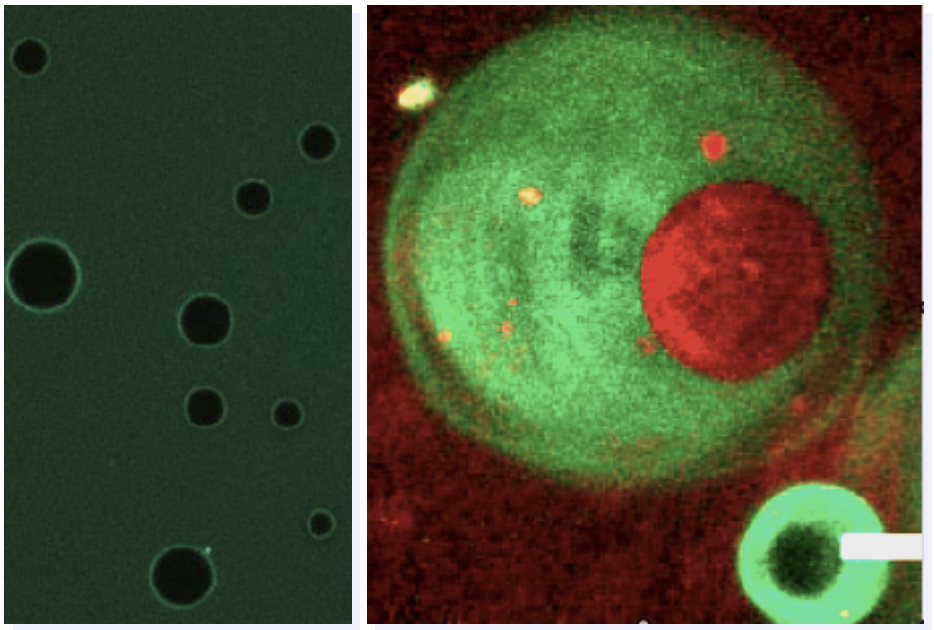

(a) (b)

Figure 2.2: (a) Images of dispersion of water droplets stabilized by 2.8 nm diameter CdSe nanoparticles in toluene. (b) After addition of 4.6 nm nanoparticles, water droplet stabilized by larger particles. 4.6 nm particles (red) displace 2.8 nm nanoparticles(green). Reproduced from reference [15].

2.2 Nanoparticle Assembly and Transport at Liquid-Liquid Interfaces

In an investigation of the self-assembly of nanoparticles at fluid interfaces, TOPO stabilized CdSe nanoparticles were dispersed in a toluene phase, and water droplets were formed with diameters of 10 μm to 100 μm within the toluene phase. Within a few seconds from droplet formation, the nanoparticles assembled at the toluene-water

interface and stabilized the droplet The nanoparticles were found to form a densely packed layer at the interface.

Over time, smaller particles were always replaced by larger ones (i.e., the exchange of the particles depends on the size) [64], as it is known that the particle assembly will occur in such a way to minimize the Helmholtz free energy. There is always a size dependence on the adsorption of nanoparticles at the interface. For example, it has been found that water droplets formed with 4.6 nm particles were stable for days, while droplets formed with the 2.7 nm particles fused or coalesced within hours. There was no droplet stabilization for particle less than $\sim$1.6 nm, because thermal fluctuations act to reduce the adsorbed particle concentration to levels below what is needed for a stable interface [64].

2.3 Effect of Contact Angle on Interfacial Tension

The contact angle between water and oil determines the position of the colloidal particles at the interface. More of the particle will be in the water phase if the particles are hydrophilic (i.e., the particles form a contact angle less than 90° with the interface), whereas, for hydrophobic particles (i.e., particles with contact angle greater than 90°) most of the particle will be in the oil phase. This can be seen schematically in Figure 1.4.

For nanometer-sized particles, the interfacial energy is on the order of the thermal energy, k_BT. The thermal energy is sufficient to allow nanoparticles trapped at the interface to move into the bulk phase. Investigations of the partition profile of 10 nm particles in water/oil two phase systems has been done. Nanoparticles with a contact angle close to 90° remained at the interface, while particles with contact angles much greater or less than 90° would move into one of the bulk phases. The change in the free energy for a single spherical particle moving from one of the bulk phases to the interface is given by one of the following equations:

$$\Delta E_p = -\pi r^2 \gamma [1 - cos(\Theta)]^2, \tag{2.1}$$

$$\Delta E_p = -\pi r^2 \gamma [1 + cos(\Theta)]^2, \tag{2.2}$$

where ΔE_p is the change in the free energy, r is the particle radius, γ is the interfacial tension, and Θ is the particle–liquid contact angle. Equation 2.1 is used when particles transfer from the water phase to the interface, while Equation 2.2 is used for particles moving from either the air or oil phases to the interface.

Partial wetting of the particle will occur for contact angles other than 0° or 180°. If the contact angle is near 0°, then the particle will essentially be in the water phase, and will most likely move into the bulk water phase. On the other hand, if the contact angle is 180°, then the particle will move into the oil phase. The amount of aggregation depends on the contact angle. The behavior of micron-sized particles has been studied using fundamental thermodynamics [56]. The attachment of the colloidal particle at either the air–liquid or liquid–liquid interface is due to a decrease in the interfacial energy. The decrease in interfacial energy depends on the contact angle, the interfacial tension, and the maximum attachment energy. The maximum attachment energy occurs when the particle is wetted by both phases equally (i.e., when $\Theta = 90°$) [56].

Micron-sized particles are effectively stuck at the interface because the interfacial attachment energy is on the order of $10^6 \times k_B T$. Since the attachment energy of nanoparticles (<10 nm) is on the order of $k_B T$, the nanoparticles can readily detach from the interface and move into the bulk phase. Even a small deviation, only a few degrees from 90°, may make it impossible for the particles to attach to the interface (i.e., the attachment becomes very poor for small particles because the interfacial tension becomes very important) [11]. The addition of salt was found to destabilize aggregates of particles at the interface. Aggregation was found to depend on the contact angle of the particle with the interface.

The adsorption of spherical particles to a spherical liquid-liquid interface was investigated theoretically by *Komura et al.* [65]. Youngs equation was used to estimate the equilibrium contact angle, for a particle absorbed at flat oil-water interfaces. *Komura et al.* argued that, same for flat interfaces, Youngs equation can also be used to estimate the contact angle of a particle at the spherical interfaces. The authors also surmised that the spherical curvature has an effect on the minimum adsorption energy for the spherical particle absorbed at the interface [65].

2.3.1 Effect of Line Tension on Particles Stabilization at the Interfaces

Oil-water interfaces make a contact angle (θ) with the particle surface. Line tension acts in the three phase contact lines around the absorbed particles at the interfaces. This tension may have an effect on particle adsorption. *Aveyard et al.* studied the effects of both positive and negative line tension on the free energy of adsorption of the spherical particles at spherically curved liquid interfaces [54]. They found that positive line tension drives small particles away from the interface of a drop, while negative line tension stabilizes emulsions. Line tension does not affect larger particles (radius>300 nm) [54]. For hydrophilic particles, (i.e., $\theta < 90°$), a larger portion of the particle surface is present in the aqueous phase. Whilst, for the hydrophobic particles, ($i.e., \theta > 90°$), most of the portion of the particles surface lies on the oil phase [3],[14], [66]. *Aveyard et al.* argued that the effect of the line tension (τ) has to be incorporated to calculate the attachment energy at the interfaces [54],[11]. The authors argued that positive line tension acts at the three phase contact angle at the interfaces. Due to positive line tension, and significant thermal energy fluctuation, small nanoparticles ($\leqslant 20$) nm can easily be removed from interfaces. For $\theta_{o/w}$ close to 90°, a stable attachment at the interfaces can be obtained. However, in these circumstances, the surfaces of the colloidal particles are partially wetted by either the water or oil phase.

2.4 Interfacial Energy of the Nanoparticle

For microscopic particles at the interface, the energy gained is much larger than k_BT, but for nanoparticles it is on the order of k_BT. Thus, microscopic particles bind more strongly than nanoparticles. At a given concentration, larger particles cover more area than smaller ones because the particles exchange more rapidly and easily as particles size decreases [1]. For this reason, smaller particles need more time to reach an equilibrium interfacial tension value. For example, the self-assembly of 2-bromo-2-methyl-propionate ligand stabilized nanoparticles of different types and sizes were observed by *Wang et al.* [55]. Hydrophilic nanoparticles were found to form a homogeneous thin film, while hydrophobic ones produced a heterogeneous film.

Not only the size of particles, but also the contact angle with the water-oil interface (i.e., the surface wettability) determines the interfacial surface activity. The terminal groups of the capping ligands are responsible for interfacial self-assembly. When the contact angle is close to 90° self-assembly can be understood clearly. Only recently has work related to self-assembly of nanoparticle with diameters less than 10 nm been done [55].

To date, only macroscopic measurements of the contact angle have been made to obtain the overall effect of nanoparticles at the interface, as it is nearly impossible to determine the contact angle of an individual nanoparticle.

2.5 Nanoparticles at the Interfaces

Molecular dynamic simulations have been done to study the interfacial assembly of surfactants and negatively charged hydrophilic silica nanoparticles [2]. At air–water interfaces, the surface tension of anionic and non-ionic surfactants were found to decrease when negatively charged silica nanoparticles were added. Also, the simulations showed that there was an increase in the interfacial activity of sodium dodecyl sulfate (SDS), an anionic surfactant, after nanoparticles were added. However, the interfacial activity for nonionic surfactants (e.g., tetraethylene glycol ethers (C_8E_4, $C_{12}E_4$, $C_{14}E_4$), and Triton X-100) was unaffected by the addition of nanoparticles. Repulsive forces between SDS and silica nanoparticles were found to be responsible for enhancing the surfactant absorption at the air–water interface. Again from simulation, the tri-chloroethylene–water (TCE–water) interface was studied. It was found that the interfacial tension of both SDS and Triton X-100 surfactants decreased when nanoparticles were introduced to the system. The addition of nanoparticles proved to have little effect on the TCE-water interfacial tension for $C_{12}E_4$, $C_{14}E_4$ systems (i.e., the tension was essentially the same with or without nanoparticle being added). The simulations showed that C_8E_4, $C_{12}E_4$, $C_{14}E_4$ molecules do not absorb at the TCE–water interfaces, rather they disperse into the TCE phase [2].

Although, it is important to know the interfacial adsorption of a system that contains both surfactants and colloidal particles, this topic has not been widely studied. The surface activity of a liquid–liquid interface can be changed by adding sur-

factants, nanoparticles, or both [2]. Experimental studies done by *Ravera et al.* showed the effect of negatively charged silica nanoparticles (D_p ∼30 nm) and the cationic surfactant hexadecyl-trimethyl-ammonium bromide (CTAB). The effectiveness of the CTAB at air–water and hexane–water interfaces decreased when charged silica nanoparticles were added. They postulated that the nanoparticles went to the interface because CTAB adsorbed on the nanoparticle surface [51].

Udayana et al. performed a molecular dynamics (MD) simulation of uncharged NPs and non-ionic tri-(ethyleneglycol)-dodecyl ether surfactant [53]. It was noticed that uncharged NPs and surfactant were confined to the oil-water interface by lowering IFT. NPs alone did not significantly change the oil-water interfacial tension. Together, surfactants and NPs showed synergistic behavior and resulted in lowered oil-water interfacial tension; this phenomenon was observed at low surfactant concentration. At higher surfactant concentrations, this synergy decreased. NPs functionalized with surfactants were not as effective at lowering the oil-water interface tension as the individual NPs or surfactants. *Udayana et al.* observed that many

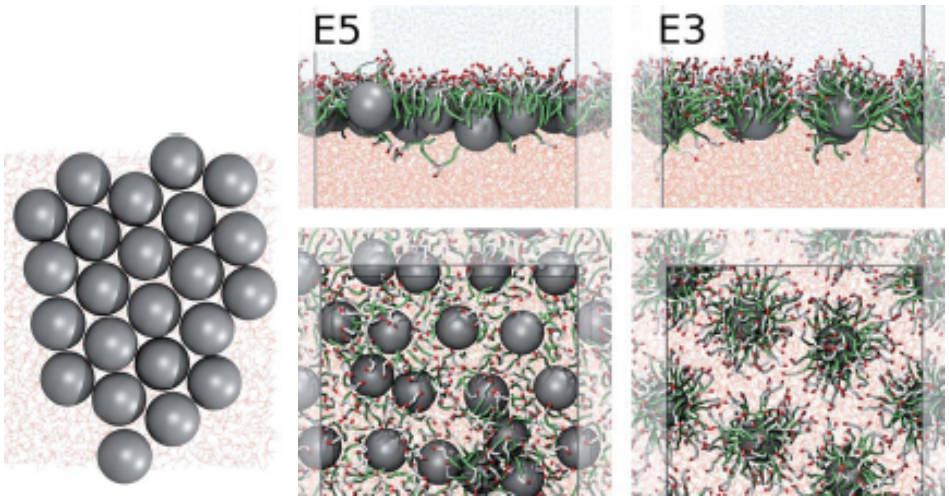

Figure 2.3: Snapshots of a packing structures of (a) unfunctionalized and (b) surfactant functionalized NPs at oil-water interface. The packing structures of a functionalized NPs are very different from their unfunctionalized one [53].

surfactants oriented in a proper direction to reduce the oil–water interfacial tension at low $C_{12}E_3$ surfactant coverage on the surface of the NP (left: system E5). At higher coverage (right: system E3), due to steric repulsion forces some surfactants formed unfavorable structures. This can be seen in Figure 2.3 and may be because, upon binding, surfactants are driven into unfavorable positions with respect to the interface. This leads to hetergenous surfactant coverage, and possibly explains the reduced efficiency [53]. It has been shown that both NPs and surfactants have a strong tendency to bind to interfaces. Surfactants lower the interfacial tension, while NPs lower the surface area. A system with both NPs and surfactants shows interesting and complex behavior at the fluid-fluid interfaces [53].

2.6 Effect of Particle Concentration on the Interfacial Properties

The time dependent interfacial tension of a water and toluene-CdSe nanoparticle suspension changes when the concentration of the bulk solution changes [1]. The time required for the system to reach equilibrium depends on particle size. For suspensions of larger particles, the system reaches the equilibrium interfacial tension more quickly than for smaller particles. Smaller particles reach equilibrium only when the particle concentration is very high, while larger particles will reach equilibrium very quickly for all concentrations. For smaller particles, at the lowest particle concentrations, equilibrium is not reached over the duration of the experiment.

Figure 2.4 and Figure 2.5 show the time dependence of the interfacial tension for CdSe-TOPO nanoparticles at the toluene–water interface. The lowest particle concentrations are represented by the curves at the top of the figure. As the particle concentration increases, the curves drop quickly with the highest concentration represented by curves nearer to the origin [1]. As the particle concentration increases, the equilibrium interfacial tension decreases until a critical concentration, c', is reached. At this concentration, the interface reaches the maximum coverage, Γ_∞, of the absorbed nanoparticles (i.e., the interface is saturated), and a susbequent increase in particle concentration will not change the equilibrium interfacial tension.

It was also found that apparent diffusion coefficients decrease with an increase in the

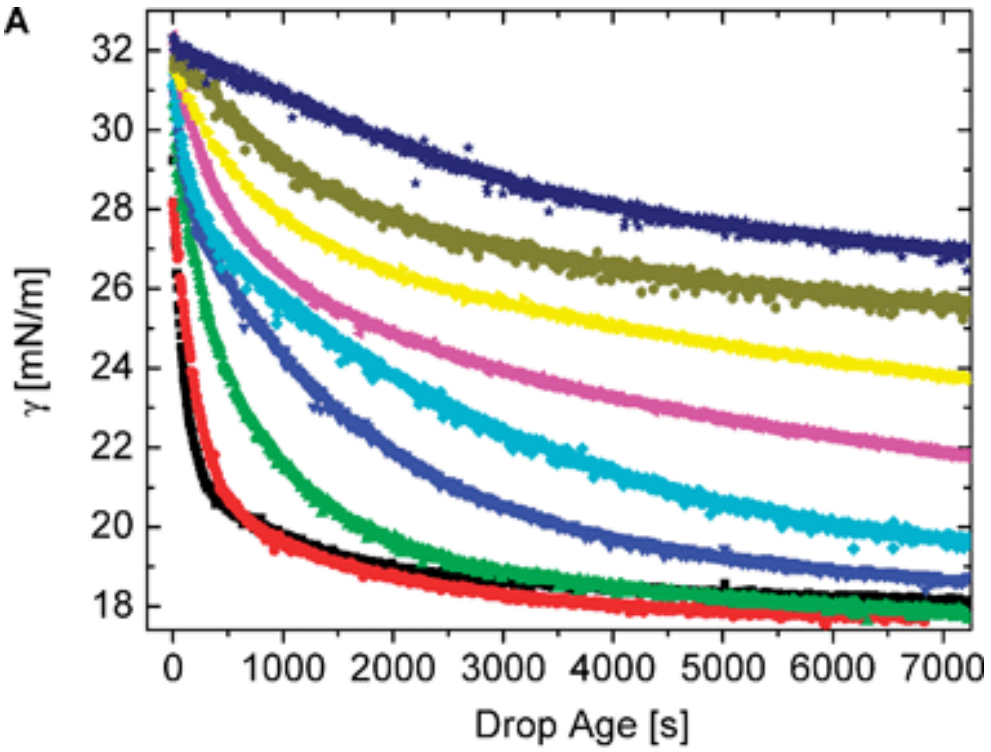

Figure 2.4: Time dependence of the interfacial tension at the toluene-water interface for 2.3 nm CdSe-TOPO nanoparticles of various concentrations [1].

particle concentration [1]. At longer adsorption times and higher particle concentrations, the interaction between particles nearer to the water-oil interface increases. It was assumed that this reduced the diffusion coefficient at the later times. There are always collisions between either nanoparticles adsorbed at the interface or desorbed from the interface, and nanoparticles approaching the interface from the bulk suspension. Over time, collisions increase within the sub-layer because the number of particles increases as the particle concentration increases. At the interface, the adsorption of additional nanoparticles is hindered by nanoparticles that are already desorbing. As shown in Figure 2.6, in the vicinity of the sub-layer, a potential barrier arises close to the interface that prevents particles from moving perpendicular to the interface. The motion of particles near the interface are influenced by two mechanisms: diffusion of the particles from the bulk to the sub-layer, and overcoming a potential barrier between the interface and the bulk. At the low concentrations, a

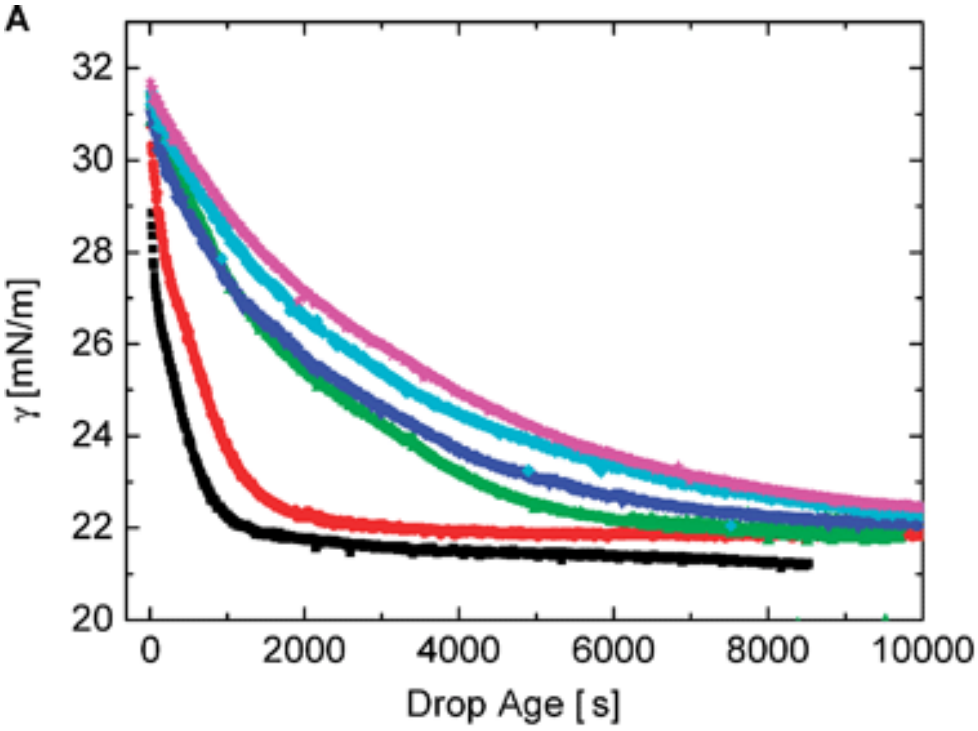

Figure 2.5: Time dependence of the interfacial tension at the toluene-water interface for 6.0 nm CdSe-TOPO nanoparticles of various concentrations [1].

distinction between the sub-layer and the interface is difficult because it becomes indistinguishable from the bulk phase. The width and position of the potential barrier depends on the strength of inter-particle interactions.

2.6.1 Dynamic Surface Tension of Non-Ionic Surfactants

Using a maximum bubble pressure instrument, *Eastoe et al.* studied the dynamic surface tension for a variety of nonionic surfactants [21]. These surfactants included the following: glucamide surfactants; di-(C5-Glu), di-(C6-Glu), di-(C7-Glu), and *n*-alkyl polyglycol ethers; $C_{10}E_4$, $C_{10}E_5$, $C_{12}E_5$ $C_{12}E_6$, $C_{12}E_7$, and $C_{12}E_8$. The surface tension was observed for different concentrations for each of the surfactants. The concentration of each surfactant was adjusted to levels above and below the critical micelle concentration (CMC) and the dynamic surface tension was observed. Immediately after a bubble was formed, the adsorption was found to be diffusion controlled. Over

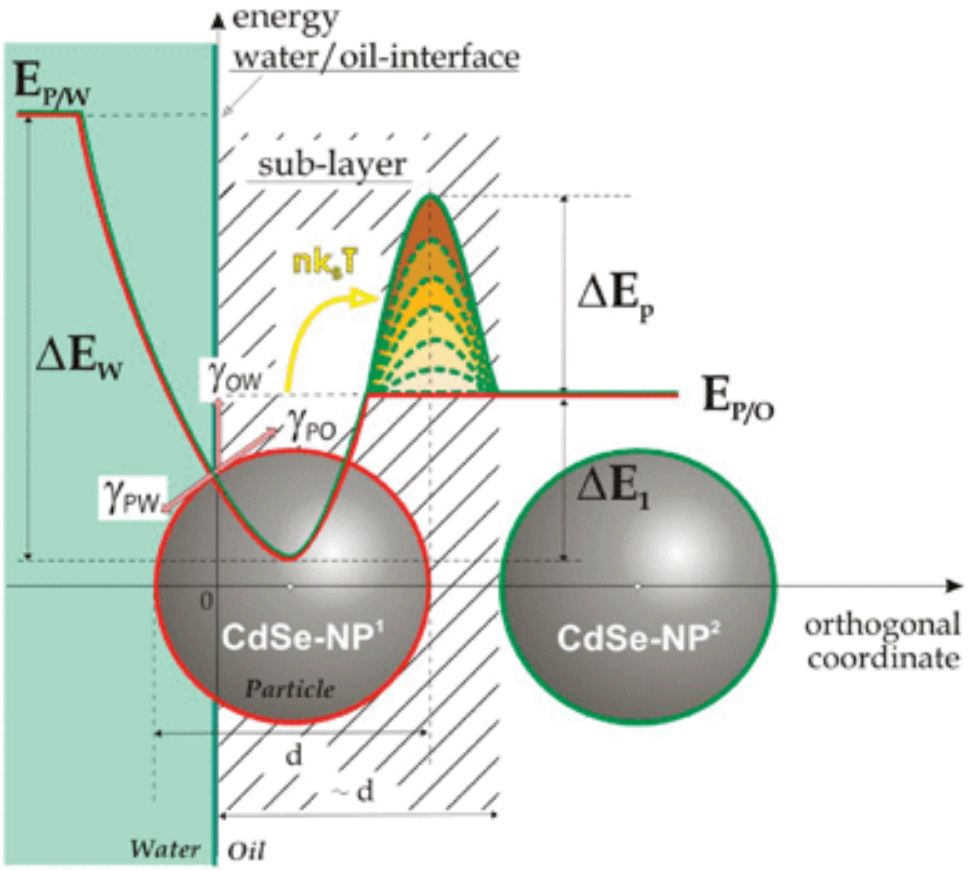

Figure 2.6: Schematic of the energetics associated with spherical CdSe-TOPO nanoparticles at the oil-water interface. CdSe-NP^1 is at the interface, while CdSe-NP^2 is in the bulk [1].

time, it was found that a mixed mechanism, diffusion–activation, was responsible for the dynamic adsorption, with the creation of an adsorption barrier of between 5 and 12 kJ/mol [21].

2.7 Effect of Temperature and Pressure on Interfacial tension

Investigations of the interfacial tension for a number of n-alkane–water systems using the emergent drop experimental technique were performed by *Zeppieri et al.*. A linear dependence was found for the interfacial tension as a function of temperature for several n-alkanes (see Figure 2.7). As the length of the carbon chain increased, the interfacial tension increases [67]. The interfacial tension between various n-alkanes and water as function of temperature and pressure was also studied by *Motomura et al.*[68]. A summary of the results can be seen in Figure 2.8 and Figure 2.9. The authors found a linear dependence between the interfacial tension and pressure, while the interfacial tension decreased as the temperature increased. *Miquilena et al.* [42] studied IFT between decane and aqueous solutions of Triton X-100 surfactant using the pendant-drop technique. Their results show that for surfactants the IFT increases with an increase in temperature. The authors also state that temperature has greater influence on the IFT for lower Triton X-100 concentrations than it does for higher bulk surfactant concentrations. A similar behavior was observed by *Ye et al.* [34] on the interfacial tension between crude oil and a gemini surfactant solution above a certain temperature. After reaching the temperature of 70^oC, the IFT for that system increased with an increase in temperature. They claimed that the increase occurs because there is diffusion of the surfactant from the interface to the oil phase. *Sottmann and Strey* [43] found that an increase in temperature causes the IFT of water–n-alkane surfactant systems to increase above a certain temperature. *Ataev* [44] determined that the IFT in water-hydrocarbon systems also increases as the temperature is raised. *Ataev* surmised that the increase may be due to an increase in the probability of impurities diffusing from the interface to the bulk phase (i.e., impurities that are present in oil phase).

2.8 Effect of Ligands on Interfacial Tension

Colloidal particles are not stable at interfaces. Increased particle stability requires a hydrophobic coating, so that that interfacial attachment of nanoparticles is achiev-

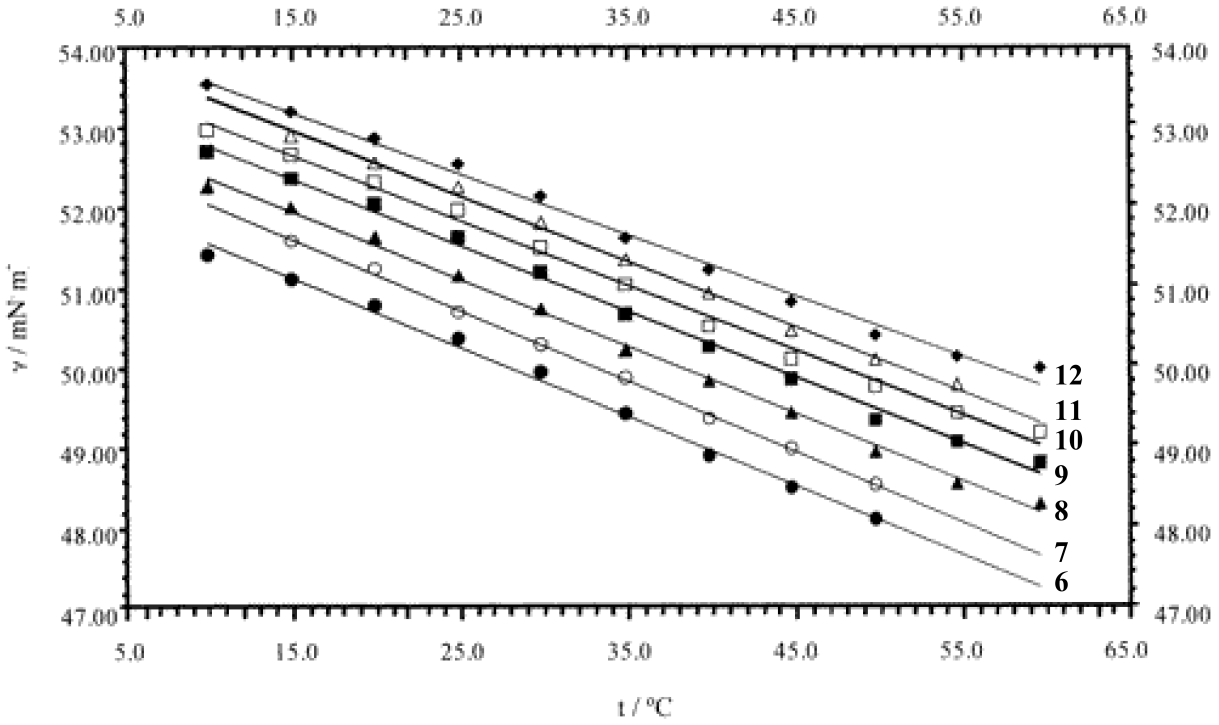

Figure 2.7: Interfacial tension values as a function of temperature for several n-alkanes. 12–dodecane, 11–undecane, 10–decane, 9–nonane, 8–octane, 7–heptane, 6–hexane [67].

able. *Duan et al.* argued that only particles with hydrophobic surface coatings are able to absorb at oil-water interfaces [69]. They observed the self assembly of hydrophilic AuNP, Ag−NPs, and hydrophobic γ-Fe_2O_3 at water-toluene interfaces. The authors reported that the particles were attached to the interface when capped with a 2-bromopropionate ligands [69]. They suggested that the ligands may make the contact angles of the nanoparticles close to 90° at the interfaces. This, in turn would drive nanoparticle self-assembly to form closely packed arrays at the water-toluene interface. *Duan et al.* used 2-bromo-2-methylpropiorate as a surface ligand on AuNPs, AgNPs, and γ-Fe_2O_3NPs [69]. The authors claimed that this provided the particles a contact angle very close to 90°. The particles were found to assemble exactly in the middle of a toluene-water interface. This indicates that an appropriate selection of capping ligands can adjust the wettability of NPs at interfaces [69]. The image of the self-assembled Au@DTBE nanoparticles at the water-toluene interface can be seen in Figure 2.10. *Du et al.* observed the energy of adsorption of

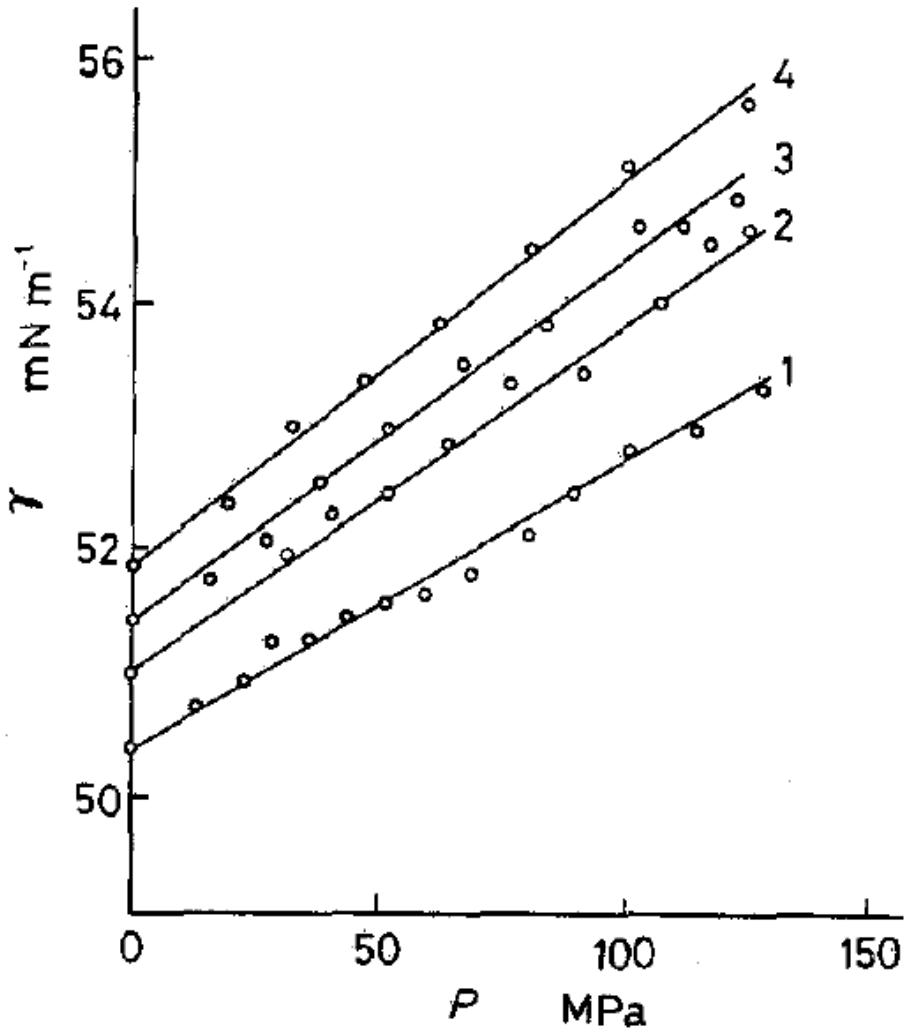

Figure 2.8: Interfacial tension of oil—water interface versus pressure at 298.15K. 1–hexane, 2–octane, 3–decane, 4–dodecane [68].

nanoparticles and microparticles at the oil-water interface and found that the change of adsorption energy (ΔE) of citrate-stabilized gold nanoparticles is proportional to the square of the particle radius [8]. They recorded a decrease of the interfacial tension for 2.5 nm citrate stabilized gold nanoparticles (Au−cit) and 2.3 nm (1-mercatoundec-11-ye)tetra(ethylene glycol) stabilized gold nanoparticles (Au−TEG)

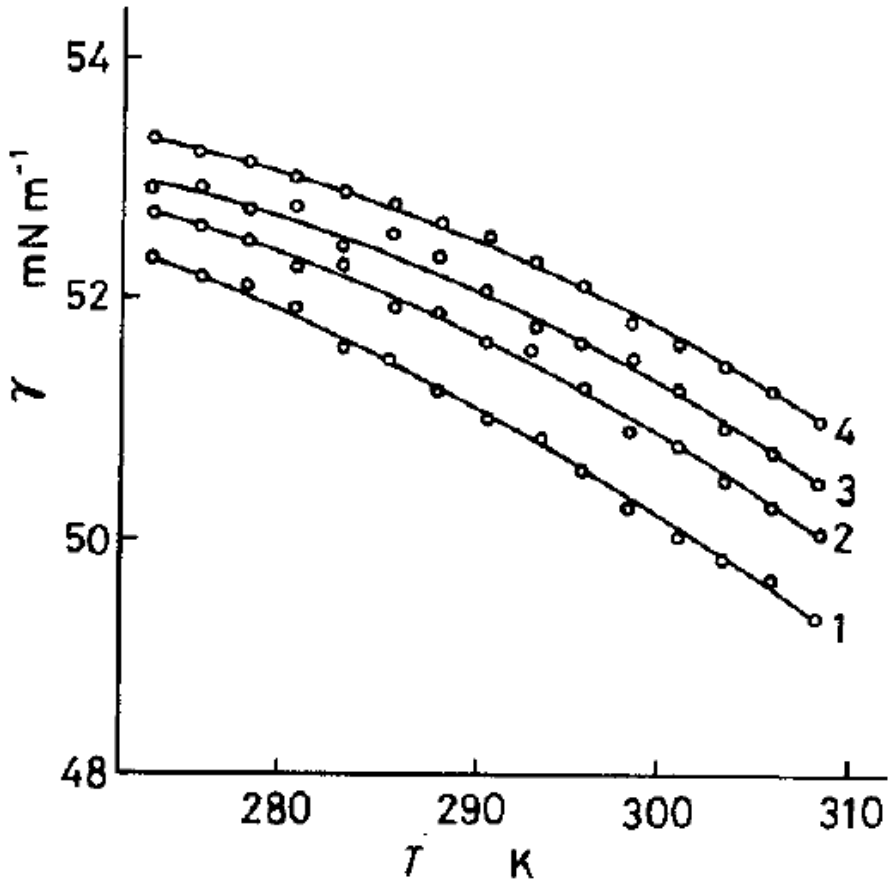

Figure 2.9: Interfacial tension of oil—water interface versus temperature at atmospheric pressure 1–hexane, 2–octane, 3–decane, 4–dodecane [68].

at the octafluoropentyl acrylate (OFPA)-water interface. By changing the concentration of salt and the organic solvent, the binding energy can be adjusted at the interface. The adsorption energy of 2.5 nm Au−cit and Au−TEG on the droplet OFPA are -5.1k_BT and -60.4 k_BT, respectively. The latter value is 12 times greater than the ΔE for similar sized Au−cit. Therefore, the ligand has an effect on the adsorption energy (i.e, interfacial tension) [8].

Ranatunga et al. performed molecular dynamics simulations to understand the behavior of surfactant-functionalized nanoparticles at oil-water interfaces [70]. They

Figure 2.10: Image of the self-assembled Au@DTBE nanoparticles at the water/toluene interface in a plastic tube [69].

studied four NPs with different surface coverage. It was found that the coating on the surface of NPs has a profound effect on the interfacial activity. They also suggested that the particles can be deformed from an idealized spherical shape at the liquid-liquid interfaces due to the flexibility of ligands on the NPs surface [70]. The composition of the ligand shell on the surface of the NPs has a profound effect on the wettability of the particles at interfaces as the stable assembly of NPs at the interface depends on particle wetting. The snapshots of characteristic behavior of surface-ligated NPs in the vicinity of an oil-water interface can be seen in Figure 2.11. *Glogowski et al.* observed that AuNPs capped with equimolar amounts of *n*-dodecanethiol and 11-mercapto-1-undecanol stabilized emulsions. However, an excess of the same ligands on the NPs surface caused inability to stabilize the emulsions. Therefore, mixed-monolayer protected NPs can be used as a new tool to stabilize emulsion water droplets in oil [71].

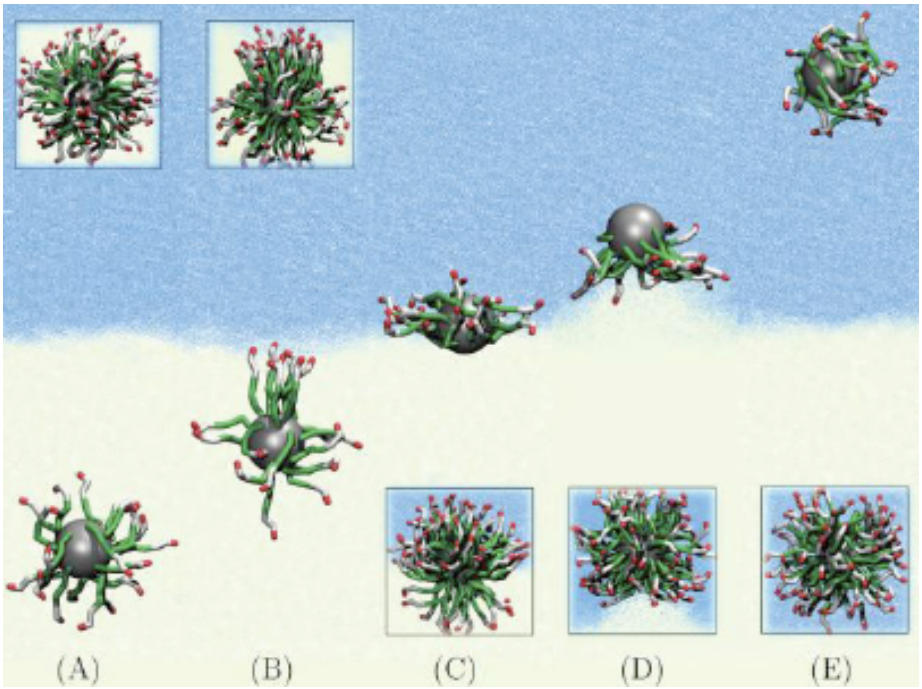

Figure 2.11: Snapshots of characteristic behavior of surface-ligated NPs in the vicinity of an oil/water interface. The regions are (A) deep in the oil phase, (B) in the oil phase close to the interface, (C) at the interface, (D) in the water phase close to the interface, and (E) deep in the water phase [70].

At the oil–water interface, self-assembly of 2-bromo-2-methyl-propionate terminus ligand stabilized nanoparticles of various size and chemical composition was discussed by *Wang et al.* [55]. Hydrophilic nanoparticles were found to form a homogeneous layer at the interface, while hydrophobic nanoparticles were found to generate heterogeneous layers. The terminal groups of the capping ligands are determined by the self-assembly of the nanoparticles at the interface.

2.9 Effect of Salt on the Interfacial Tension at Liquid–Liquid Interfaces

Simovic and Prestidge investigated the adsorption behavior of hydrophilic silica nanoparticles at the polydimethylsiloxane (PDMS) droplet-water interface [48]. It was found that the change in free adsorption energy, (ΔG), and maximum adsorption density, (Γ_{max}) in increased pH conditions were insignificant. These values were significantly increased with an increased salt concentration. At low salt concentration, the hydrophilic silica nanoparticles adsorbed at the liquid droplets with negligible interfacial accumulation. As the salt concentration was increased, particle-droplet and particle-to-particle lateral electrostatic repulsion was reduced. This leads to an increase in particles assembly at the interface. The authors demonstrated that the particles adsorbed very densely at the interface when double-layer thickness is reduced to a few nanometers [48].

The dynamic interfacial tension between a commercial soybean oil–water, and soybean oil–brine interface at three temperatures (5°C, 20°C and 50°C) has been studied [46]. Since there are a number of impurities in the commercial oil, they have a dramatic effect on the dynamic interfacial tension.

The presence of the salt (NaCl) in the oil–brine system, decreased the interfacial tension compared to a oil–water interface. It was postulated that the polar nature of the salt caused impurities in the oil to be concentrated at the oil–brine interface, thus reducing the interfacial tension. The solubility of the polar impurities changes not only with salt concentration, but also with temperature. Thus, changes in temperature also cause an increase in the rate of reduction in interfacial tension. The higher the temperature the greater the rate of reduction in the tension. Without salt, higher temperatures caused a smaller rate of reduction in the interfacial tension. This observation may be due to a reduction in the adsorption of impurities present in the oil, or on the dependence of the temperature, or both. These effects can be seen in Figure 2.12. The study was also conducted on the same system for soybean oil that had been purified by passing the oil through a glass column packed with a mixture of Florisil and silica gel. By removing the impurities in the oil, the interfacial tension did not change substantially over time. The dynamic interfacial

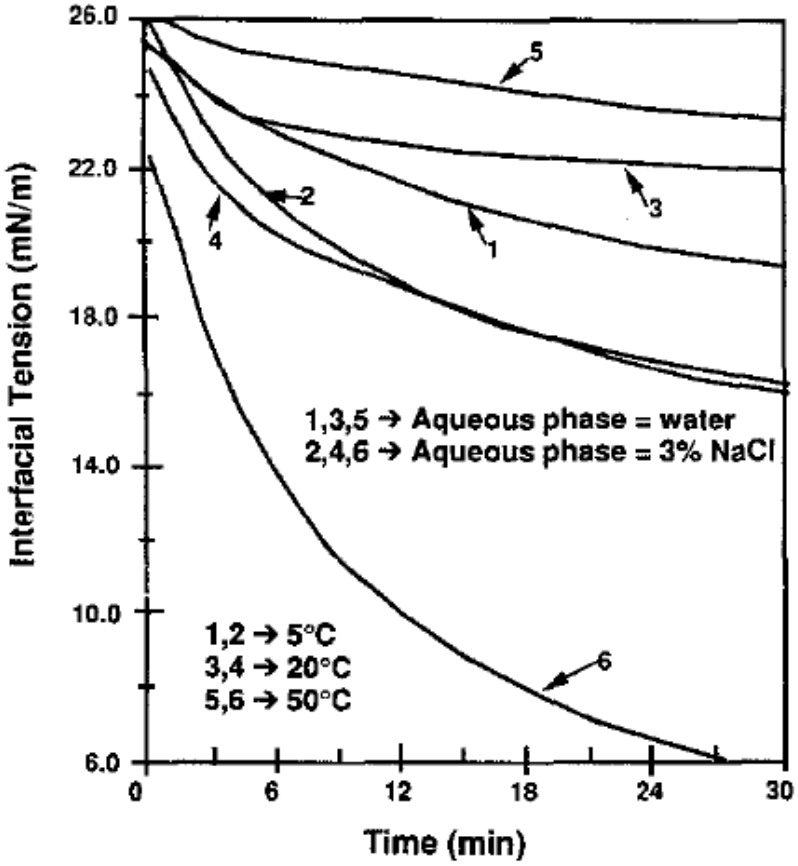

Figure 2.12: Interfacial tension between commercial soybean oil and water in the presence and absence of NaCl (3%) at three temperatures [46].

tension for a number of experimental conditions can be seen in Figure 2.13. The effect of salt on the interfacial tension for purified soybean oil–water systems with added surfactants (i.e., stearic acid, oleic acid, ricinolic acid, and linoleic acid) was also investigated. This was done to see the effect of salt and impurities in the systems in a controlled way. Simply by adding the surfactants to the purified oil there was a noticeable drop in the initial interfacial tension. Also for the case ricinoleic acid (9-*cis*-12-hydroxyoctadecenoic acid), there was a substantial drop in the interfacial tension for brine versus water. Again, these effects can be seen in Figure 2.14. In the case of ricinoleic acid, the drop in interfacial tension may be due to the presence of an –OH group close to the double bond within the molecule.

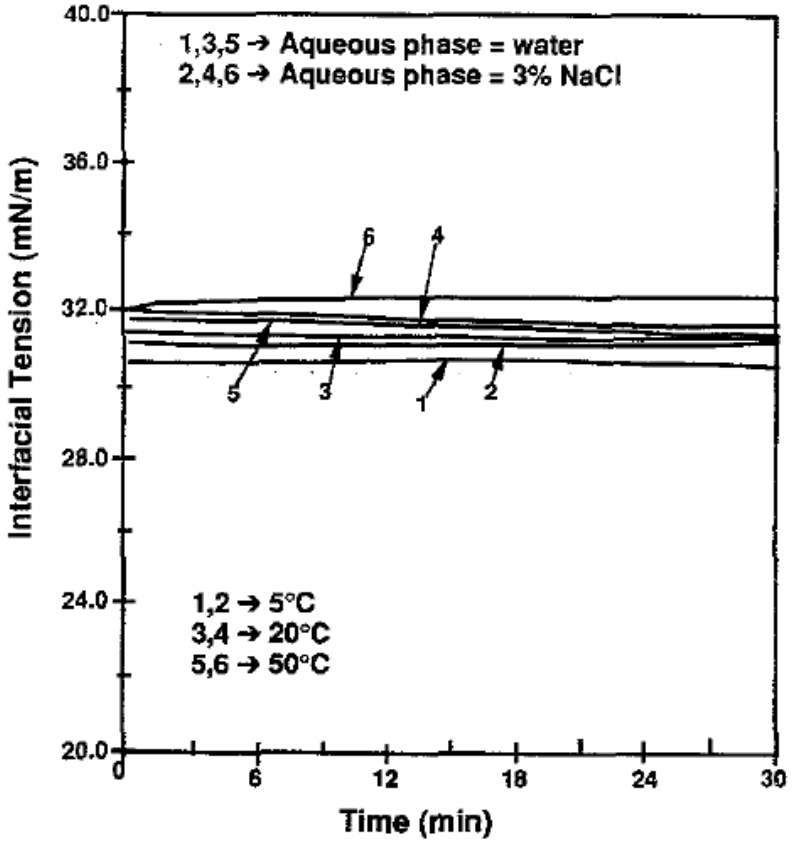

Figure 2.13: Interfacial tension between purified soybean oil and water in the presence and absence of NaCl (3%) at three temperatures [46].

2.10 Effect of Ethanol at Oil–Water Interfaces

Reincke et al. showed that citrate capped gold nanoparticles formed a randomly packed colloidal monolayer at the water–heptane interface after adding ethanol. More nanoparticles would gather at the interface as the concentration of ethanol increased. These results were confirmed by electrophoretic measurements which showed that the ethanol reduced the particle surface charge density [56].

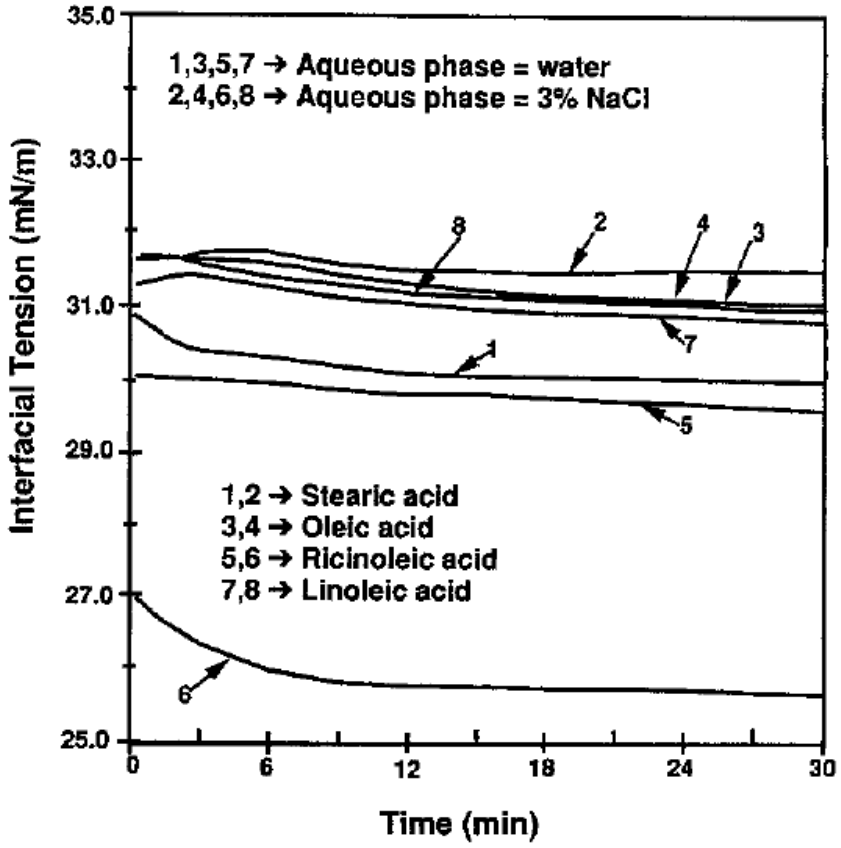

Figure 2.14: Dynamic interfacial tension for 0.1% fatty acid: purified oil–water systems in the presence and absence of NaCl (3%) at 323K [46].

2.11 Effect of pH on the Stability of Particles at Oil–Water Interfaces

The pH of aqueous solutions in contact with an organic phase also has an effect on IFT. The organic phase in contact with the water phase provides an electrical negative charge at the organic-aqueous interface. This is due to the adsorption of hydroxyl ions (OH^-) at the interface from the bulk aqueous phase which leads to a decrease in the IFT [72], [73], [74], [75],[76].

Reincke et al. showed that by changing the pH of the aqueous phase, 4-mercaptobenzoic

acid capped 8 nm AuNPs can be attached and detached from the water-heptane interface. The particles can also be re-dispersed in the aqueous phase [56]. No particles were found to attach at the interface when NPs were introduced to the water-heptane interface; this is due to the particles hydrophilic nature. The pH of the aqueous phase was then adjusted by adding dilute HCl. This resulted in protonation of the AuNPs, and caused them to adsorb to the interface; the particles formed a purple film at the water-heptane interface; this can be seen in Figure 2.15. The authors observed

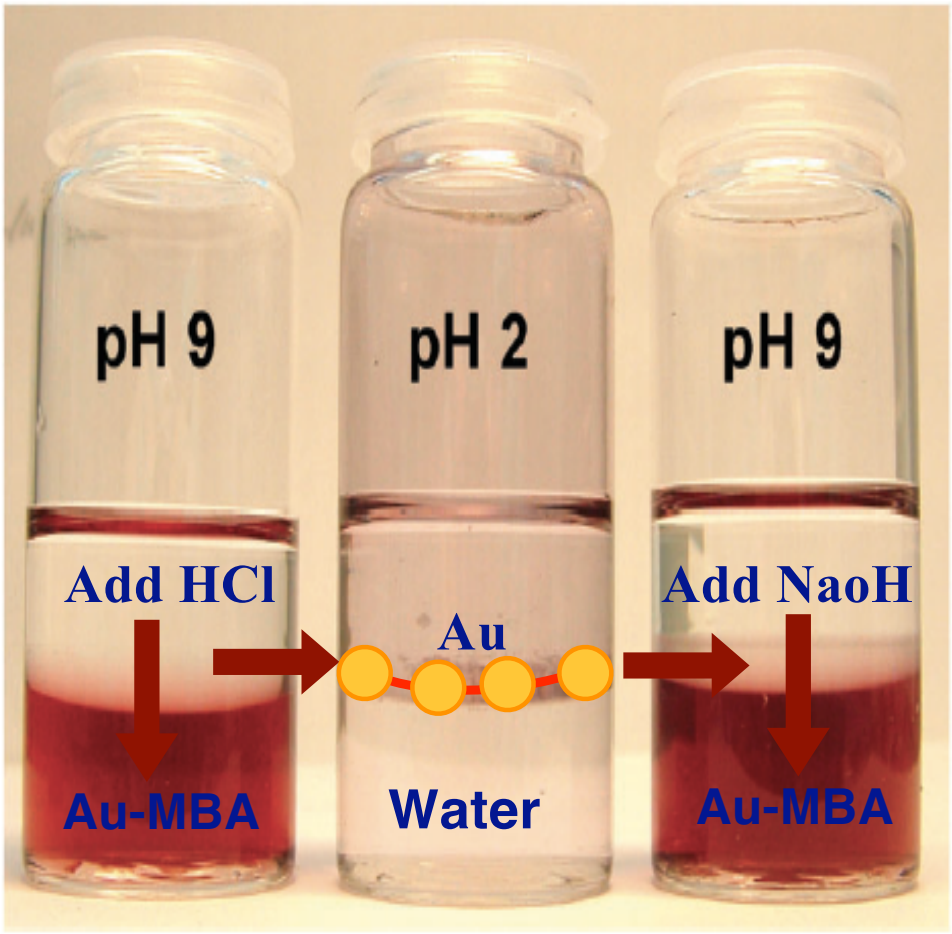

Figure 2.15: Photographs display the HCl and NaoH effect on aqueous solutions of 4-MBA capped 16 nm AuNPs at heptane-water interface heptane [56].

reversible interfacial self-assembly when the pH of the aqueous solution was adjusted

to a value of 9. The color of the aqueous solution returned to its original red color at this pH. This confirmed the detachment of the AuNPs from the interface [56].

Reincke et al. et al. also studied, the self assembly of charge-stabilized colloidal Au and CdTe at the water-heptane interface. The particles are capped with 3-MPA

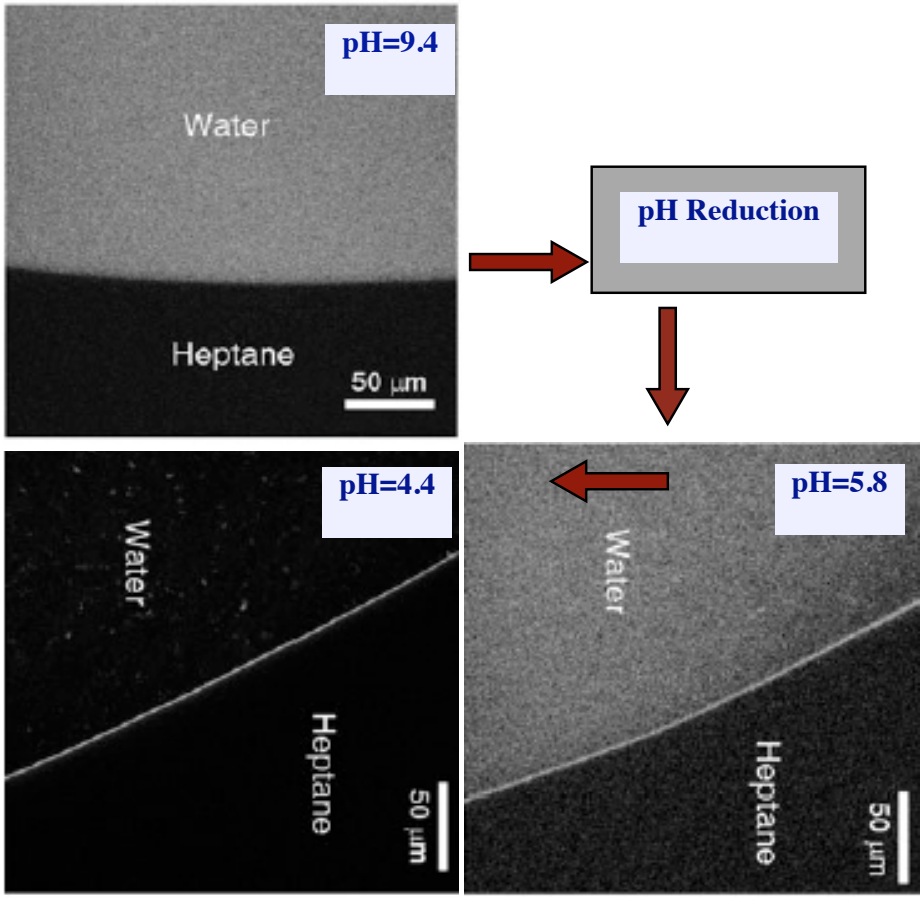

Figure 2.16: Confocal images show the pH effect on an aqueous solution of 3-MPA capped CdTe nanoparticles at the heptane-water interface. With the reduction of pH (from 9.4 to 4.4), more CdTe particles drive to the interface [Reprodued from reference [56].

and 4-MBA. At low pH, the surface charge density reduced due to the protonation of the carboxylic acid groups on the surfaces. This lead to an increase in surface hydrophobicity, and allowed a greater number of nanoparticles to attach at the water-heptane interface. At high pH, surface charge density is increased due to the de-

protonation of the carboxylic acid groups this results in expulsion of particles from the interface into the bulk water phasen [56]. The pH effect on an aqueous solution of 3-MPA capped CdTe nanoparticles at the heptane-water interface is shown in Figure 2.16. *Simovic and Prestidge* investigated the adsorption of hydrophobic silica nanopartcles at the PDMS droplet-water interface and found that when the pH of the aqueous phase was increased, particle adsorption was reduced [47]. This may have been due to the increment of interaction between the droplet and particle in addition to particle-particle electrostatic repulsion. On the other hand, particle adsorption increased with increased salt concentration.

2.12 Effect of Impurities on Interfacial Properties

In order to investigate the interfacial properties of liquid–liquid interfaces, it is necessary to check for the presence of surface-active trace impurities. From observations of water–*n*-alkane systems, it has been found that many alkanes, as obtained from chemical suppliers, often contain many impurities and fail to satisfy the stringent requirements necessary for interfacial studies. In order to get reliable results, the impurities in these stock alkanes must be removed. The procedures used to purify a substance and test that it is pure enough for interfacial studies of air–water interfaces can also be applied to water–oil interfaces. There are a few methods to remove the impurities from the oil phase: (1) A solid adsorbent column filled with basic alumina, or (2) shaking the oil with water for a few hours. By using one or a combination of these methods, the impurities can be removed from an oil phase.

Any study of the adsorption properties of amphiphiles at the water–oil interface, must have impurities removed from both the water and the oil phases. Impurities may have a very strong effect on the interfacial properties. For example, a strong effect of impurities on interfacial tension for a *n*-decane–water interface can be seen in Figure 2.17. At the same time, when the phases are free of impurities, the interfacial tension has a constant and definite value [59].

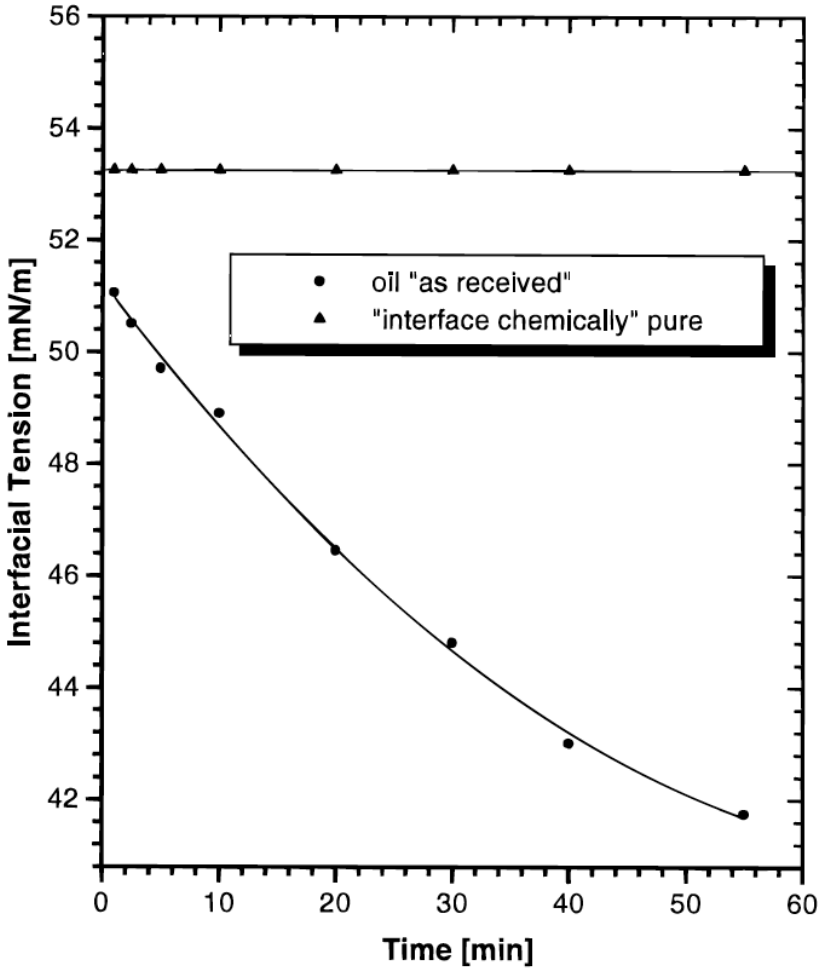

Figure 2.17: Water–n-decane interfacial tension [59].

2.13 Effect of the hydrocarbon chain length on the interfacial tension

Investigations of the interfacial tension of different hydrocarbons at the water–oil interfaces were done. It was found that the interfacial tension value depends on the carbon number, N_c of the n-alkane. As the chain length increases, the interfacial tension also increases. This is shown in Figure 2.18.

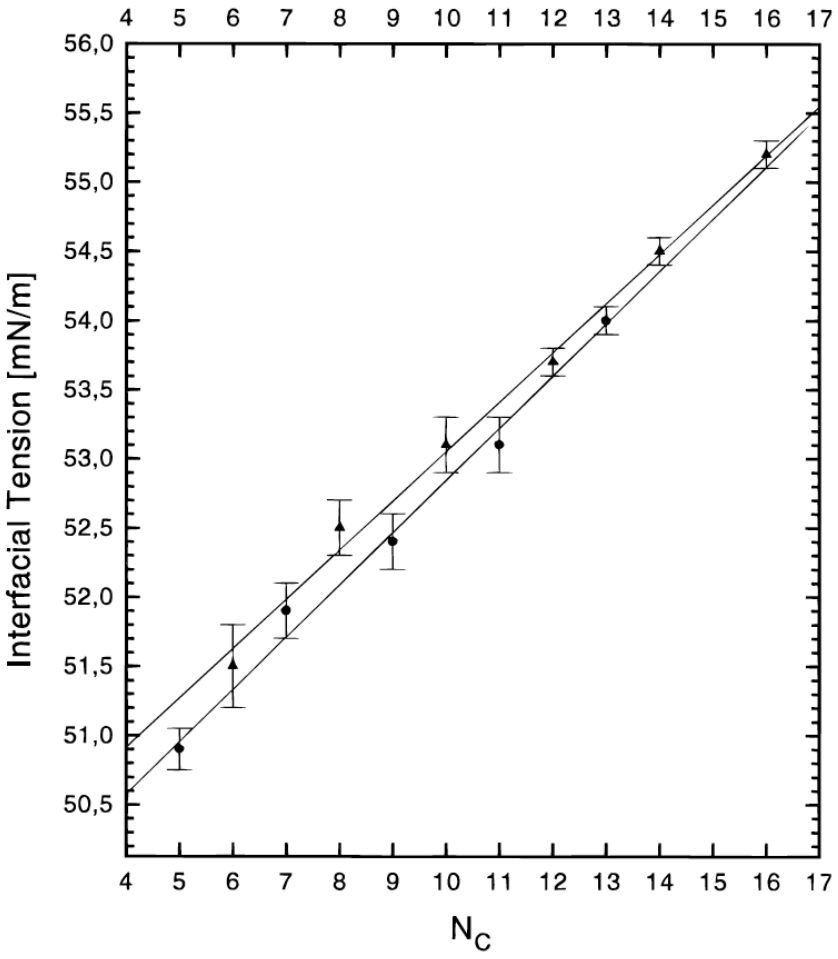

Figure 2.18: Water–n-alkane interfacial tension [59].

2.14 Effect of Particle Shape on the Stability at Interfaces

Bresme and Faraudo determined the dependence of the stability of NPs at the liquid interfaces on particle geometry [77]. Particles with an aspect ratio, α, larger than a critical value are not stable at liquid-liquid interfaces. The effect of the particle geometry on the free energy of three nanoparticles with the same surface area, but different shapes can be seen in Figure 2.19. The oblate (disk) shaped particles are the most stable while spherical nanoparticles and prolate (rod) shaped particles are

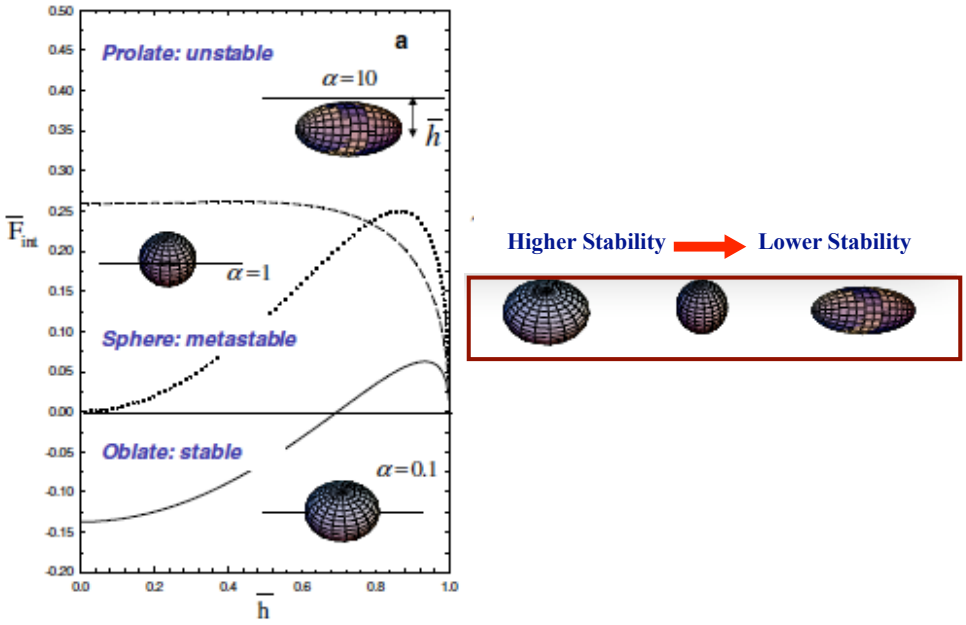

Figure 2.19: Schematic view of effect of particle shape on the stability [13].

metastable and unstable at the interface, respectively [77],[13]. Until now, many investigations performed at the liquid-liquid interface have dealt with spherical, low aspect ratio colloidal particles [78], [79]. The interfacial assembly of high aspect ratio non-spherical particles at the interfaces is still an open question [13].

2.15 Effect of Janus Particles at the Interfaces

Janus particles, named after the Roman god of doorways, are particles with two faces. The interfacial activity of Janus particles is many times greater than homogeneous particles [6]. The amphiphilic character of surfactants, and physical properties of nanoparticles are combined in Janus particles. This opens up a new and exciting research area related to the development of nanotechnology and emulsion stabilization [6]. Some of the most common Janus nanoparticles consist of gold (Au) and another material. Nanoparticles of gold (Au) and ironoxide (Fe_3O_4) were synthesized to determine the effect of Janus particles on interfacial activity [18]. The surface activity of nanoparticles was studied at room temperature using the Pendant drop method.

The Au–Fe_3O_4 Janus nanoparticles were dispersed in an n-hexane phase. A water drop was made in this phase. Immediately after the water drop was formed, the Janus particles moved to the interface and the interfacial tension of the water–n-hexane began to decrease and eventually reached an equilibrium value. The interfacial tension of the Janus particles was found to be lower than that for either homogeneous Au or Fe_3O_4 nanoparticles. From this study, it was found that Janus particles are more effective at decreasing interfacial tension. It was concluded that the Janus particles aligned, thus reducing the interfacial tension, at the liquid–liquid interface. This can be seen schematically in Figure 2.20. The long-chain hydrocarbon end of the gold side stays in the hexane phase, while the iron oxide remains in the water phase. The drop in the interfacial tension was found to be higher for the Janus particles than the homogeneous nanoparticles, as can be seen in Figure 2.21.

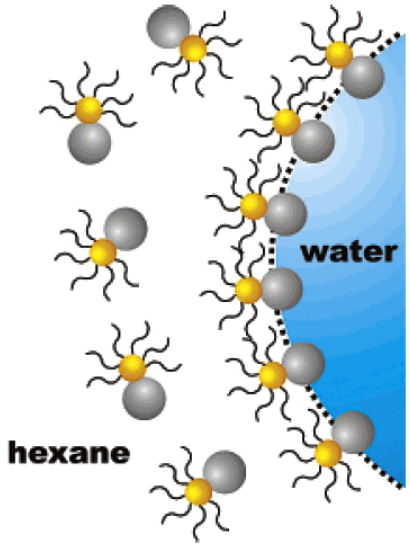

Figure 2.20: Schematic representation of Janus nanoparticles at the hexame–water interfaces [18].

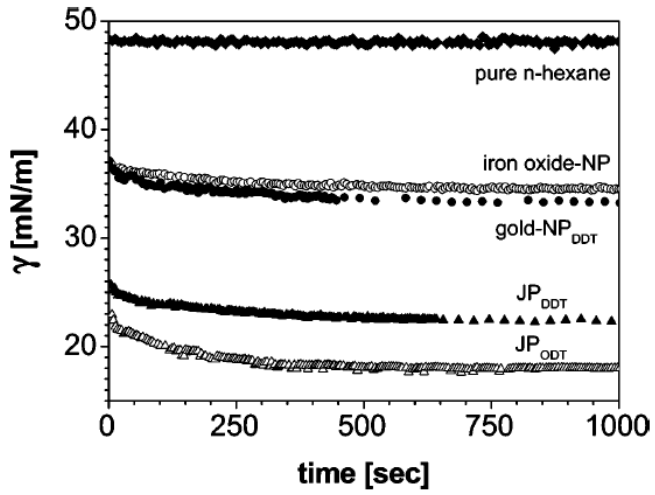

Figure 2.21: Interfacial tension of water–hexane versus time for various nanoparticle types. DDT: dodecanethiol, ODT: octadecanethiol, NP: homoegneous nanoparticles, JP: Janus particle [18].

2.16 Colloidal Stability at the Interface and DLVO Theory

The Derjaguin, Landau, Verwey, and Overbeek theory (DLVO) states that the stability of colloidal systems is dependent upon its total potential energy function (V_T). The total potential is sum of the three potential contributions:

$$V_T = V_A + V_R + V_S \tag{2.3}$$

whereV_S is potential of the solvent, V_A and V_R are van der Waals attractive and repulsive potential between the particles, respectively. However, V_S has a small contribution to the total potential energy over few nanometers of separation. DLVO theory demonstrates the effects of van der Waals and electrostatic interactions between two approaching surfaces. The net force due to van der Waals interaction is attractive. The electrostatic interactions between like-charged particles is repulsive; whereas for the unlike charged particles, the interaction is attractive. The apparent net force acting between two particles, approaching each other, in the solution can

be obtained by adding van der Waals and electrostatic interactions [80], [81]. The energy barrier arises due to the repulsive force prevent particles in approaching each other. If high repulsion exist among particles, dispersion tries to prevent flocculation and the colloidal system turns to be stable. The zeta potential indicates magnitude of the interaction between colloidal particles or determine the stability of colloidal systems. The large positive or negative zeta potential value represents that particles in the suspension repel each other. However, particles with low zeta potential indicate that particles adhere with each other or flocculate in the solution. Particles having zeta potentials more than +30 mV or more than -30 mV are considered stable in the suspension.[82]. *Smith et al.* studied adsorption of charged nanoparticles at the oil-water interface [83]. Using DLVO theory, authors investigated interaction potentials for negatively charged hexadecane droplets with anionic polystyrene (PS) latex particles or cationic gold nanoparticles. They found that with an increase of ionic strength; there is a decrease in the decay length of electrostatic repulsion. Hence, the electrical double layer around the particles and oil tends to shrink. As a consequence, van der Waals attractions and interfacial attractions begin to govern at the interfaces. This enhances particle adsorption at the oil-water interface. Using small-angle scattering experiments, for PS latex particles, they found that the highest particle adsorption occurred at average ionic strength and low pH. For cationic gold particle, using DLVO calculations, authors observed that the particle adsorption at the interface is highest at the neutral pH.

2.17 Summary

This chapter surveyed the roles that bulk nanoparticle concentration, size, shape, wettability, and surface ligands, play on the behavior of NPs at liquid-liquid interfaces. The effects of salt concentration and pH were also discussed.

The next chapter provides the overview of experimental procedures, methods and materials used for the experiments performed in Chapter 5, 6 and 7.

Chapter 3

Experimental Methods and Materials

This chapter presents the experimental procedures for synthesis of alkhanethiol capped gold nanoparticles and describes the materials, and methods used in this work. This chapter also outlines the characterization techniques used to study the nanoparticles.

3.1 Axisymmetric Drop Shape Analysis

Axisymmetric Drop Shape Analysis (ADSA) is a powerful technique for measuring interfacial tensions and contact angles of pendant drops, sessile drops and bubbles. Numerous methodologies have been developed for the measurement of interfacial tensions, but of these, ADSA is considered to be the most powerful. This is primarily due to the high accuracy, simplicity, and versatility of the technique [84]. Through the use of digital image analysis, ADSA is well suited for automated computer implementation. Automated ADSA systems fit the shape of the droplet to a mathematical model based on the classical Laplace equation of capillarity [85].

Advantages of using pendant and sessile drop methods are as follows: (1) only small quantities of liquid are required, (2) the technique can be used to study both liquid–vapor and liquid–liquid interfaces. The methods can be applied to a wide range of materials—from organic liquids to molten metals, from pure solvents to concentrated

solutions. The technique can be applied at low or high temperatures, and from vacuum conditions to high pressure. In automated systems, a least-squares algorithm using the interfacial surface tension as a fitting parameter fits the Laplace equation of capillarity:

$$\Delta P = \gamma \left(\frac{1}{R_1} + \frac{1}{R_2} \right) \tag{3.1}$$

where R_1 and R_2 are the principle radii of curvature of the droplet , ΔP is the pressure difference across the curved interface.

When fitting this equation to experimental data, the surface or interfacial tension is a parameter that is varied until a good fit is established. In recent years, the use of automated systems for measuring interfacial properties of fluids (i.e., surface tensions, and interfacial tensions), has not only improved the accuracy of the measurements, but it has also permitted the study of phenomena that were not possible or difficult to investigate in the past. Examples include: ultra-low interfacial tensions, the relaxation of absorption layers, and dynamic surface tensions [84]. Using a modern desktop computer, the time required for a single interfacial tension measurement has been reduced from hours of dedicated work to just a few seconds. Thousands of time-independent measurements can be performed, unattended, in a single day. The only information required to use the ADSA method is the local gravitational constant, the density of the two phases, and several arbitrary, yet accurate coordinate points selected from the droplet profile [85].

A range of scientific disciplines have shown strong interest in accurate measurements of interfacial and surface tensions. From a technology standpoint, surface and interfacial tension measurements are important because of the role they play in several chemical processes (e.g., gas absorption, distillation, extraction, etc.). The IFT measurements were made using Axisymmetric Drop Shape Analysis (ADSA) [84], [85], [86], [87],

3.1.1 Equipment For Temperature Measurement

A constant temperature chamber (stainless steel, 13 cm long, 5 cm wide and 7 cm tall with three quartz windows for viewing the sample) was made for this analysis. The pendant drop profiles were viewed by a camera through the windows in the

chamber. A syringe was inserted from the top of the chamber to form a pendant drop of water. A glass cuvette containing the colloidal suspensions was held within the constant temperature chamber. The chamber was well insulated and the chamber's temperature was measured using a high precision temperature probe to ensure that it remained constant. A schematic of the setup can be seen in Figure 3.1.

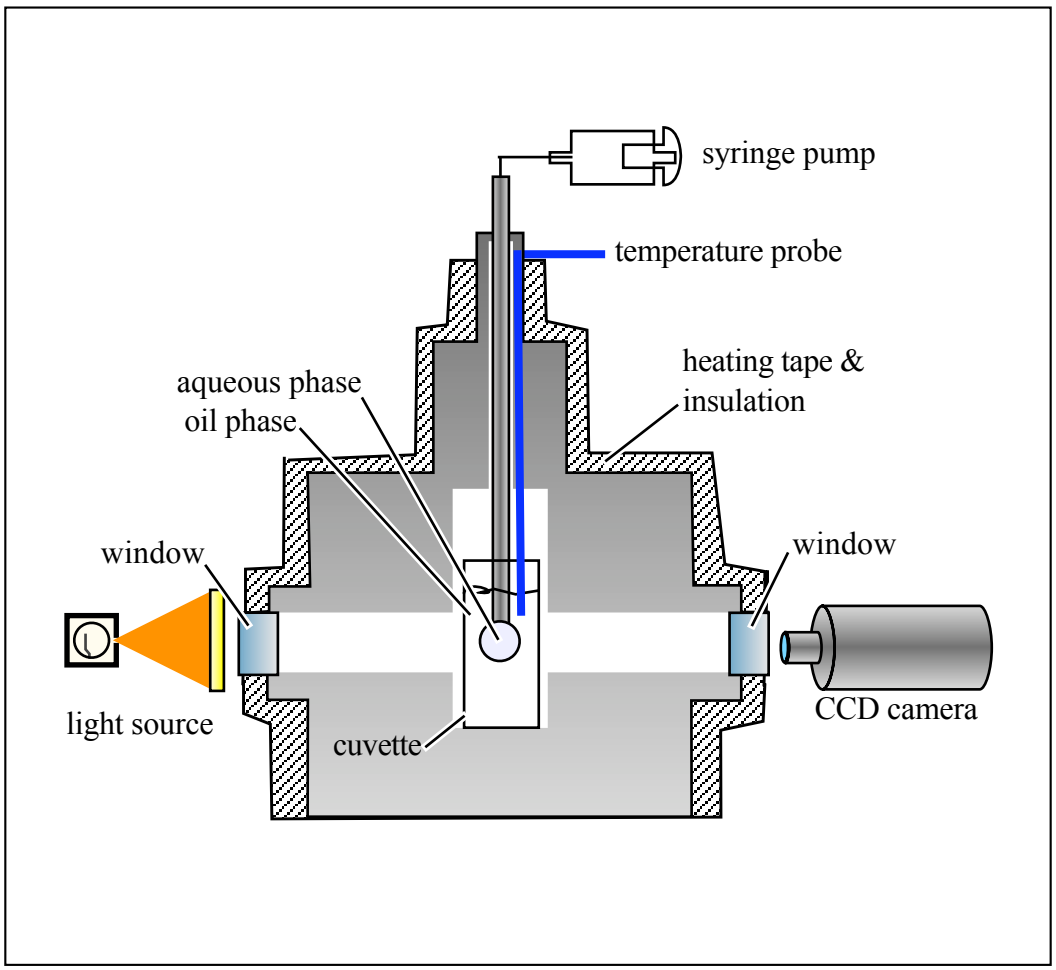

Figure 3.1: Schematic of different components of temperature chamber.

3.2 Materials and Experimental Procedures

3.2.1 Materials Used in the Work

In Table 3.1 a list of materials that were used in the work is shown. Some of the chemicals, alkanes in particular, were purified prior to their use in interfacial tension measurements.

Table 3.1: Materials

Chemical	**Formula**	**Source**	**Purity**	**M.W. [g/mol]**	**B.P. [C°]**	**M.P. [C°]**	ρ **[g/cm^3]**
chloroauric acid	$HAuCl_4 \cdot X\ H_2O$	Sigma-Aldrich	99.9+%	393.83	254	25	3.9
tetraoctylammonium bromide	$C_{32}H_{68}NBr$	Sigma-Aldrich	98%	546.82	—-	98	—
sodium borohydride	$NaBH_4$	Sigma-Aldrich	99%	37.83	400	36	1.074
toluene	C_7H_8	Alfa-Aesar	99.8%	92.13	110.6	-93	0.867
1-hexanethiol	$CH_3(CH_2)_5SH$	Sigma-Aldrich	95%	118.24	148	-81	0.84
1-dodecanethiol	$C_{12}H_{26}S$	Sigma-Aldrich	≥98%	202.40	266	-7	0.845
ethanol	C_2H_6O	Commercial Alcohol	99%	46.06	79	-117	0.8
hexane	$CH_3(CH_2)_4CH_3$	VWR	99.9%	86.18	68	-95	0.66
n-nonane	C_9H_{20}	Sigma-Aldrich	≥99%	12 2.1 ± 0.9 14	151	-53	0.718

3.3 Experimental Procedures

The experimental procedures consist of synthesizing gold nanoparticles and then testing their effect on interfacial tension.

3.3.1 Axisymmetric Drop Shape Analysis (ADSA)

Interfacial tension measurements of capped gold nanoparticles at hydrocarbon-water interfaces were performed by pendant drop experiments using Axisymmetric Drop Shape Analysis (ADSA). These measurements include the following steps: (1) image acquisition, (2) image processing and (3) numerical calculations to fit the Laplace equation. The hardware of ADSA consists of the following components: a CCD camera, image-digitizing board, optical components (i.e., focusing elements), a light source, and a cell holder. An experimental setup is shown in Figure 3.2.

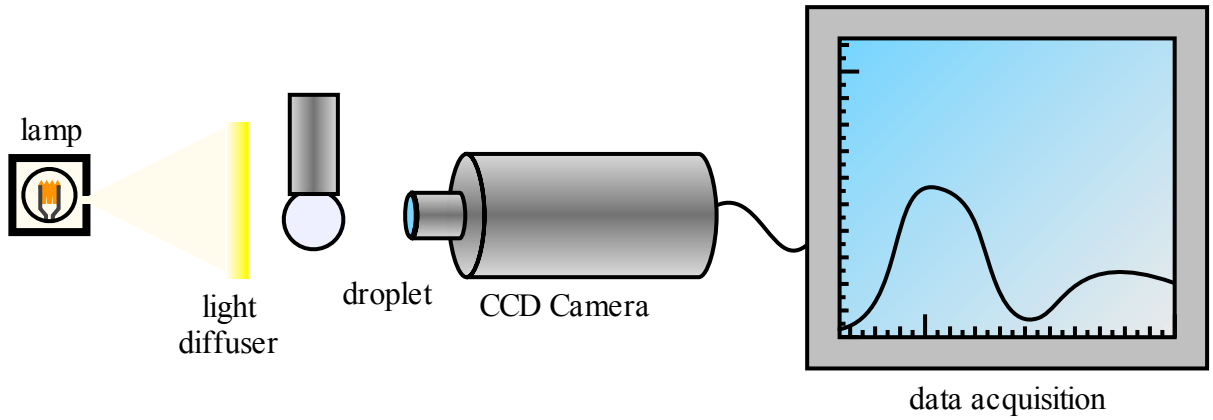

Figure 3.2: Schematic of the axisymmetric drop shape analysis (ADSA) system

In ADSA, a white light source illuminates the pendant drops that are hanging from the tip of the stainless steel needle. It is necessary to have an uniformly illuminated drop with little heat transferred from the lamp. For this reason, the light passes through a heavily frosted light diffuser prior to image capture. In order to precisely control the volume of the droplet formed, a stepper motor is used. Images of the droplet are captured by using an image-digitizing board to capture individual frames from the CCD camera. After the image has been acquired, software (Video Contact

Angle 2500 XE) fits the shape of the droplet to the Laplace equation of capillarity [85], [86], [87].

3.4 Experimental

3.4.1 Nanoparticle Synthesis, Preparation, and Characterization

A series of gold nanoparticle colloids were synthesized using a technique established by *Brust et al.*[88] and subsequently modified by *Hostetler et al.*[89].

The size of the synthesized nanoparticles can be controlled by changing the (1) thiol to Au ratio, (2) the reduction temperature, or (3) the rate at which the reducing agent is added to the solution [89]. The core size has a pronounced effect on the chemical and physical properties of the nanoparticles. Several material characterization techniques are used to verify the composition of the particles; such as, ultraviolet visible spectroscopy (UV-Vis), high-resolution transmission electron microscopy (HRTEM), Energy-dispersive spectroscopy (EDS) and proton nuclear magnetic resonance spectroscopy (^{1}HNMR).

Synthesis of capped gold nanoparticles

n-alkanethiol-capped gold nanoparticles were synthesized using a procedure developed by *Hostetler et al.*[89] and *Brust et al.* [88]. Synthesis begins by dissolving 1.5g of tetraoctylammonium bromide ($N(C_8H_{17})_4Br$) in 80 mL of toluene. In the second step, the aqueous solution of 0.31g of hydrogen tetrachloroaurate trilydrate ($HAuCl_4 \cdot 3\,H_2O$) in 25 mL deionized water is prepared at room temperature. The organic solution is added to the aqueous phase and stirred. Immediately, a two-layer system was formed. The system was kept stirring until the bottom layer (the aqueous phase) became transparent and, the top layer (the organic phase) became orange-brown. This assures the transfer of all Au^{+3} from the aqueous phase into the organic phase. During this reaction step, the phase transfer reagent ($(N(C_8H_{17})_4Br)$) was transferred $AuCl_4^-$ from the aqueous phase to organic layer. At the end of the

reaction, it formed a complex structure with the cationic part of the phase transfer reagent. The organic phase was decanted, and the desired amount of dodecanthiol in 25 mL of toluene was added to the decanted organic phase and vigorously stirred. In the final step, an aqueous solution of 0.389 $NaBH_4$ in 25 mL of deionized water was made, and added to the system at the reduction temperature 30°C. Immediately, the pale, yellow, organic phase turned dark brown. Stirring, at the reduction temperature, was continued for 30 minutes, and then further stirred at room temperature for three hours. The organic phase was decanted, and concentrated to $\sim$ 5mL by rotary evaporator. The reduced organic phase was precipitated by adding 30 mL of ethanol.

The colloidal solution was then kept for cooling in ice for one hour. Next, the black precipitate was filtered using filter paper. The collected precipitate was further washed, with 80 mL of ethanol and 350mL of acetone several times. Finally, the dodecanethiol capped gold nanoparticles were dried in a petri dish open to air. The synthesized thiol capped gold nanocrystals form a stronger bond to the Au [89]. The overall reaction processes can be seen in Equations 1a and 1b below:

$$\text{(1.a)}\ AuCl_4^- + N(C_8H_{17})_4^+(C_6H_5Me) \longrightarrow\ N(C_8H_{17})_4^+AuCl_4^-(C_6H_5Me)$$

$$\text{(1.b)}\ mAuCl_4^-(C_6H_5Me) + nC_{12}H_{25}SH(C_6H_5Me) + 3\,me^- \longrightarrow$$
$$4\,mCl^- + (Au_m)(C_{12}H_{25}SH)_n(C_6H_5Me)$$

The dried samples were further cleaned by ethanol, to completely remove all impurities and free ligands. The particles were then re-dispersed in hexane and dried in a round flask cleaned by ethanol, and again re-dispersed in hexane. The cleaning procedure was repeated at least 25 times to confirm the removal of free ligands and by-products before performing various characterizations discussed in the following sections. The sample was stored in a -20°C freezer for further use. During the reaction, NaCl and sodium borate, may be produced as byproducts. Similar procedures were used to synthesize *n*-hexanethiol capped gold nanoparticles. In this case, the surfactant *n*-hexanethiol was added instead of *n*-dodecanethiol.

3.4.2 Nanoparticle Characterization

The nanoparticle colloids were synthesized at $30°C$ using the experimental conditions shown in Tables 3.2 and 3.3. During the synthesis, either n-hexane-1-thiol or n-dodecane-1-thiol was added to the colloidal solution to act as a capping agent, resulting in a total of five colloidal suspensions.

Table 3.2: Synthesis conditions for the nanoparticle suspensions.

Condition	Ratio of gold atoms to capping molecules	Cap
(a)	1:8	dodecanethiol
(b)	6:1	dodecanethiol
(c)	12:1	dodecanethiol

Table 3.3: Synthesis conditions for the nanoparticle suspensions.

Condition	Ratio of gold atoms to capping molecules	Cap
(d)	6:1	hexanethiol
(e)	8:1	hexanethiol

To avoid interference from free surfactant molecules, the synthesized nanoparticles were rinsed with ethanol and re-dispersed in hexane. This process was repeated 25 to 30 times to ensure that the nanoparticles were free of excess capping ligand. The size distributions of the synthesized nanoparticles were determined by analyzing TEM images of the material. UV-VIS and proton NMR measurements were then performed to confirm that free ligands were completely absent in the colloidal suspensions used to measure nanoparticle adsorption at the hexane-water interface.

HR-TEM analysis

High-resolution transmission electron microscopy (HR-TEM) was performed using a FEI Titan microscope at 300 kV and JEOL 2010F TEM (Phillips CM12) electron

microscope operating at 60kV. A drop of the synthesized colloid was placed onto a 400 mesh copper TEM grid coated with formvar. The samples were dried in air for at least one hour prior to analysis.

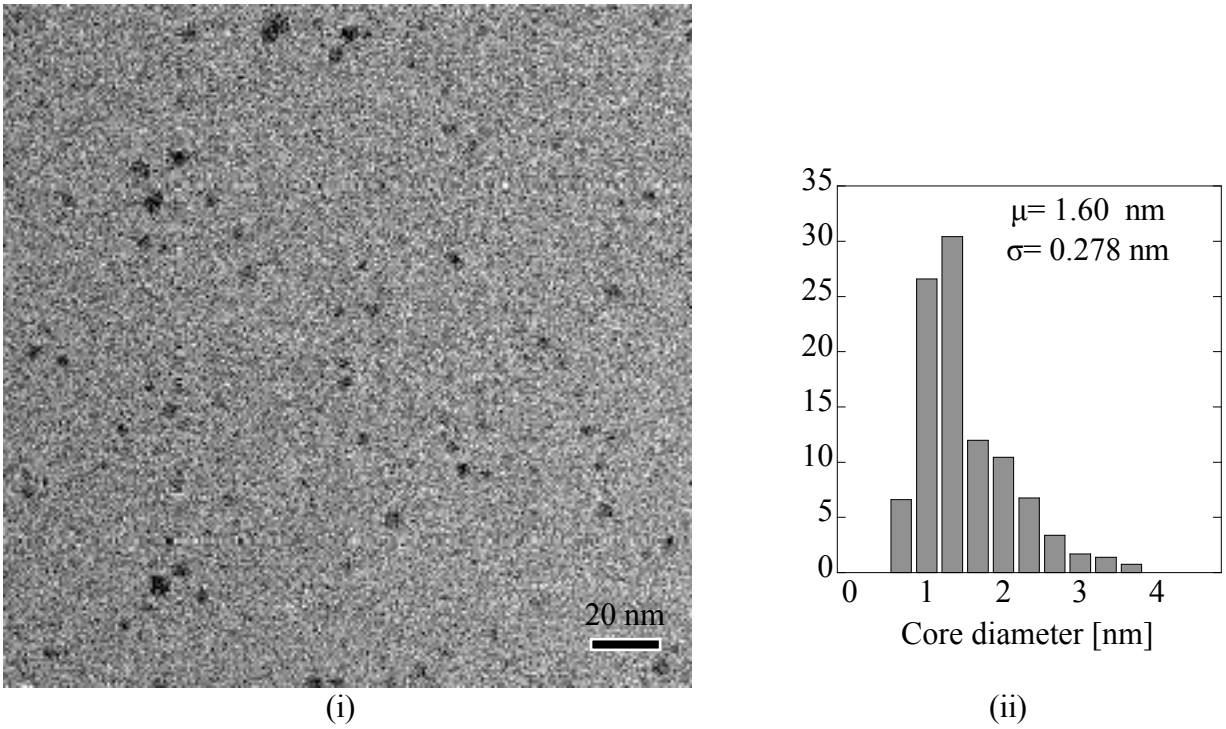

Figure 3.3: TEM image and associated size distribution for 1.6 nm gold nanoparticles synthesized using condition (a) capped with *n*-dodecane-1-thiol are shown respectively in (i) and (ii).

Figure 3.3 illustrates the TEM images and associated size distribution for 1.6 nm gold nanoparticles synthesized under condition (a) and capped with *n*-dodecane-1-thiol. Nanoparticle diameters were determined by image analysis using the ImageJ software. The average size of the *n*-dodecane-1-thiol nanoparticles synthesized under condition (a) was found to be $\mu = 1.60$ nm with a standard deviation of $\sigma = 0.278$ nm. The particles were found to have a log normal distribution. Figure 3.4 shows an HR-TEM image of the 1.6 nm gold nanoparticles, and the corresponding selected area electron diffraction (SAED) pattern of HR-TEM image is also shown. As seen in this figure,

(ii)

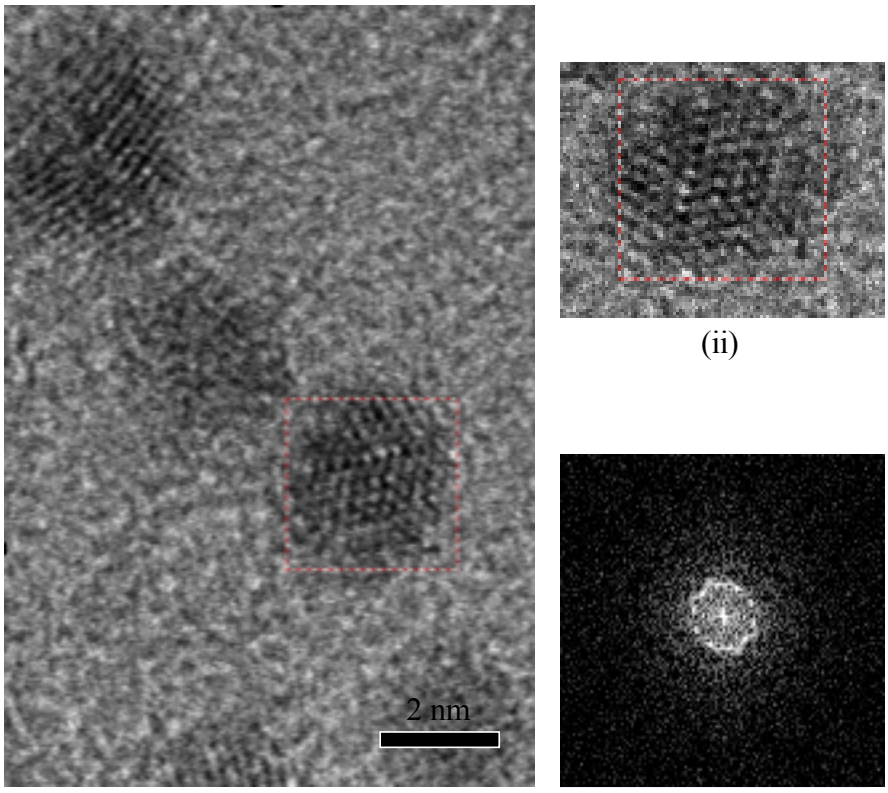

(ii)

(i) (ii)

Figure 3.4: HR-TEM image, selected area and associated SAED are shown respectively in (i), (ii) and (iii); for 1.6 nm gold nanoparticles synthesized using condition (a) capped with *n*-dodecane-1-thiol.

the diffraction pattern consists of rings or spotty ring patterns and illustrates that AuNPs have a crystalline structure. Energy-dispersive spectroscopy (EDS) was carried out to better understand the chemical composition of gold nanoparticles. Figure 3.5 shows the EDS spectra of 1.6 nm *n*-dodecane-1-thiol capped gold nanoparticles. EDS displays peaks solely ascribed to gold. In addition to gold peaks, carbon peaks are also shown in the spectra. The latter signals arise from the carbon coated formvar film on the copper grid used for analyzing the synthesized gold nanoparticles.

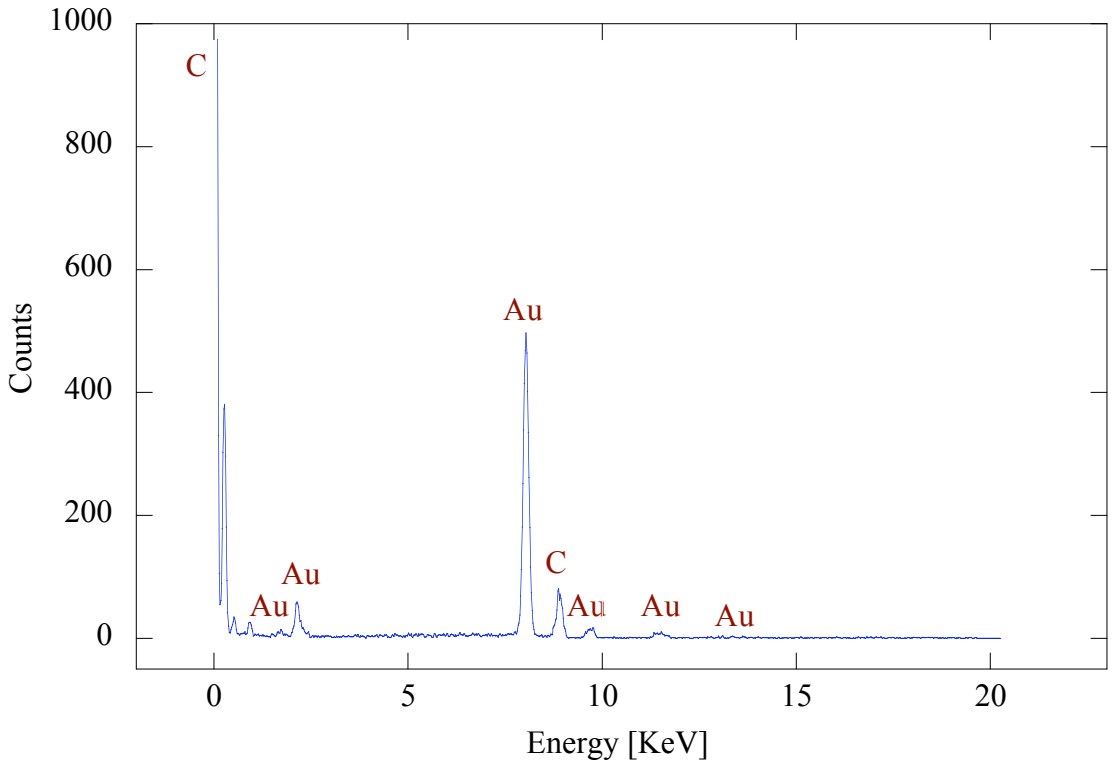

Figure 3.5: EDS spectrum for 1.6 nm gold nanoparticles synthesized using condition (a) capped with n-dodecane-1-thiol.

Figure 3.6 shows the TEM images and associated size distribution for 2.8 nm gold nanoparticles synthesized under condition (b) and capped with n-dodecane-1-thiol. The average size of the n-dodecane-1-thiol capped nanoparticles synthesized under conditions (b) were larger than those of condition (a); they were found to be $\mu = 2.78$ nm with a standard deviation of $\sigma = 0.273$ nm. The HR-TEM images and EDS spectrum of the particles are shown in Figures 3.7 and 3.8. As in Figure 3.3, Figure 3.9 and 3.10, show TEM images and SAED for 4.4 nm n-dodecane-1-thiol capped AuNPs. For 2.9 nm and 4.3 n-hexane-1-thiol capped AuNPs, TEM images and SAED are shown respectively in Figure 3.12, Figure 3.13 and Figure 3.15, Figure 3.16. The average size of the n-dodecane-1-thiol capped nanoparticles synthesized under conditions (c) were found to be $\mu = 4.4$ nm with a standard deviation of $\sigma = 0.6$ nm. The average size of the n-hexane-1-thiol capped nanoparticles synthesized under conditions (d) were found to be $\mu = 2.9$ nm with a standard deviation of $\sigma = 0.188$

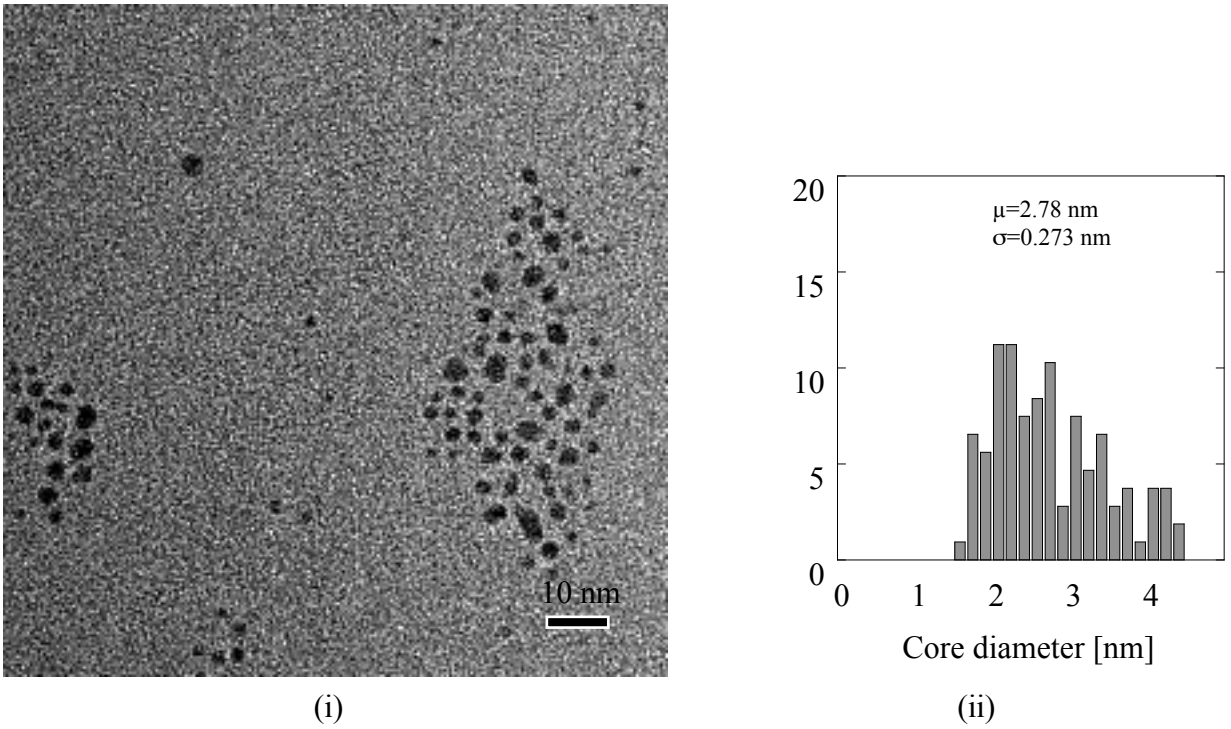

Figure 3.6: TEM image and associated size distribution for 2.8 nm gold nanoparticles synthesized using condition (b) capped with n-dodecane-1-thiol are shown respectively in (i) and (ii).

nm; while the average size of the n-hexane-1-thiol capped nanoparticles synthesized under conditions (e) were found to be $\mu = 4.3$ nm with a standard deviation of $\sigma = 0.7$ nm. Analysis of HR-TEM, EDS and SAED patterns are the same as 1.6 nm dodecane-1-thiol capped AuNPs. As can be seen from Figure 3.8 and Figure 3.14, the EDS spectrum illustrates the evidence of gold nanoparticles in the capped dodecanethiol and hexanethiol AuNPs. In addition to gold peaks, copper and carbon peaks are also shown in the spectra. The latter signals arise from the carbon coated formvar film on the copper grid used for analyzing the synthesized gold nanoparticles. The SAED pattern confirms the crystal structure formation for all particles. *Chen et al.* also obtained similar EDS spectra and selected area electron diffraction (SAED) pattern for dodecanethiol capped gold nanoparticles [90]. From Figures 3.11 and

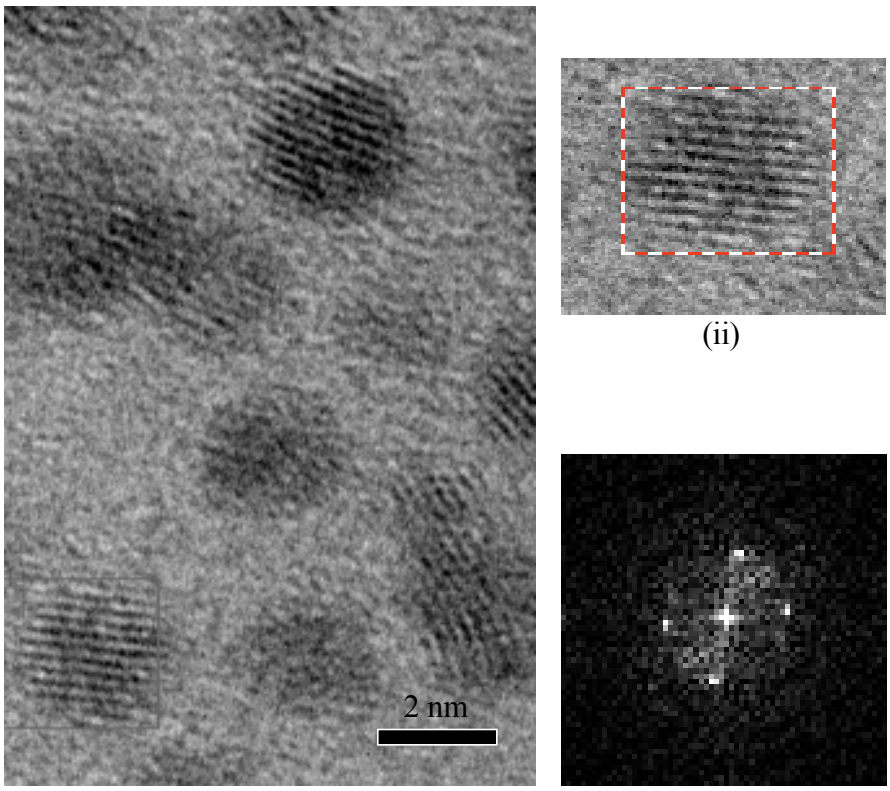

Figure 3.7: HR-TEM image, selected area and associated SAED are shown respectively in (i), (ii) and (iii); for 2.8 nm gold nanoparticles synthesized using condition (b) capped with *n*-dodecane-1-thiol.

3.17, it can be seen that the histogram is symmetrical, and the distance between the two successive peaks is 0.23 nm, corresponding to the (111) planes for gold. Similar results have been obtained by *Liang et al.* [91].

UV-Vis Absorbance Spectra

An Ocean Optics USB2000+ UV–VIS Absorbance Spectrophotometer was used to obtain the spectra of the nanoparticle colloids. Pure hexane, as supplied by Sigma-Aldrich, was used for the reference spectrum in these measurements. The spectra,

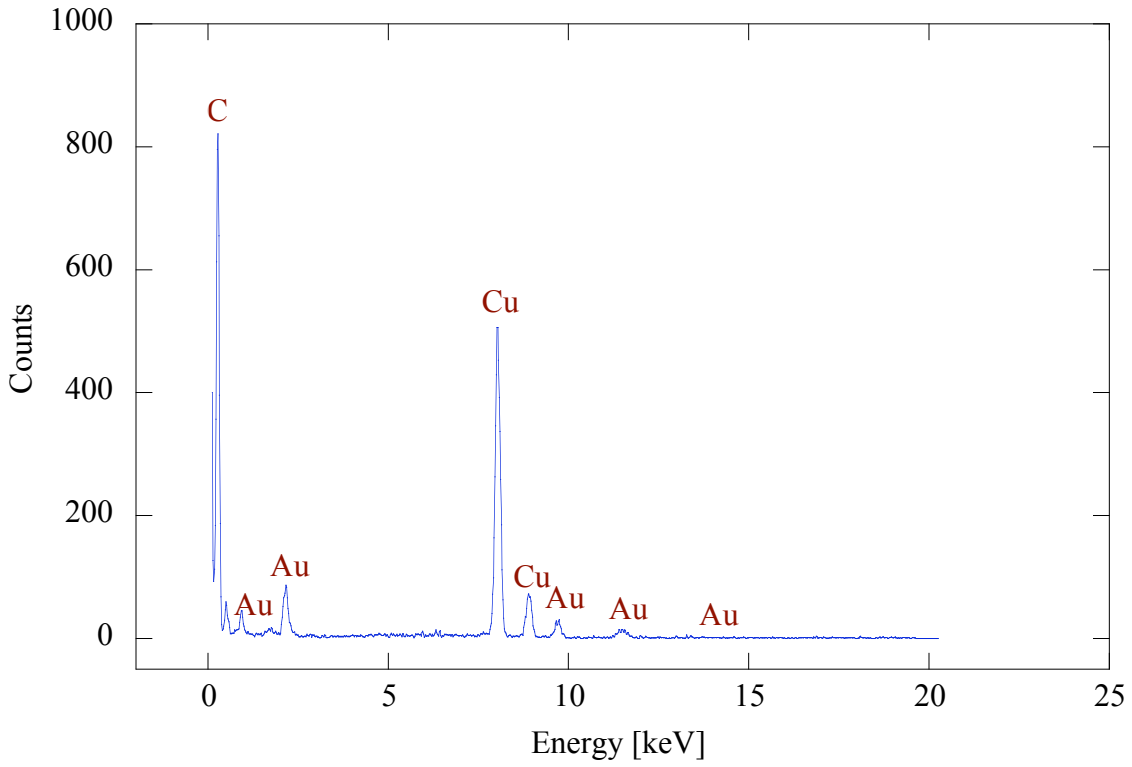

Figure 3.8: EDS spectrum for 2.8 nm gold nanoparticles synthesized using condition (b) capped with *n*-dodecane-1-thiol.

which were taken in the range of 250-850 nm, can be seen in Figure 3.18 and Figure 3.19. From Figure 3.18, it is evident that the expected plasmon resonance peak for gold nanoparticles is undetectable for condition (a). A single plasmon resonance peak is just visible for conditions (b) and (c) at ∼510 nm and ∼540 nm, respectively. From Figure 3.19, it can be seen that a single plasmon resonance peak is visible for conditions (d) and (e) at ∼510 nm and ∼540 nm, respectively. This result is consistent with the work of *Hostetler et al.* [89] and *Alvarez et al.* [92].

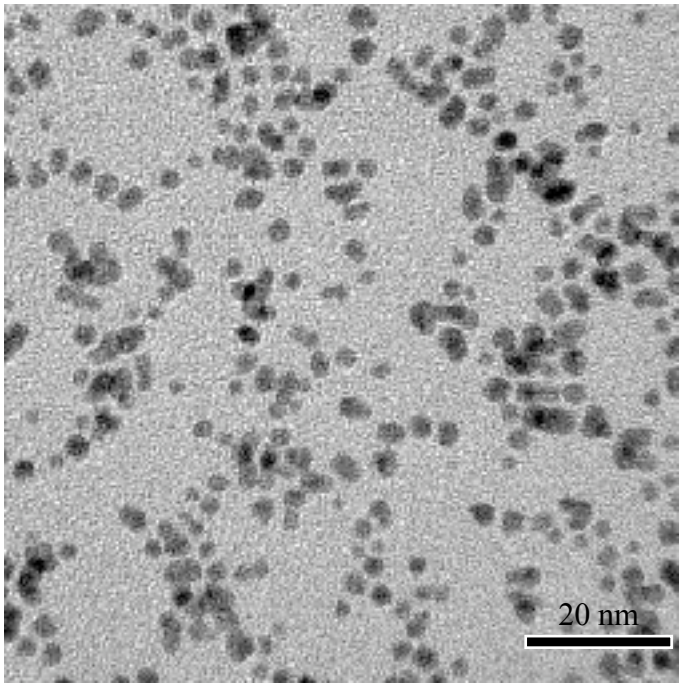

(i)

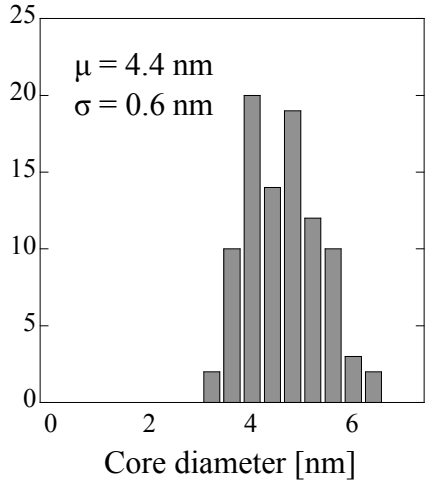

(ii)

Figure 3.9: TEM image and associated size distribution for 4.4 nm gold nanoparticles synthesized using condition (c) capped with *n*-dodecane-1-thiol are shown respectively in (i) and (ii).

NMR Spectra

Proton NMR (^{1}H-NMR) spectra were taken using a BRUKER 500 $Shield^{@TM}$ spectrometer. NMR spectra of stock *n*-dodecane-1-thiol solution and suspensions of nanoparticles capped with *n*-dodecane-1-thiol for conditions (a), (b) and (c) are shown in Figure 3.20. The stock *n*-dodecane-1-thiol was prepared by dissolving 1 mL of pure dodecanethiol into 1.5 mL $CDCl_3$. NMR samples of the synthesized nanoparticles were made by suspending ∼14 mg of the nanoparticles into 1.5 mL of $CDCl_3$. The resulting concentrations of suspensions (a), and (b),(c) for this analysis were 1.31×10^{20} particles/L and 2.54×10^{19} particles/L, respectively. For nanoparticles synthesized under condition (a), Figure 3.20, shows three multiplets located at

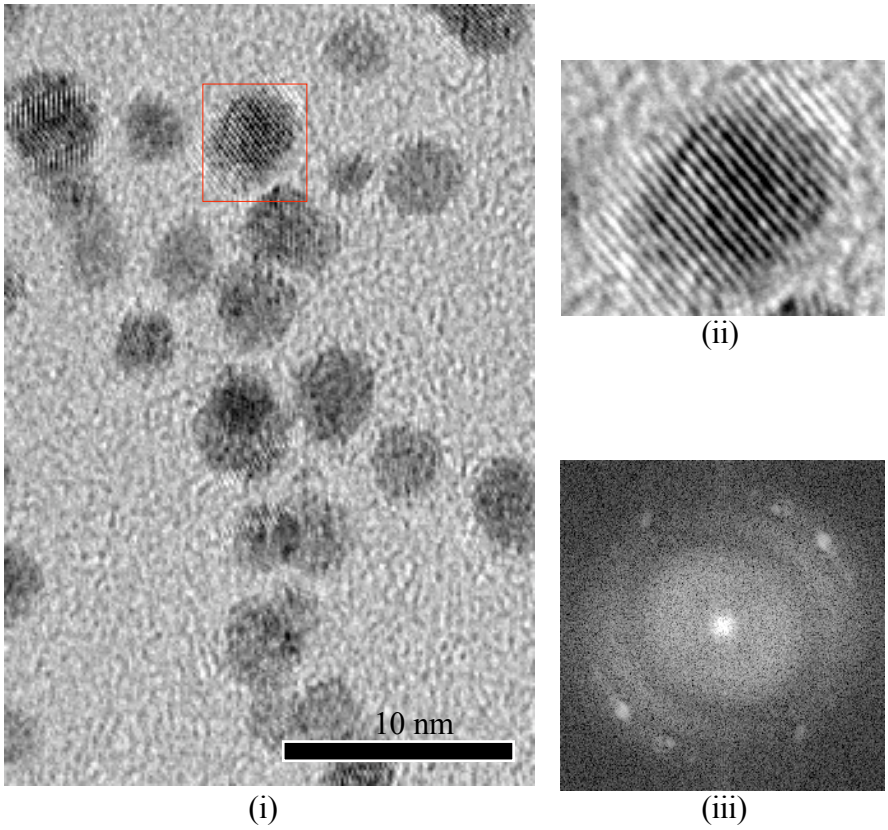

Figure 3.10: HR-TEM image, selected area and associated SAED are shown respectively in (i), (ii) and (iii); for 4.4 nm gold nanoparticles synthesized using condition (c) capped with *n*-dodecane-1-thiol.

1.546 PPM, 1.26 PPM and 0.892 PPM.

The NMR spectra obtained for nanoparticles synthesized under experimental condition (b) and (c) yielded three broad multiplets at 1.547 PPM, 1.266 PPM and 0.893 PPM. These results are also consistent with *Hostetler et al.* [89]. The resulting spectra for the capped nanoparticles differ from the spectrum obtained for stock *n*-dodecane-1-thiol solution. For the capped nanoparticles, all of the observed peaks are broader than those of stock *n*-dodecane-1-thiol sample. It is known that an NMR peak at 2.58 PPM is associated with a proton attached to the –SH group. This peak

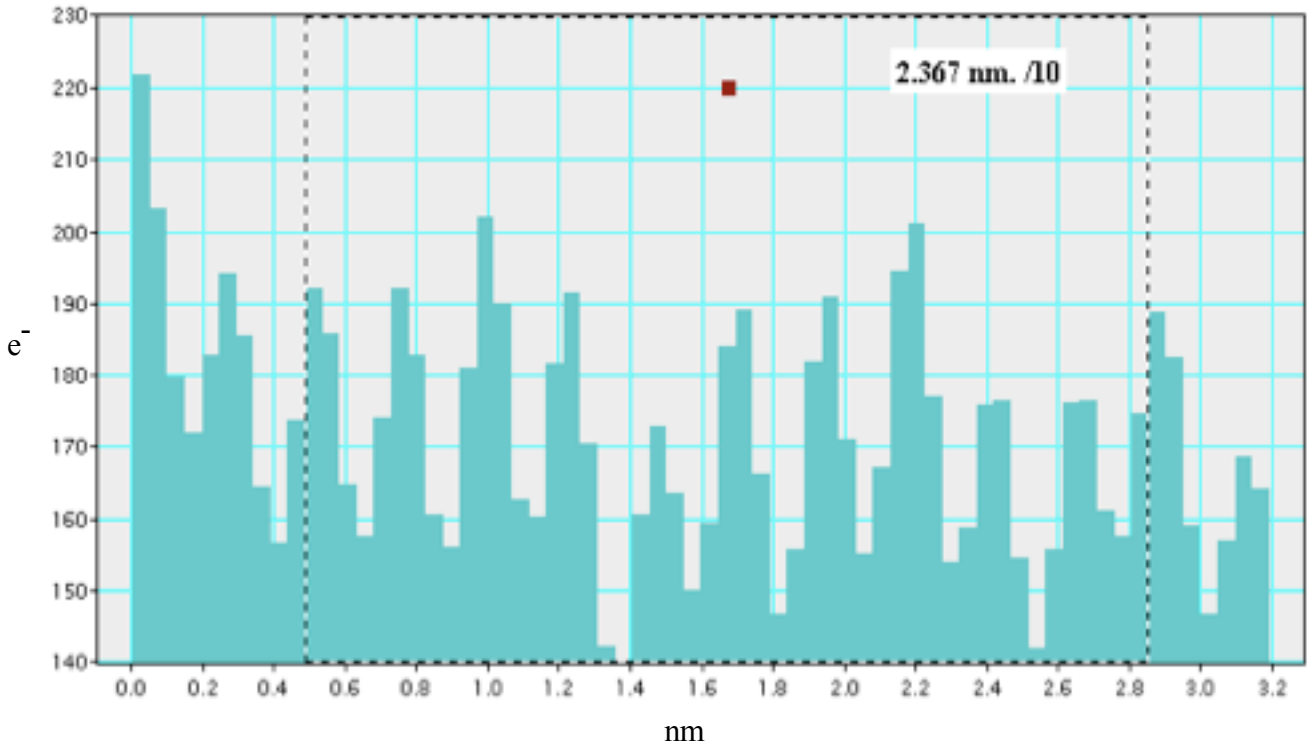

Figure 3.11: Histogram spectrum for 4.4 nm gold nanoparticles synthesized under condition (c) capped with *n*-dodecane-1-thiol is shown .

can be seen in the spectra of the stock *n*-dodecane-1-thiol, but is not observed in the spectra for the capped nanoparticles. The lack of this peak indicates that the thiol group is attached to the gold nanoparticle surface, thus quenching the 2.58 PPM peak associated with the proton of the thiol. The NMR peak at 0.88 PPM in the stock *n*-dodecane-1-thiol is associated with the terminal $-CH_3$ group. In the capped nanoparticle samples, this peak is not significantly shifted (i.e., only a small shift from 0.88 PPM to ∼0.89 PPM is observed). Such a small shift indicates that the methyl group of the *n*-dodecance-1-thiol cap is far from the nanoparticle surface.

NMR spectra of stock *n*-hexane-1-thiol and nanoparticles capped with *n*-hexane-1-thiol produced under condition (d) and (e) are shown in Figure 3.21. The measurement for the stock *n*-hexane-1-thiol was prepared by dissolving 1 mL of the

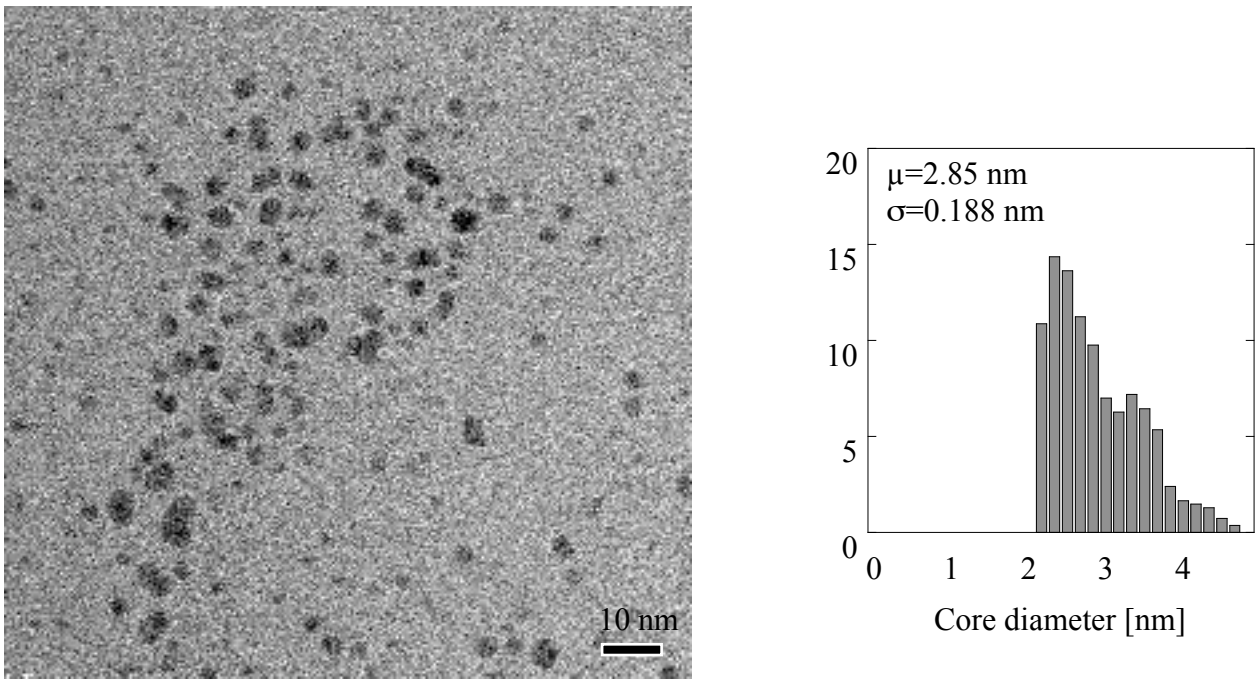

Figure 3.12: TEM image and associated size distribution for 2.9 nm gold nanoparticles synthesized under condition (d) and, capped with *n*-hexane-1-thiol are shown respectively in (i), (ii) and (iii).

hexanethiol into 1.5 mL $CDCl_3$. NMR samples of the synthesized nanoparticles were made by dissolving ∼10 mg of the nanoparticles into 1.5 mL of $CDCl_3$. The resulting particle concentration was 3.66×10^{19} particles/L. In Figure 3.21 , the peaks for the stock *n*-hexane-1-thiol are found at 0.933 PPM, 1.33 PPM, 1.648 PPM, and 2.57 PPM. Three multiplets of the *n*-hexane-1-thiol capped gold nanoparticles are seen at 1.55 PPM, 1.27 PPM, and 0.856 PPM. The NMR peak at 2.58 PPM is associated with a proton attached to the –SH group. This peak is observed in the spectra of the stock *n*-hexane-1-thiol, but is not seen in the spectra for the capped nanoparticles. The lack of this peak indicates that the thiol group is attached to the gold nanoparticle surface, thus quenching the 2.58 PPM peak associated with the proton of the

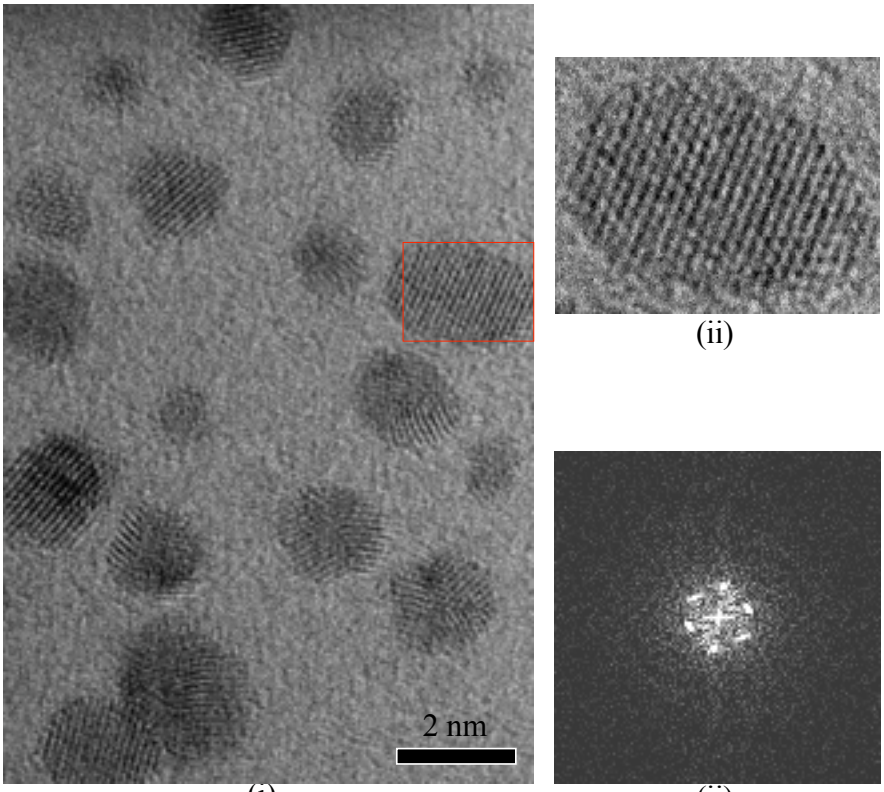

Figure 3.13: HR-TEM image, selected area and associated SAED are shown respectively in (i), (ii) and (iii); for 2.9 nm gold nanoparticles synthesized using condition (d) capped with *n*-hexane-1-thiol.

thiol. These results confirm that the thiol group is completely attached to the gold nanoparticle surface. Here, greater proximity of the $-CH_3$ group to the nanoparticle surface results in more significant shift from 0.933 PPM to 0.856 PPM.

3.5 Summary

This chapter outlines the procedure of gold nanoparticle synthesis based on the technique established by *Hostetler et al.*[89] and *Brust et al.* [88]. The size distributions of the synthesized nanoparticles were determined by analyzing TEM images of the

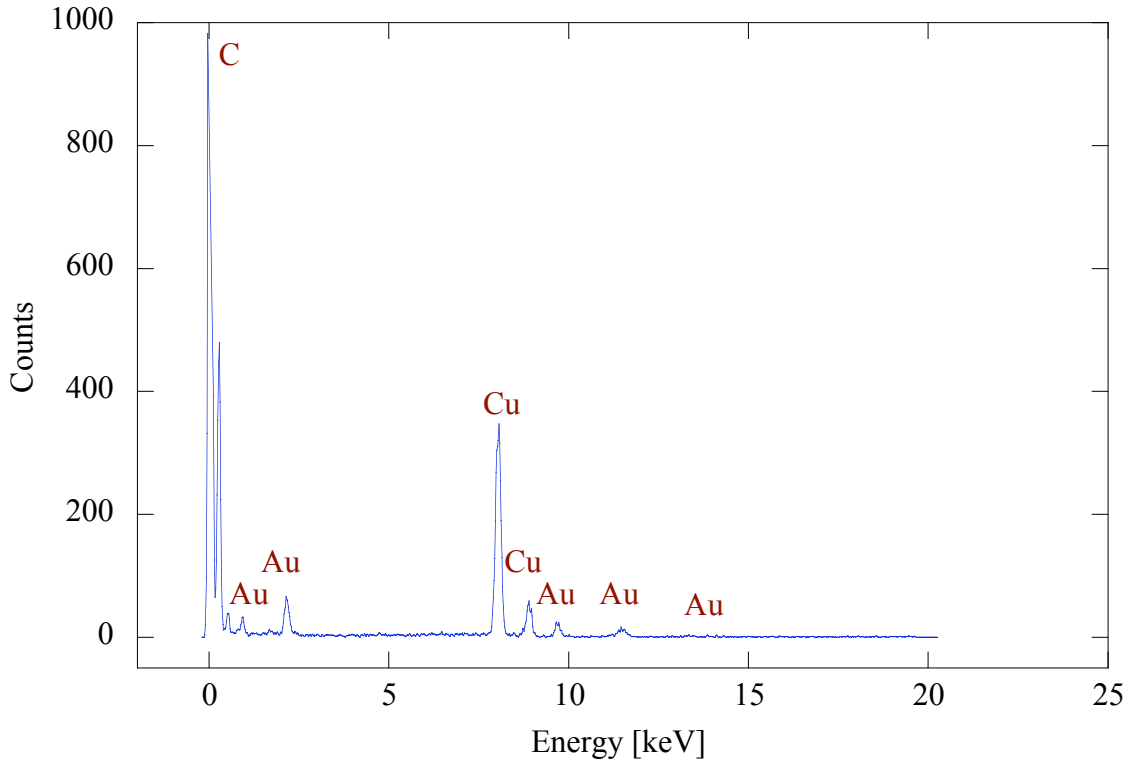

Figure 3.14: EDS spectrum for 2.9 nm gold nanoparticles synthesized under condition (d) capped with *n*-hexane-1-thiol is shown .

particles. EDS spectra showed evidence of gold in the spectrum. A SAED pattern illustrates the crystal structure of the capped nanoparticles. This chapter also shows the UV-vis and NMR measurement data for all synthesized nanoparticles.

The next chapter describes the theoretical consideration and sample preparation for the performed experiments.

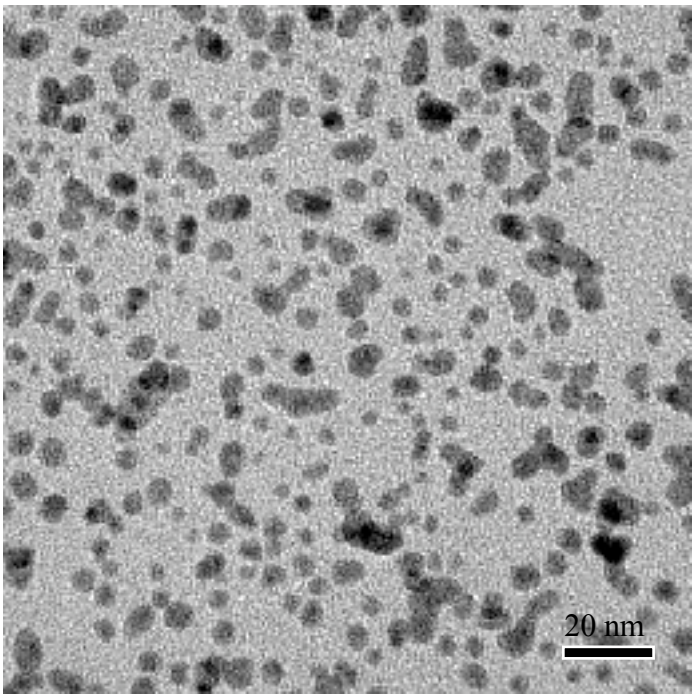

(i)

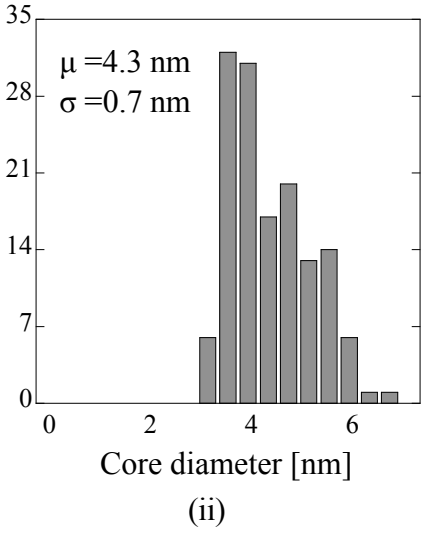

(ii)

Figure 3.15: TEM image and associated size distribution for 4.3 nm gold nanoparticles synthesized using condition (e) capped with *n*-hexane-1-thiol are shown respectively in (i) and (ii).

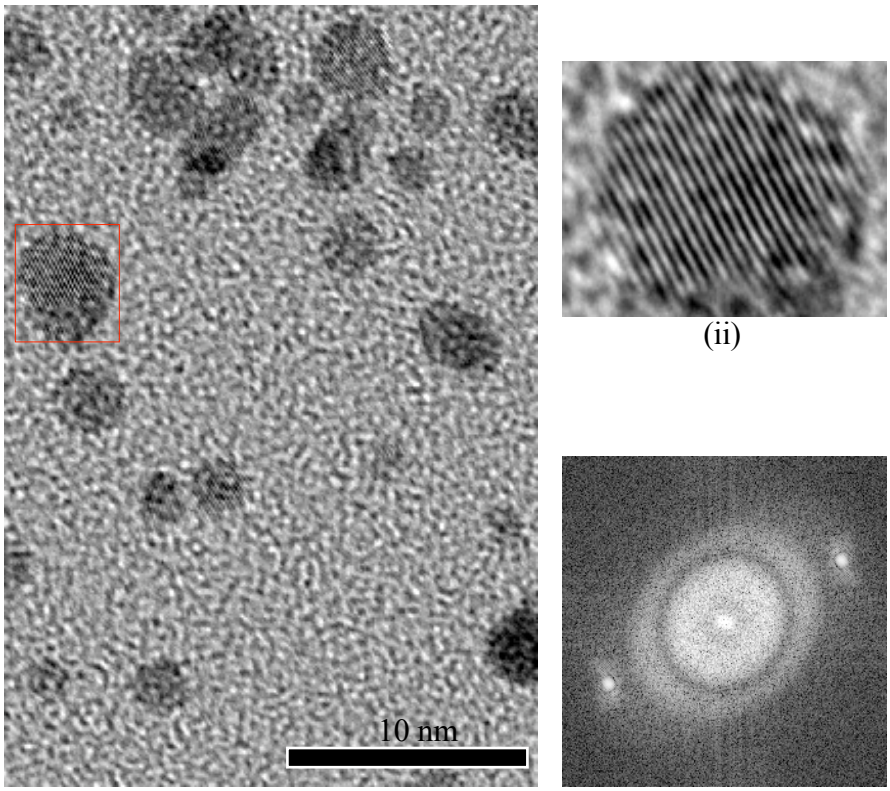

Figure 3.16: HR-TEM image, selected area and associated SAED are shown respectively in (i), (ii) and (iii); for 4.3 nm gold nanoparticles synthesized using condition (e) capped with *n*-dodecane-1-thiol.

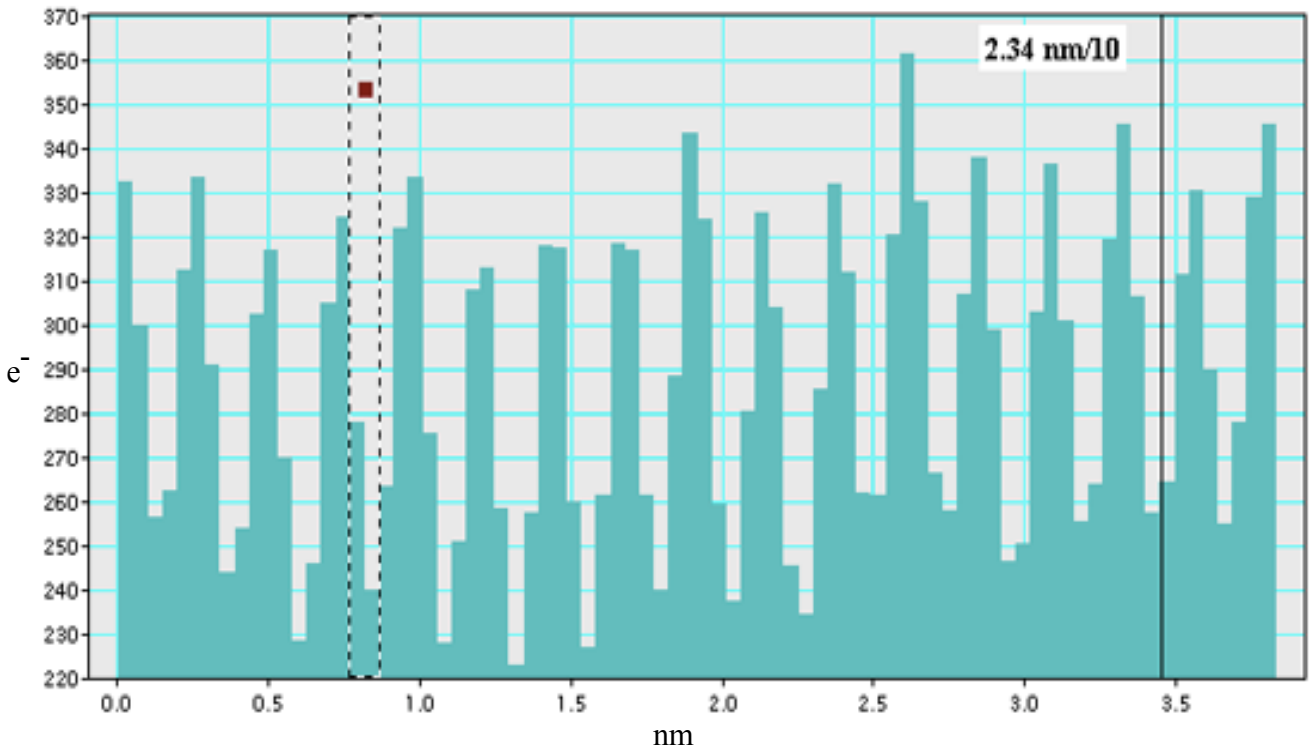

Figure 3.17: Histogram spectrum for 4.3 nm gold nanoparticles synthesized under condition (e) capped with *n*-hexane-1-thiol is shown .

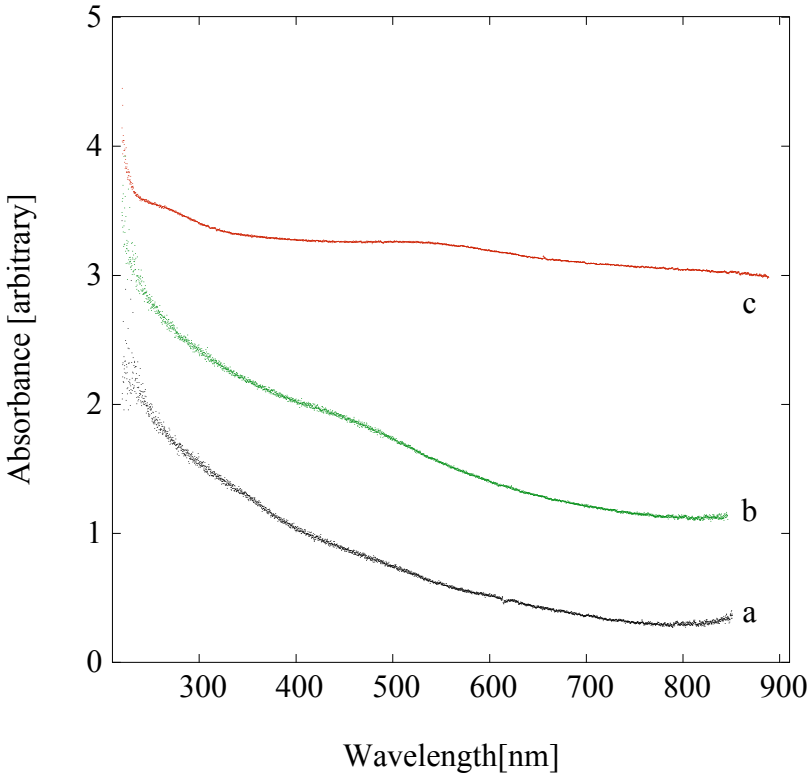

Figure 3.18: UV–Vis spectra of 1.6 nm, 2.8 nm and 4.4 nm *n*-dodecane-1-thiol capped gold nanoparticles produced under conditions (a), (b) and (c).

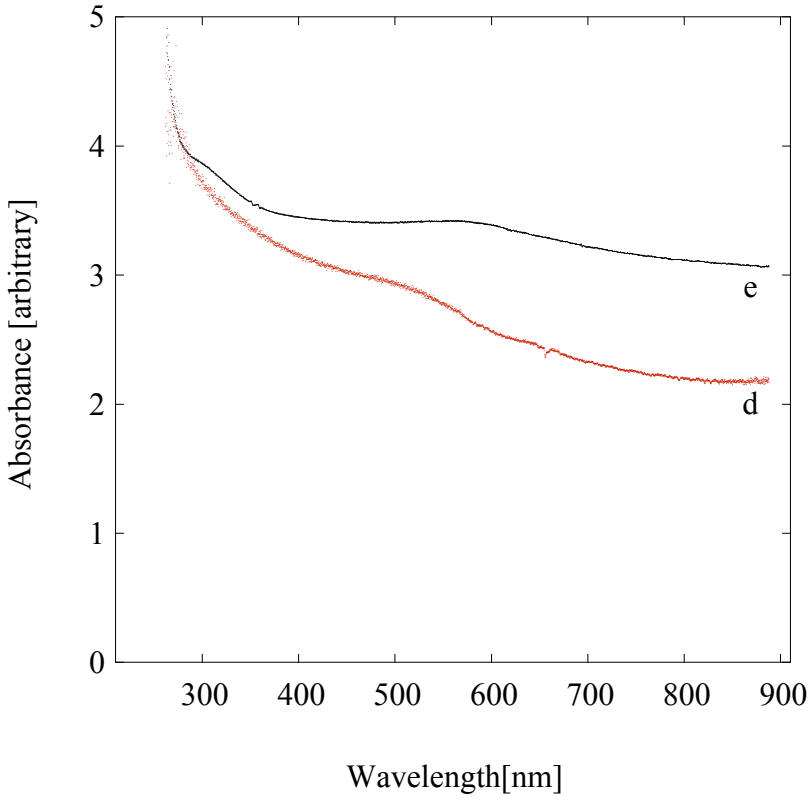

Figure 3.19: UV–Vis spectra of 2.9 nm and 4.3 nm *n*-hexane-1-thiol capped gold nanoparticles produced under conditions (d) and (e).

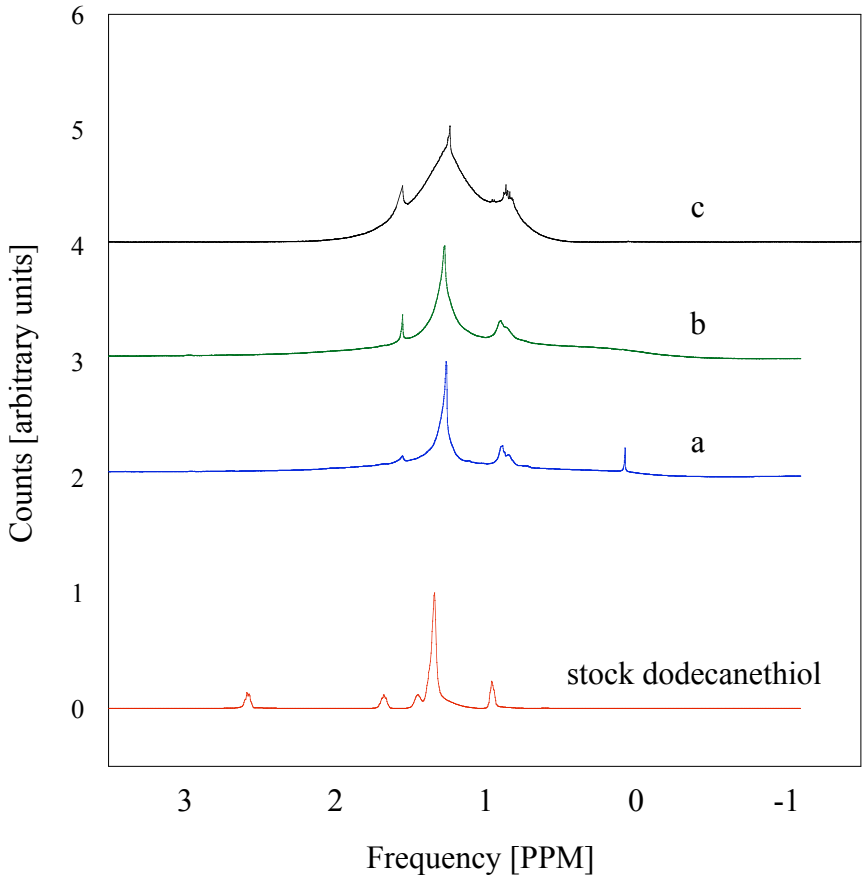

Figure 3.20: NMR spectra of stock *n*-dodecane-1-thiol and nanoparticles produced under conditions (a),(b) and (c) (i.e., nanoparticles capped with *n*-dodecane-1-thiol).

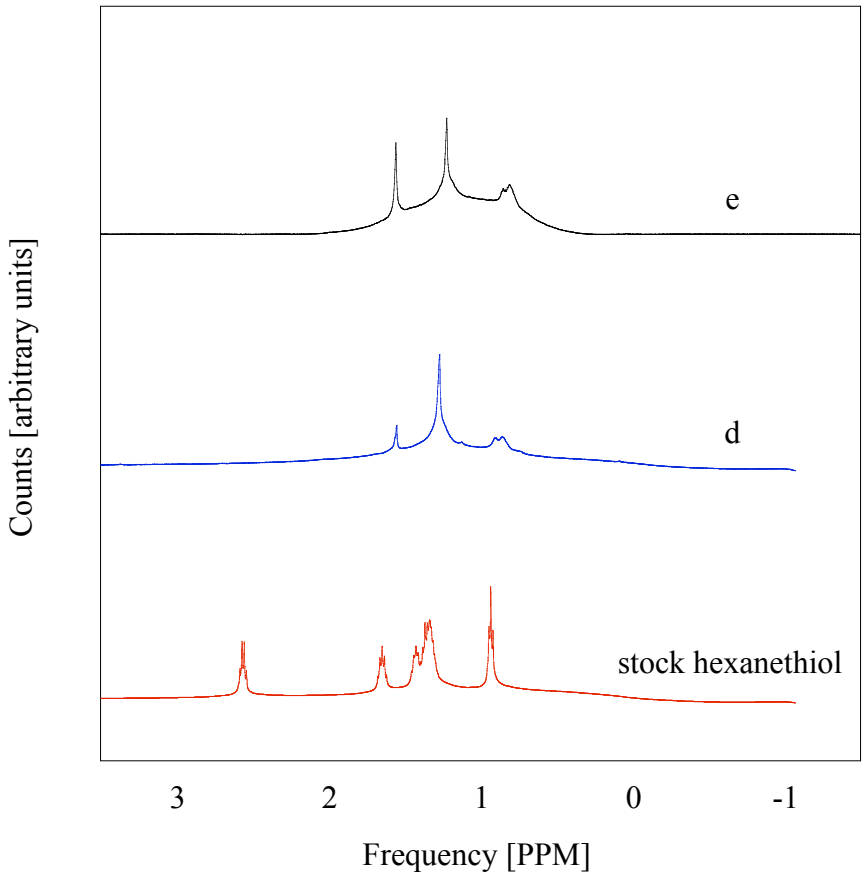

Figure 3.21: NMR spectra of stock *n*-hexane-1-thiol and nanoparticles produced under condition (d) and (e) (i.e., nanoparticles capped with *n*-hexane-1-thiol).

Chapter 4

Theoretical Considerations and Sample Preparation

This chapter describes the theories used for the analysis of the experimental results. The sample preparation is described, in brief, for all of the experiments that were performed.

4.1 Theoretical Considerations For Unmixed Nanoparticles

Equilibrium between nanoparticles in the bulk and nanoparticles adsorbed at the hexane–water interface is assumed to obey the Langmuir equilibrium isotherm:

$$\Gamma = \Gamma_{max} \cdot \frac{C}{a_L + C} \tag{4.1}$$

where Γ_{max} is the monolayer capacity of the liquid-liquid interface, reflecting the maximum amount of nanoparticles that can be adsorbed, a_L is the Langmuir parameter, and C is the bulk nanoparticle concentration at equilibrium. Assuming ideal behavior, an assumption valid at low nanoparticle concentrations, the adsorption density and bulk nanoparticle concentration at equilibrium are related by the Gibbs adsorption equation:

$$\Gamma = -\frac{1}{RT}\frac{d\gamma}{d(\ln C)} \tag{4.2}$$

Combining Equation 4.1 and Equation 4.2, yields the well-known Langmuir-Szyszkowski equation which relates explicitly, the interfacial tension to nanoparticle concentration in the bulk phase [93]:

$$\gamma = \gamma_0 - RT \cdot \Gamma_{max} \cdot \ln\left(1 + \frac{C}{a_L}\right) \tag{4.3}$$

where γ_0 is the interfacial tension of the hexane–water interface in the absence of nanoparticles. When diffusion controls the adsorption kinetics of gold nanoparticles, the theory of Ward and Tordai applies [19]:

$$\Gamma(t) = 2\sqrt{\frac{D}{\pi}}\left(C\sqrt{t} - \int_0^{\sqrt{t}} C_s(0, t-\tau)d(\sqrt{t})\right) \tag{4.4}$$

where C_s is the nanoparticle concentration in the subsurface (a region of the bulk solution immediately next to the hexane–water interface) and D is the diffusion coefficient of nanoparticles in the bulk phase. The asymptotic forms of the time dependence of dynamic interfacial tension for $t \longrightarrow 0$ and $t \longrightarrow \infty$ are given by [94]:

$$\gamma(t) = \gamma_0 - 2RTC\sqrt{\frac{Dt}{\pi}} \tag{4.5}$$

$$\frac{d\gamma}{d(t^{+\frac{1}{2}})}|_{t\to 0} = -2RTC\sqrt{\frac{D}{\pi}} \tag{4.6}$$

$$\gamma(t) = \gamma_\infty + \frac{RT \cdot \Gamma^2}{C}\sqrt{\frac{\pi}{4Dt}} \tag{4.7}$$

$$\frac{d\gamma}{d(t^{-\frac{1}{2}})}|_{t\to \infty} = \frac{RT \cdot \Gamma^2}{C}\sqrt{\frac{\pi}{4D}} \tag{4.8}$$

where γ_∞ is the interfacial tension at equilibrium (i.e., as $t \longrightarrow \infty$). The latter quantity is obtained from the intercept of a plot of long-time dynamic interfacial tension data against $t^{-\frac{1}{2}}$. The Langmuir isotherm parameters can be estimated from a fit of the Langmuir-Szyszkowski equation to equilibrium surface pressure data, $\gamma_0 - \gamma_\infty$. The Szyszkowski isotherm permits an estimation of the maximum adsorption density, Γ_{max}, Langmuir parameter, a_L, the minimum molecular area occupied by a nanoparticle at the interface, A_{min}, and the Gibbs free energy of adsorption, ΔG_{ads}. These values may be estimated using the following equations [95], [96]:

$$A_{min} = \frac{1}{\Gamma_{max} \cdot N_A} \tag{4.9}$$

$$\Delta G_{ads} = -RT \cdot \ln\left(\frac{1}{a_L}\right) \tag{4.10}$$

where N_A is the Avogadro's number.

Should the adsorption kinetics be controlled by diffusion of nanoparticles in the bulk phase at all times, one should find that $D_0 = D_\infty$. This is not the case for the adsorption of nanoparticles at liquid-liquid interfaces – a fact attributed to the presence of an adsorption barrier, such that $D_\infty \ll D_0$ [97, 1].

For sufficiently dilute colloidal suspensions, such as the ones considered here, the Stokes-Einstein equation should be expected to provide a reasonably accurate prediction of the diffusion coefficient of nanoparticles in solvent:

$$D_{S-E} = \frac{k_B T}{6\pi\eta r} \tag{4.11}$$

where k_B is the Boltzmann constant, η is the viscosity of the solvent and r is the nanoparticle radius. The Stokes-Einstein equation derives, with the assumption that a single rigid solute sphere is diffusing in a continuum of solvent. The net velocity (v) of this sphere is directly proportional to the force acting on it (i.e. force = f ·v). As the sphere moves slowly, according to Stokes law, this friction coefficient f is equal to $6\pi\eta r$. Einstein stated that the force, acting on the sphere, is equal to negative chemical potential gradient. The assumption in this analysis is that the velocity or flux is assumed to vary with the chemical potential gradient. This equation is valid when the solute is larger than the solvent. However, experimentally it is found to be inaccurate in the non-ideal solutions [98]. During the early stages of adsorption from sufficiently dilute nanoparticle suspensions, one expects $D_0 = D_{S-E}$. In the context of the theory put forth by *Liggieri* and co-workers [20] for mixed diffusion-activation controlled adsorption, the analysis of late-time dynamic IFT data provides an apparent diffusion coefficient which depends on the magnitude of the adsorption barrier [20]:

$$D_\infty = D_0 exp\left(-\frac{\Delta E}{k_B T}\right) \tag{4.12}$$

where ΔE is the activation energy of the barrier and D_0 is the diffusion coefficient.

It is assumed above that there is no interaction among nanoparticles at the liquid-lquid interface. To clarify this assumption, Frumkin models can be applied instead

of Langmuir. The Frumkin adsorption isotherm and equation of state respectively, are given by [99],[100]:

$$\frac{C}{a_L} = \frac{\Gamma}{\Gamma_\infty - \Gamma} \cdot \exp\left(\frac{K\Gamma}{\Gamma_\infty}\right) \tag{4.13}$$

$$\gamma = \gamma_0 + RT \cdot \Gamma_\infty \cdot \left(\ln\left(1 - \frac{\Gamma}{\Gamma_\infty}\right) - \frac{K}{2} \cdot \left(\frac{\Gamma}{\Gamma_\infty}\right)^2\right) \tag{4.14}$$

where, parameter K represents the interaction among the particles. The value of K > 1, shows an evidence for favoring any interaction among the studied non-mixed nanoparticles . For K$\leqslant$1, indicates that no interaction exists among the particles. [100],[101].

4.2 Theoretical Considerations For Nanoparticle Mixtures

For insignificant surface interactions, the Langmuir isotherm that is used for single components can also be generalized for two component systems [102], [103]. The generalized Langmuir isotherm for two component systems (eg. A and B), is given by:

$$\Gamma_A = \frac{\Gamma_{max} K_{L,A} C_A}{1 + K_{L,A} C_A + K_{L,B} C_B} \tag{4.15}$$

$$\Gamma_B = \frac{\Gamma_{max} K_{L,B} C_B}{1 + K_{L,A} C_A + K_{L,B} C_B} \tag{4.16}$$

where $K_{L,i} = \frac{1}{a_{L,i}}$ represents to component i. C_A and C_B are the concentration of components A and B in the bulk, respectively. The corresponding equation for surface pressure $\Pi = \gamma_0 - \gamma$ is:

$$\Pi(C_A, C_B) = -RT\Gamma_{max} \cdot \ln\left(1 - \frac{\Gamma_A}{\Gamma_{max}} - \frac{\Gamma_B}{\Gamma_{max}}\right) \tag{4.17}$$

Equations 4.15, 4.16 and 4.17 are valid only if $\Gamma_{m,A}$ and $\Gamma_{m,B} \approx \Gamma_{max}$. Otherwise an improved approach or model is needed for multicomponent systems [102].

Using non-ideal interactions in binary mixtures (NIBM) theory, the mole fraction of adsorbed nanoparticles at the interfacial layer at the water–hexane interface can be estimated by [104], [105], [95], [106] :

$$\frac{X_1^2 \cdot \ln\left(\frac{C_{1,t}}{C_{1,t}^0 \cdot X_1}\right)}{(1-X_1)^2 \cdot \ln\left(\frac{C_{2,t}}{C_{2,t}^0 \cdot (1-X_1)}\right)} = 1 \tag{4.18}$$

where X_1 is the mole fraction of type-1 nanoparticles at the interface; α is the mole fraction of type-1 nanoparticles in the bulk suspension; $C_{1,t}$ and $C_{2,t}$ are the molar concentrations of type 1 & 2 nanoparticles in the bulk suspension; $C_{1,t}^0$ and $C_{2,t}^0$ are the molar concentration of type 1 & 2 nanoparticles that would be needed to produce the same interfacial tension as a binary mixture of nanoparticles having a total molar concentration of C_t. Further, it is also known that $C_{1,t} = \alpha C_t$ and $C_{2,t} = (1-\alpha)C_t$.

The interaction parameter, β, represents the interaction between the two components in a mixed nanoparticle interfacial layer and, assuming a monolayer of nanoparticles at the interface, it can be calculated as follows:

$$\beta = \frac{\ln\left(\frac{C_{1,t}}{C_{1,t}^0 \cdot X_1}\right)}{(1-X_1)^2} \tag{4.19}$$

The parameter β measures the deviation from an ideal mixing of the two nanoparticle types and it is proportional to the free energy of mixing in the system. If $\beta = 0$ then there is ideal mixing between the two types of nanoparticles and no interaction between the two types of nanoparticles is observed. A negative value of β indicates that there is an attractive interaction between the two nanoparticle types, when compared to the attraction between nanoparticles of the same type. A positive value of β indicates that there is a repulsive interaction between the two types of nanoparticles.

4.3 Measurements

Below are the sample preparation methods and measurements for the experiments outlined in Chapters 5, 6 and 7.

4.3.1 Sample Preparation for the Experiments Performed in Chapter 5

Dynamic interfacial tension measurements

The effect of nanoparticles on the dynamic interfacial tension was investigated using a series of colloids of varying nanoparticle concentration, achieved by diluting each of the three kinds 1.6 nm, 2.8 nm *n*- dodecane-1-thiol capped and 2.9 nm *n*-hexane-1-thiol capped synthesized nanoparticles in pure hexane. A drop of deionized ultra-pure water ($\sim$18.2 MΩ·cm) was formed at the end of a steel needle placed into the colloidal suspension and images of this drop were recorded over time. Image aquisition and determination of dynamic interfacial tension by axisymmetric drop shape analysis (ADSA) were performed using the VCA 2500 XE equipment and software (AST Products, Billerica, MA).

Calibration and verification of ADSA system

All glassware, syringes, and equipment were well cleaned using either acetone, tetrahydrofuran, or both. Before use in the ADSA measurements, the hexane (Sigma-Aldrich, $\geqslant$ 99% purity) was shaken with a nearly equal volume of ultrapure water for thirty minutes to achieve equilibrium between the two phases. The water was then removed and the process repeated a total of three times in order to remove trace impurities from hexane. The interfacial tension of pure water droplets in hexane treated in this manner was then measured. The purity of hexane-water interface was confirmed and, is shown in Appendix 8.2. A constant interfacial tension value of 51.2 $\pm$ 0.4 mN/m was found at a temperature of 295.5 K for these droplets, which is consistent with the literature value of 51.4 mN/m reported by *Goebel and Lunkenheimer* [59]. Prior to any interfacial measurement, the equipment was checked by measuring the interfacial tension of a pure water droplet in equilibrated hexane to verify that the measured interfacial tension had not deviated from the established value of 51.2 mN/m.

4.3.2 Sample Preparation for the Experiments Performed in Chapter 6

The interaction behaviour of mixtures of nanoparticles at the interfacial layer was investigated by preparing a series of nanoparticle suspensions containing two types of nanoparticles at various concentrations in pure hexane. A droplet of deionized ultra-pure water ($\sim$18.2 MΩ·cm) was then formed at the end of a steel needle placed into the colloidal suspension and images of the droplet were recorded over time. A similar procedure, as discussed in Section 4.3.1, was followed for the dynamic interfacial tension measurements, and calibration of ADSA system.

4.3.3 Sample Preparation for the Experiments Performed in Chapter 7

Colloidal suspensions were prepared by adding the synthesized nanoparticles to either pure hexane or nonane. Prior to use, the hexane and nonane (Sigma-Aldrich, $\geqslant$ 99% purity) were shaken with approximately equal volume of ultrapure ($\sim$18.2 MΩ·cm) water for thirty minutes in order to achieve equilibrium between the two phases. The water was then removed and the process was repeated a total of three times in order to remove trace impurities from both the hexane and nonane. The aqueous phases used in this study were made from deionized ultra-pure water to which various amounts of either NaCl (J. T. Baker), NaOH (Caledon), or HCl (Fisher Scientific) were added to adjust the ionic strength and pH of the solution. As a control, the equilibrium IFT of pure water droplets was measured in the system resulting in constant IFT values of 51.2 $\pm$ 0.4 mN/m for water–hexane and 52.2 $\pm$0.3 mN/m for water–nonane at a temperature of 297.65 K. These values are consistent with literature values for water–hexane (51.4 mN/m) and water–nonane (52.4 mN/m) as reported by *Goebel and Lunkenheimer* [59]. The reported interfacial tension values are the average of at least two measurements. The pH was measured using a calibrated pH meter (VWR SB21, Symphony) with an uncertainty of $\pm$0.01. The experiments were carried out at temperatures in the range of 25^{o}C to 43^{o}C using a fresh sample solution at constant pH and bulk nanoparticle concentration. The dynamic interfacial tension measurements, and calibration of ADSA system were done as described in Section

4.3.1.

4.4 Summary

This chapter illustrates the theoretical formulae necessary for analysis of the experimental data (analysis is shown in chapters 5, 6 and 7). It also outlines the procedure followed for sample preparation in each investigation performed in this thesis.

The next chapter provides the effect of factors, i.e., bulk concentration, particle size and nature of the capping agent on the adsorption kinetics of AT-AuNPs at the hexane-water interface.

Chapter 5

Effect of Bulk Concentration, Particle Size and Capping Agent on Interfacial Tension

This chapter discusses the effect that nanoparticle bulk concentration, particle size and nature of the capping ligand has on the IFT at the water-hexane interface. The pendant drop technique was used to characterize the adsorption behavior of *n*-dodecane-1-thiol and *n*-hexane-1-thiol capped gold nanoparticles. UV-Vis spectroscopy and proton NMR measurements were performed to confirm the removal of free ligands from the nanoparticle suspensions prior to their use. The characteristics of the adsorption process was obtained by analysis of dynamic interfacial tension data as a function of particle concentration in the bulk.

5.1 Effect of Particle Concentration and Size on the Interfacial Properties

Time dependent interfacial tension measurements were performed on the hexane–water interface. For these measurements, *n*-dodecane-1-thiol and *n*-hexane-1-thiol capped nanoparticles were suspended in the hexane phase prior to the formation of

the interface. It was found that the dynamic interfacial tension decreases with time for all cases as shown below.

5.1.1 Concentration Effect on the Dynamic Interfacial Tension for *n*-Dodecane-1-Thiol Capped Gold Nanoparticles

Figures 5.1 and 5.2 illustrate that at higher particle concentrations, the rate at which the interfacial tension decreases is greater and a lower interfacial tension is reached at equilibrium. For each observed concentration, the equilibrium dynamic interfacial tension (i.e., $t \longrightarrow \infty$) was obtained by fitting straight lines to γ vs. $t^{-\frac{1}{2}}$ data at late times and reading γ_∞ as the intercept (cf. Equation 4.7). These results can be seen in Tables 5.1 and 5.2. Semi-log plots of the equilibrium interfacial tension vs. nanoparticle concentration are shown in Figure 5.3. It is evident that as the nanoparticle concentration increases, the equilibrium interfacial tension decreases until a critical concentration, c', is reached for which the interface reaches maximum coverage, Γ_∞, by absorbed nanoparticles (i.e., the surface is saturated). The values of c' for 1.6 ± 0.28 nm and 2.8 ± 0.27 nm particles are 2.12×10^{17} particle/L and 8.28×10^{16} particles/L respectively.

Table 5.1: Adsorption behavior for n-dodecane-1-thiol capped gold nanoparticles synthesized under condition (a) at the hexaxe–water interface. These particles were sized using a log-normal fit; resulting in a mean particles size of $\mu = 1.60$ nm with a standard deviation of $\sigma = 0.278$ nm.

Nanoparticle concentration C [particle/L]	Equilibrium int. tension γ_∞[mN/m]	Diffusivity [m^2/s] D_0	D_∞
2.12×10^{15}	40.70	4.42×10^{-10}	1.98×10^{-10}
8.51×10^{15}	35.58	8.14×10^{-11}	5.70×10^{-12}
2.12×10^{16}	32.85	9.90×10^{-12}	3.54×10^{-13}
4.26×10^{16}	30.90	3.63×10^{-12}	1.56×10^{-13}
2.12×10^{17}	26.30	2.57×10^{-13}	7.31×10^{-15}
2.55×10^{17}	26.07	1.39×10^{-13}	2.73×10^{-15}

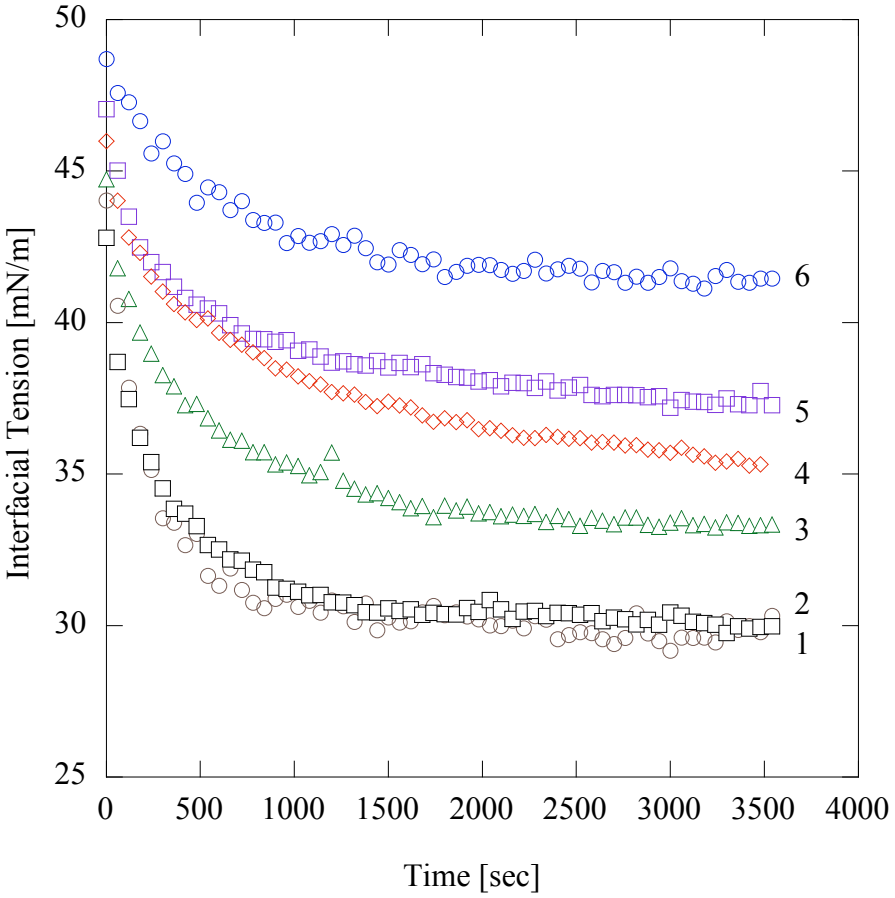

Figure 5.1: Interfacial tension of a water droplet in hexane with 1.6 ± 0.28 nm Au capped n-dodecane-1-thiol nanoparticles at various concentrations: (1) 2.55×10^{17} particles/L, (2) 2.12×10^{17} particles/L, (3) 4.26×10^{16} particles/L, (4) 2.12×10^{16} particles/L, (5) 8.51×10^{15} particles/L,and (6) 2.12×10^{15} particles/L.

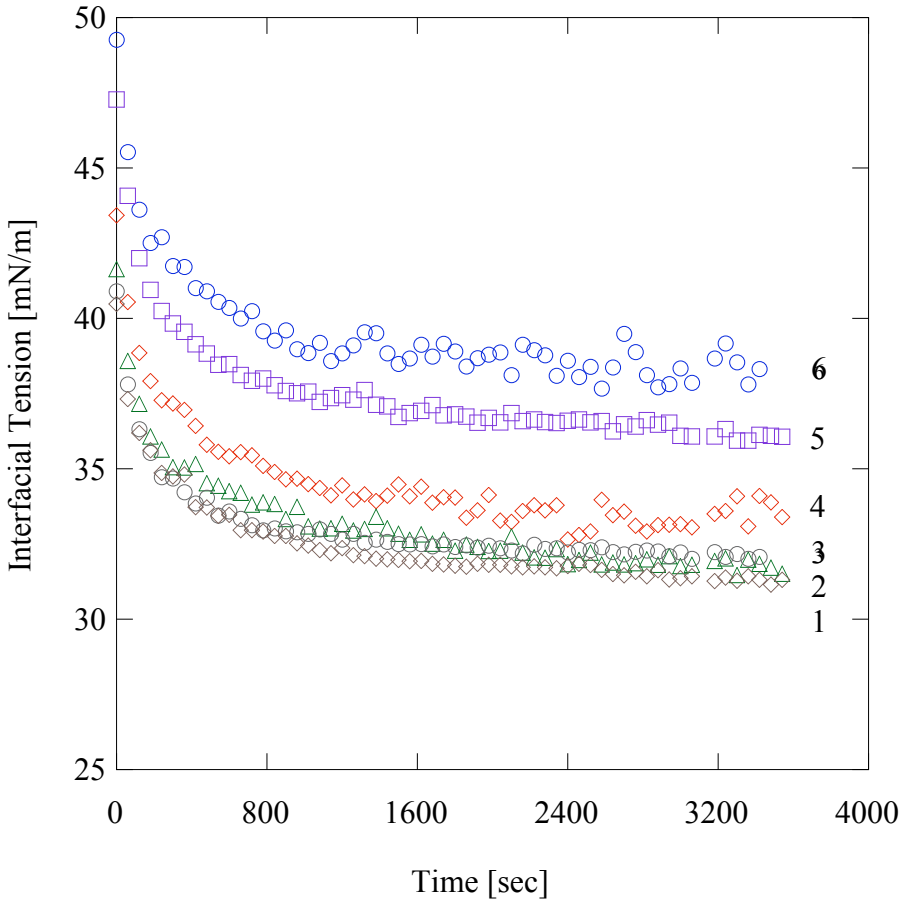

Figure 5.2: Interfacial tension of a water droplet in hexane with 2.8 ± 0.27 nm Au capped n-dodecane-1-thiol nanoparticles at various concentrations: (1) 1.27×10^{17} particles/L, (2) 8.48×10^{16} particles/L, (3) 4.24×10^{16} particles/L, (4) 2.12×10^{16} particles/L, (5) 8.48×10^{15} particles/L, and (6) 4.24×10^{15} particles/L

Table 5.2: Adsorption behavior for n-dodecane-1-thiol capped gold nanoparticles synthesized under condition (b) at the hexane–water interface. These particles were sized using a log-normal fit; resulting in a mean particles size of $\mu = 2.78$ nm with a standard deviation of $\sigma = 0.273$ nm.

Nanoparticle concentration C [particle/L]	Equilibrium int. tension γ_∞[mN/m]	Diffusivity [m^2/s] D_0	D_∞
4.24×10^{15}	36.47	3.54×10^{-10}	5.16×10^{-12}
8.48×10^{15}	34.60	1.29×10^{-10}	1.41×10^{-12}
2.12×10^{16}	32.30	1.37×10^{-11}	3.72×10^{-13}
4.24×10^{16}	31.0	3.52×10^{-12}	9.16×10^{-14}
8.48×10^{16}	29.69	7.56×10^{-13}	1.07×10^{-14}
1.27×10^{17}	29.62	2.24×10^{-13}	6.55×10^{-15}

5.1.2 Concentration Effect on the Dynamic Interfacial Tension for *n*-Hexane-1-Thiol Capped Gold Nanoparticles

As with Figures 5.1 and 5.2, Figure 5.4 also shows that there is an effect on the interfacial tension associated with nanoparticle concentration. The rate at which the interfacial tension decreased was also found to be higher for n-hexane-1-thiol capped nanoparticles as concentration was increased. Again, the equilibrium interfacial tension was found to be lower at higher nanoparticle concentrations. These results can be seen in Table 5.3. With an increase in the nanoparticle concentration, the equilibrium interfacial tension also decreased until the critical concentration, $c' = 8.61 \times 10^{16}$ particles/L, was reached.

5.1.3 Size Effect on the Dynamic Interfacial Tension

For larger particles (2.8 ± 0.27 nm), the interfacial tension falls very sharply when the droplet is initially formed. The interfacial tension also falls for smaller nanoparticles (1.6 ± 0.28 nm), but not as sharply as for the larger ones. As soon as the water droplet is formed in the hexane-Au suspension, nanoparticles go to the interface. The total

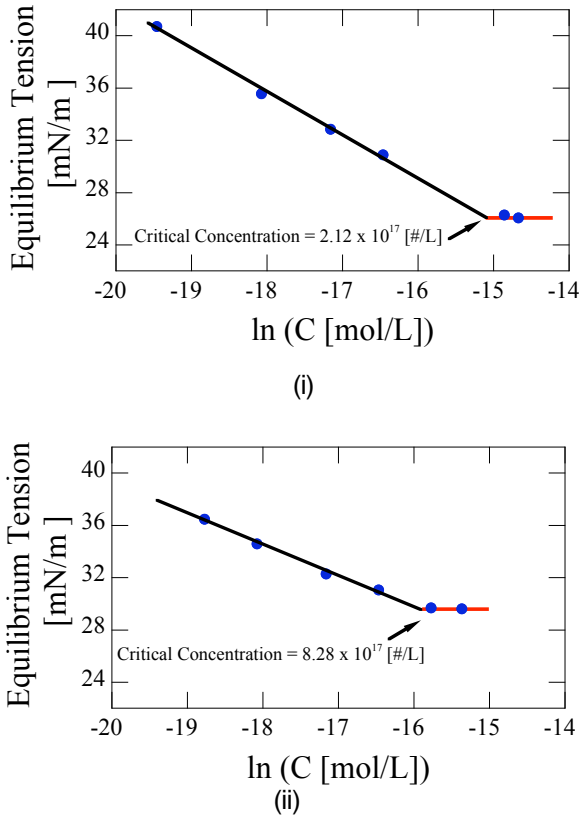

Figure 5.3: Extrapolated equilibrium interfacial tension of (i) 1.6 ± 0.28 nm and (ii) 2.8 ± 0.27 nm Au capped n-dodecane-1-thiol nanoparticles showing the critical concentration [particle/L]. The straight line represents a fit on the Gibbs adsorption isotherm.

free energy of the system decreases as a result. The change in free energy associated with adsorption of a single particle is given in Equation 1.1, which shows that for constant temperature, $\gamma_{o/w}$, $\gamma_{p/w}$, and $\gamma_{p/o}$, larger particles are more stably attached at the liquid-liquid interface. On the contrary, smaller particles are more easily displaced as a result of thermal fluctuations. For a given bulk concentration, greater surface coverage is initially achieved by adsorption of larger particles, hence a greater initial reduction of the interfacial tension is observed. As $t \longrightarrow \infty$, equilibrium coverage of the interface is achieved faster for larger nanoparticles. For the same bulk concentration of $(4.25 \pm 0.1) \times 10^{16}$ particles/L, Figure 5.5 shows that the interfacial tension is slightly smaller for the larger nanoparticles (31.87 mN/m vs. 33.33 mN/m).

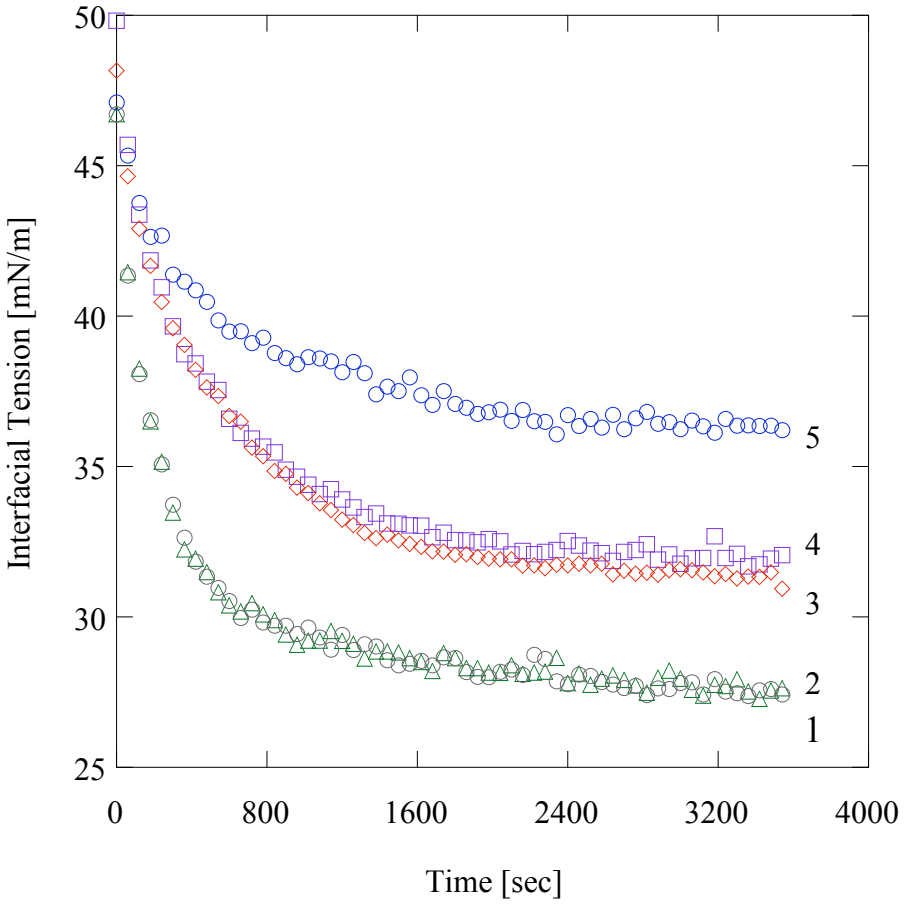

Figure 5.4: Plot of the interfacial tension of a water droplet in hexane with 2.9 ± 0.19 nm Au capped n-hexane-1-thiol nanoparticles at various concentrations: (1) 1.30×10^{17} particles/L, (2) 8.65×10^{16} particles/L, (3) 2.16×10^{16} particles/L, (4) 8.61×10^{15} particles/L and (5) 4.32×10^{15} particles/L.

Similar observations have been made by *Kutuzov et al.*[1].

Table 5.3: Adsorption behavior for n-hexane-1-thiol capped gold nanoparticles synthesized under condition (c) at the hexane–water interface. These particles were sized using a log-normal fit; resulting in a mean particles size of $\mu = 2.85$ nm with a standard deviation of $\sigma = 0.188$ nm.

Nanoparticle concentration C [particle/L]	Equilibrium int. tension γ_∞[mN/m]	Diffusivity [m^2/s] D_0	D_∞
4.32×10^{15}	31.70	3.70×10^{-10}	9.12×10^{-13}
8.61×10^{15}	29.70	2.38×10^{-10}	5.39×10^{-13}
2.16×10^{16}	28.24	2.83×10^{-11}	3.54×10^{-15}
8.65×10^{16}	25.25	1.31×10^{-12}	6.62×10^{-15}
1.30×10^{17}	25.22	5.79×10^{-13}	2.91×10^{-15}

5.2 Effect of Nature of the Capping Agent on the Interfacial Properties

Figure 5.6 demonstrates a significant effect of the chain length of alkanethiol ligands on adsorption behaviour. Specifically, at the same bulk concentration of $(8.56 \pm 0.18) \times 10^{16}$ particles/L, the longer n-dodecane-1-thiol is apparently more effective at shielding the polar gold core than n-hexane-1-thiol, thereby decreasing the hydrophilic character and reducing the surface activity of n-dodecane-1-thiol stabilized gold nanoparticles relative to nanoparticles of the same size that are stabilized with n-hexane-1-thiol. Figure 5.6 shows that a significantly lower value of interfacial tension is reached following the adsorption of n-hexane-1-thiol stabilized gold nanoparticles (27.63 mN/m vs. 32.07 mN/m) for nanoparticles of the same size stabilized with n-dodecane-1-thiol).

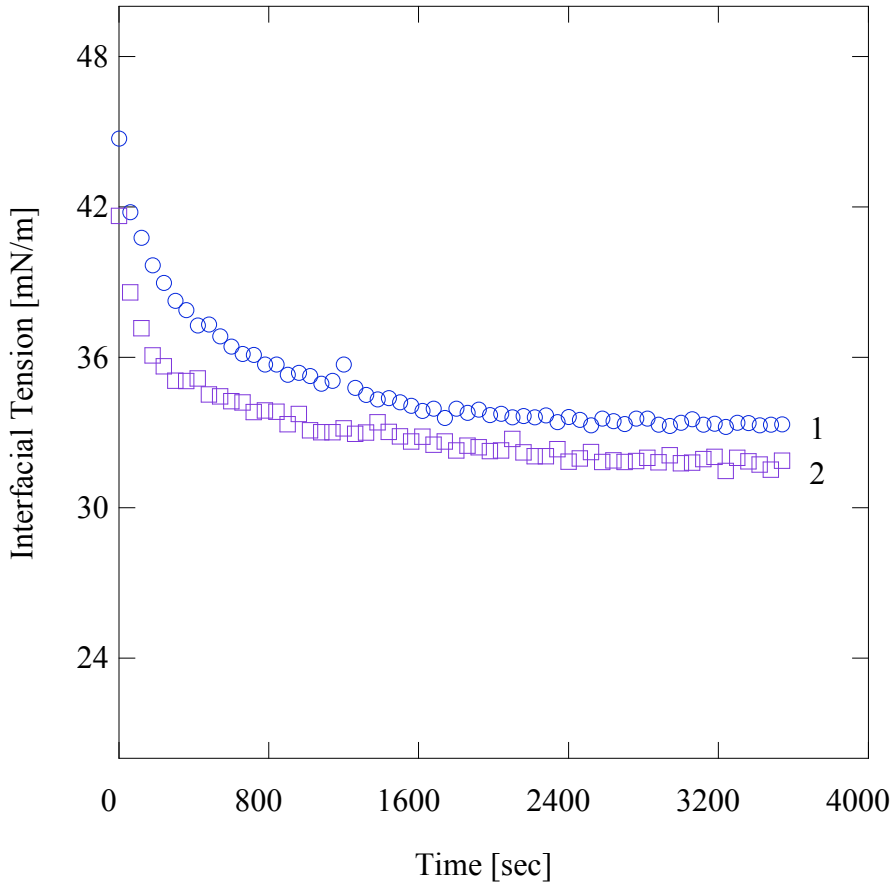

Figure 5.5: Time dependence of the interfacial tension for the adsorption of Au capped *n*-dodecane-1-thiol nanoparticles of different diameters (1) 1.6 ± 0.28 nm and (2) 2.8 ± 0.27 nm at the same bulk concentration ($4.25 \pm 0.1 \times 10^{16}$ particles/L).

5.3 Adsorption Kinetics of *n*-Dodecane-1-Thiol- and *n*-Hexane-1-Thiol-Stabilized Gold Nanoparticles

In this section, the gold nanoparticle adsorption data obtained are quantitatively analyzed. For 1.6 ± 0.28 nm *n*-dodecane-1-thiol particles, the Langmuir-Szyszkowski isotherm is characterized by a maximum adsorption density, $\Gamma_\infty = 1.27 \times 10^{-6}$

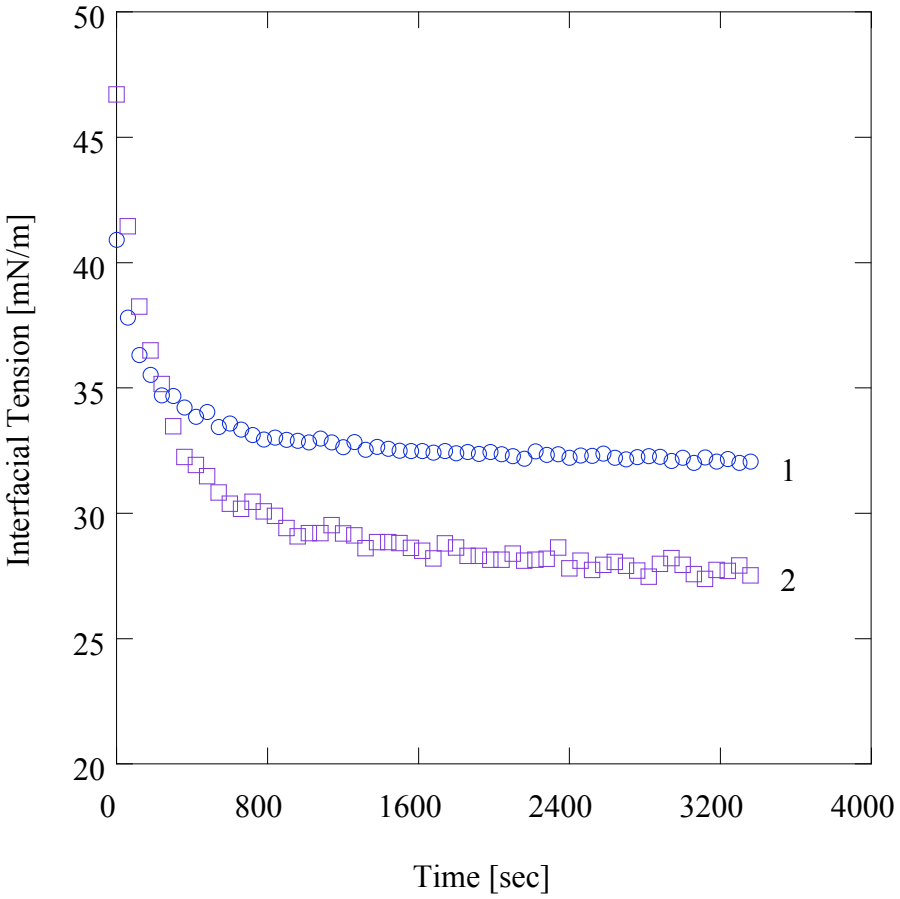

Figure 5.6: Time dependence of the interfacial tension for the adsorption of Au capped (1) n-dodecane-1-thiol and (2) n-hexane-1-thiol nanoparticles of almost same diameters (~ 3 nm) at same bulk concentration ($8.56 \pm 0.18 \times 10^{16}$ particles/L).

mol/m^2, and Langmuir parameter, $a_L = 1.15 \times 10^{-7}$ mol/m^3. It is instructive to compare the value of Γ_∞ to what would be expected for some simple closely-packed arrangements of particles at the liquid-liquid interface, as shown in Figure 5.7. For the 1.6 nm particles, the theoretical maximum adsorption density is $\Gamma_{sq} = (0.71 \pm 0.23) \times 10^{-6}$ mol/m^2 for the square arrangement and $\Gamma_{tri} = (0.82 \pm 0.27) \times 10^{-6}$mol/m^2 for the triangular one. The experimental value, $\Gamma_{max} = 1.27 \times 10^{-6}$ mol/m^2 is thus consistent with Γ_{tri} (i.e., hexagonal). Similarly, the Langmuir-Szyszkowski isotherm for the 2.8 ± 0.27 nm n-dodecane-1-thiol stabilized particles is charac-

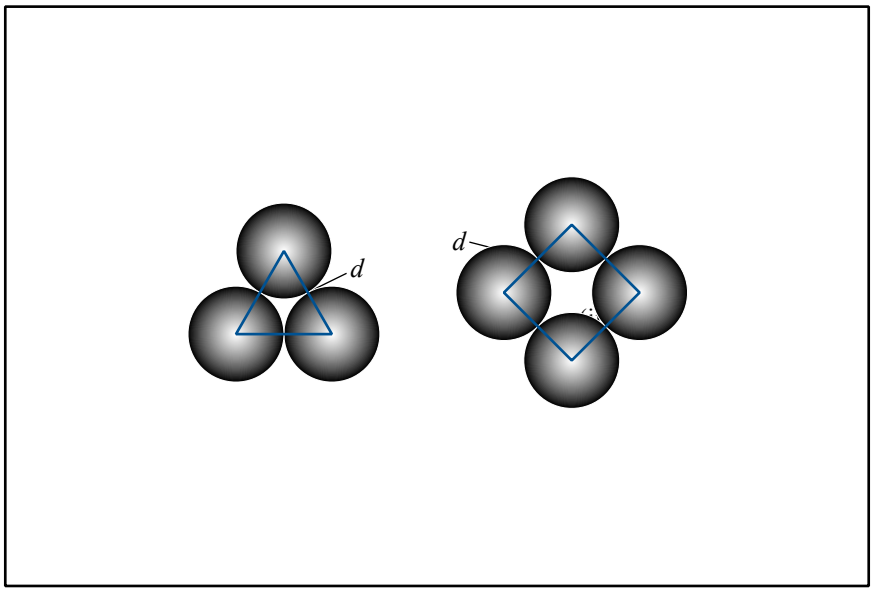

Figure 5.7: Particle packing arrangements at the interface (i) triangular and (ii) square arrangement.

terized by a maximum adsorption density, $\Gamma_{max} = 8.43 \times 10^{-7}$mol/m^2 and Langmuir parameter, $a_L = 4.89 \times 10^{-9}$mol/m^3. For this particle size, one estimates $\Gamma_{sq} = (2.2 \pm 0.42) \times 10^{-7}$mol/m^2 and $\Gamma_{tri} = (2.5 \pm 0.5) \times 10^{-7}$ mol/m^2. The latter value is consistent with experiment. The same is true of the 2.9 ± 0.19 nm *n*-hexane-1-thiol stabilized particles, for which the Langmuir-Szyszkowski isotherm is characterized by a maximum adsorption density of $\Gamma_{max} = 7.82 \times 10^{-7}$mol/m^2 and Langmuir parameter, $a_L = 2.38 \times 10^{-10}$ mol/m^3, whereas $\Gamma_{squ} = (2.00 \pm 0.27) \times 10^{-7}$mol/m^2 and $\Gamma_{tri} = (2.31 \pm 0.3) \times 10^{-7}$mol/m^2. Albeit rough, these estimates indicate a closely packed arrangement of the adsorbed nanoparticles at the hexane-water interface, as also found by *Kutuzov et al.*[1] for CdSe nanoparticles at the toluene-water interface. Figure 5.8 shows fits of the Langmuir isotherm to experimental data for 1.6 nm and 2.8 nm *n*-dodecane-1-thiol capped gold nanoparticles studied. Maximum or nearly maximum coverage of the interface is evidently achieved at equilibrium for all bulk concentrations considered,(i.e., $\Gamma \cong \Gamma_{max}$).

Using Equation 4.5 and Equation 4.7, the diffusivity of gold nanoparticles may be estimated from early- and late-time interfacial tension data, respectively. These

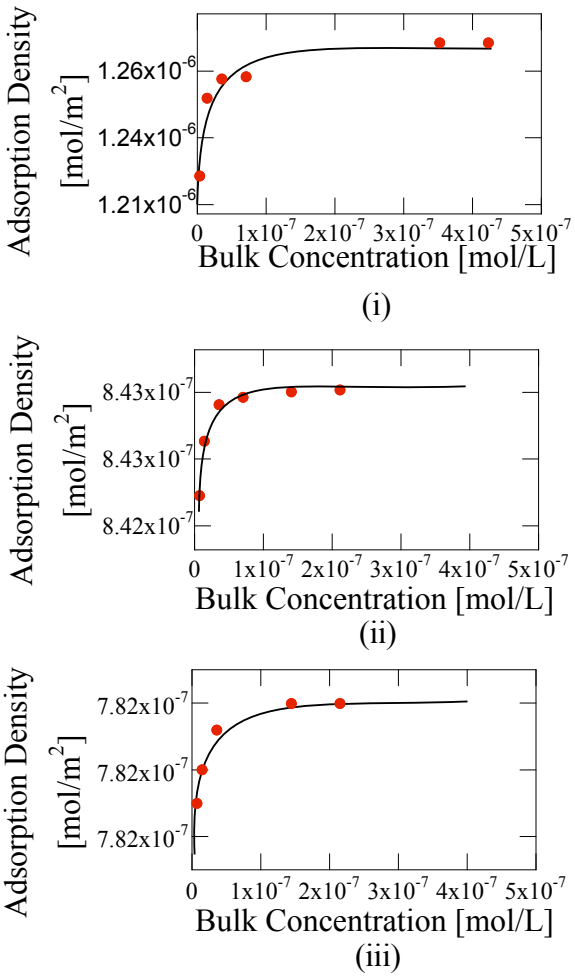

Figure 5.8: Equilibrium adsorption density of (i) 1.6±0.28 nm (ii) 2.8±0.27 nm Au capped n-dodecane-1-thiol nanoparticles and (iii) 2.9 ± 0.19 nm n-hexane-1-thiol nanoparticles as a function of bulk nanoparticle concentration.

estimates provide insight into the kinetics of the adsorption process. Should the adsorption kinetics be controlled by diffusion of nanoparticles in the bulk phase at all times, one should find $D_0 = D_\infty$. For dilute colloidal solutions such as the ones considered here, the Stokes-Einstein equation (See Equation 4.11) should be expected to provide a reasonably accurate prediction of the diffusivity of nanoparticles in hexane. Calculations of D_0 and D_∞ from dynamic interfacial tension data for each kind of gold nanoparticles synthesized are summarized in Tables 5.1, 5.2 and 5.3. We

find $D_0 > D_\infty$ typically by at least an order of magnitude, for all but the smallest nanoparticle concentration. Both D_0 and D_∞ decrease with increasing concentration of the bulk solution. Early-time ($t \longrightarrow 0$) diffusivity estimates, D_0, are plotted as a function of bulk nanoparticle concentration in Figure 5.9, where the predictions of nanoparticle diffusivity provided by the Stokes-Einstein equation are also shown for comparison. For the 1.6 nm and 2.8 nm *n*-dodecane-1-thiol stabilized nanoparticles the D_{S-E} values are $(8.92 \pm 1.56) \times 10^{-10}$ m^2/s and $(5.00 \pm 0.48) \times 10^{-10}$ m^2/s, respectively, whereas for the 2.9 nm *n*-hexane-1-thiol stabilized nanoparticles D_{S-E} $= (4.79 \pm 0.3) \times 10^{-10}$ m^2/s. Only for the lowest bulk concentrations, D_0 is seen to agree well with D_{S-E}, suggesting that diffusion in the bulk hexane phase controls the adsorption kinetics only under conditions of low coverage of the hexane-water interface by nanoparticles. Over increasing adsorption times ($t \longrightarrow \infty$) and for adsorption from higher bulk concentrations, where high coverage of the interface by nanoparticles is realized at earlier times, the estimates of diffusion coefficient afforded by Equation 4.5 are significantly lower than the D_{S-E} values. Similar observations have been made by *Kutuzov et al.*[1] for CdSe nanoparticles at the toluene-water interface. These authors have suggested that an adsorption barrier rapidly sets in with increasing surface coverage, as a result of increasing collisions in the sub-layer between nanoparticles desorbed from the interface with nanoparticles approaching the interface from the bulk solution. In the context of the theory put forth by *Liggieri* and co-workers [20] for mixed diffusion-activation controlled adsorption, the preceding analysis of experimental data provides an apparent diffusion coefficient which depends on the magnitude of the potential barrier and free diffusion coefficient as follows [20]:

$$D = D_f Exp\left(-\frac{\Delta E}{k_B T}\right) \tag{5.1}$$

where ΔE is the activation energy of the barrier and D_f is free diffusion coefficient. In the absence of an energy barrier to adsorption (i.e. when adsorption is limited by free diffusion of nanoparticles from the bulk solution to the subsurface), D_f is equal to D_{S-E}.

Taking the effective diffusivity equal to D_∞ values obtained from experiments with the highest nanoparticle concentrations, the estimated values of the potential barrier to adsorption, ΔE, are 4.4×10^{-20}J and 4.6×10^{-20}J , respectively, for the 1.6 nm

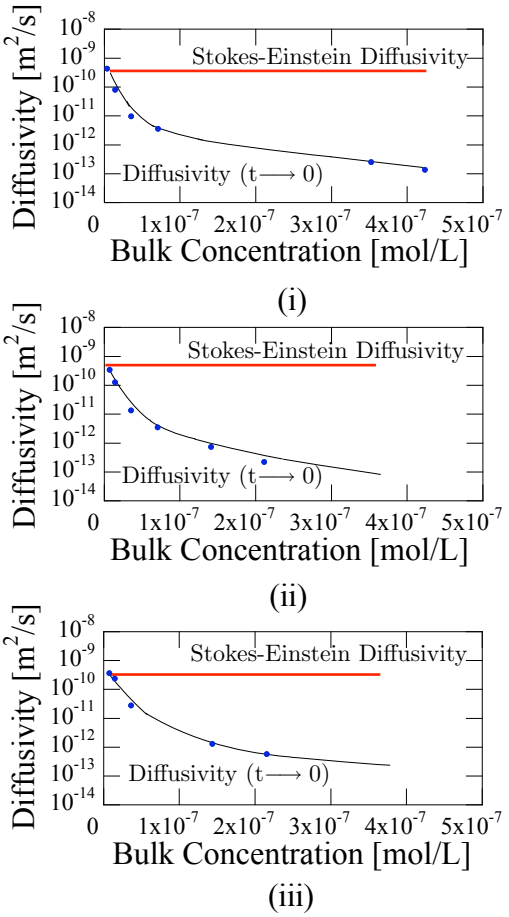

Figure 5.9: Diffusivity of (i) 1.6 ± 0.28 nm (ii) 2.8 ± 0.27 nm Au capped n-dodecane-1-thiol nanoparticles and (iii) 2.9 ± 0.19 nm n-hexane-1-thiol nanoparticles as a function of bulk nanoparticle concentration.

and 2.8 nm n-dodecane-1-thiol stabilized particles, and 4.8×10^{-20}J for the 2.9 nm n-hexane-1-thiol stabilized particles. These values are approximately equal to $10 k_B T$, as also found by *Kutuzov et al.*[1] for TOPO-stabilized Cd-Se nanoparticles of different sizes at the toluene-water interface. The latter authors suggested that, under conditions of high coverage of the interface with nanoparticles, the adsorption process is controlled by the rate of desorption of already adsorbed nanoparticles, such that the activation energy, ΔE, is roughly given by Equation 1.1. For all nanoparticles tested in this work, we find this suggestion consistent with a contact angle of about

157° (measured from the aqueous phase). Alternatively, equating ΔE to W_{ads}, the work that a particle must do against surface pressure [21], and using experimentally measured surface pressure data, we find equilibrium contact angles of $117° \pm 14°$ and $148° \pm 4°$ for the 1.6 nm and 2.8 nm n-dodecane-1-thiol stabilized particles, respectively, and $150° \pm 4°$ for the 2.9 nm n-hexane-1-thiol stabilized particles [107]. Such interpretations, however, must be viewed with great caution. When deformable soft organic ligands cover the particle surface, assessment of the energetics of nanoparticle localization at a fluid-fluid interface via determination of an equilibrium contact angle in the framework of Youngs theory is challenged by molecular dynamics simulations [70]. Further work is clearly needed before predictions of the magnitude of the adsorption barrier can be made.

5.4 Summary

This chapter describes the adsorption kinetics of alkhane-thiol capped of gold nanoparticles at the water-hexane interface. The effect of nanoparticle size, particle concentration and nature of the capping agent on the interfacial tension was discussed at the water–hexane interface. The characteristics of the adsorption process at the early stages, as $t \longrightarrow 0$, and the later stages, $t \longrightarrow \infty$, were obtained from the time evolution of the interfacial tension. At the interface, the particles first undergo free diffusion, then adsorption of the particles occurs due to the ordering and rearrangement of the nanoparticles at the interface, and, finally, by the formation of a monolayer due to the collection of the nanoparticles at the interface. By increasing the interfacial coverage, the diffusion-controlled adsorption for the nanoparticles at the interface changes to an interaction-controlled assembly. While performing these experiments, two factors were taken into consideration: (1) the concentration of nanoparticles, and (2) nanoparticle size. Two kinds of ligand stabilized gold nanoparticles were used to investigate the effect of ligand chain length on the adsorption behavior at the interface. It was found that the nanoparticle size, particle concentration and nature of the capping agent all have a profound impact on the interfacial properties.

The next chapter describes the interfacial properties of mixtures of these nanoparticles, having different sizes and capping agents.

Chapter 6

Interaction Behaviour During Adsorption of Mixtures of Alkanethiol Capped Gold Nanoparticles at the Hexane–Water Interface

This chapter addresses the adsorption properties of mixtures of gold nanoparticles at the hexane-water interface. The interaction parameters for mixtures of nanoparticles at the interface were also estimated. 1.6 nm, 2.8 nm, and 4.4 nm nanoparticles capped with n-dodcane-1-thiol and 4.3 nm particles capped with n-hexane-1-thiol were used in this study. The interfacial properties of mixtures of these nanoparticles, having different sizes and capping agents, were then studied. The nature and strength of the interaction between the nanoparticles within a mixture may be assessed in the context of the theory of non-ideal interactions in binary mixtures (NIBM) put forward by *Rosen* and coworkers [104], [105], [95], [106]. The NIBM theory has been used to determine an interaction parameter between the surfactant components in a mixture and the composition of mixed adsorption layers using the equilibrium interfacial tension isotherms. Using the NIBM theory, the mole fraction of adsorbed nanoparticles at the interfacial layer at the water–hexane interface can be estimated. Using

Equation 4.18 and Equation 4.19, the mole fraction of nanoparticles at the interface, X_1, and interaction parameter, β were estimated at the water-hexane interface. β, represents the interaction between the two particles in a mixed nanoparticle interfacial layer. These parameters were estimated using interfacial tension isotherms that were obtained for each type of nanoparticle prior to mixing and data obtained for the mixed suspensions. These equations can be seen in Chapter 4.

6.1 Adsorption of 4.4 nm *n*-Dodecane-1-Thiol and 4.3 nm *n*-Hexane-1-Thiol Capped Gold Nanoparticles at the Hexane–Water Interface

Experiments were performed to investigate the adsorption kinetics of 4.4 nm *n*-dodecane-1-thiol and 4.3 nm *n*-hexane-1-thiol-stabilized gold nanoparticles at the hexane–water interface. Figures 6.1 and 6.2 show the time-dependent interfacial tension measurements of *n*-dodecane-1-thiol and *n*-hexane-1-thiol-capped nanoparticles at the hexane–water interface. For these measurements, 4.4 nm *n*-dodecane-1-thiol and 4.3 nm *n*-hexane-1-thiol-capped nanoparticles were in the hexane phase prior to forming the droplet. The asymptotic forms of the time dependence of dynamic interfacial tension for $t \longrightarrow 0$ and $t \longrightarrow \infty$ were used to estimate the diffusivity of gold nanoparticles for early, D_0, and late times, D_∞ [94]. For each observed concentration, the equilibrium dynamic interfacial tension (i.e., $t \longrightarrow \infty$) was obtained by fitting straight lines to γ versus $t^{-\frac{1}{2}}$ at late times and by determining γ_∞ at the intercept; this technique was developed by *Fainerman et al.* [94] for surfactants. The slope of a plot of early time data (t$\lesssim$500 sec) of $\gamma(t)$ versus $t^{\frac{1}{2}}$ was used to calculate D_0. By using Equation 4.5 and Equation 4.7, the diffusion coefficients, D_0 and D_∞ for the nanoparticle suspensions may be estimated using both early-time and late-time interfacial data, respectively. The estimated values for D_0 and D_∞ from the dynamic interfacial tension data for each kind of gold nanoparticle are summarized in Tables 6.1 and 6.2. For dilute colloidal suspensions, such as the ones presented here, the Stokes-Einstein equation (See Equation 4.11) is expected to provide a reasonably accurate prediction for the diffusivity of nanoparticles in hexane. For 4.4 nm *n*-dodecane-1-thiol, and 4.3 nm *n*-hexane-1-thiol-capped gold nanoparticles, the

Stokes-Einstein diffusion, D_{S-E}, values were found to be $(3.36 \pm 0.45) \times 10^{-10}$ m^2/s and $(3.47 \pm 0.56) \times 10^{-10}$ m^2/s, respectively.

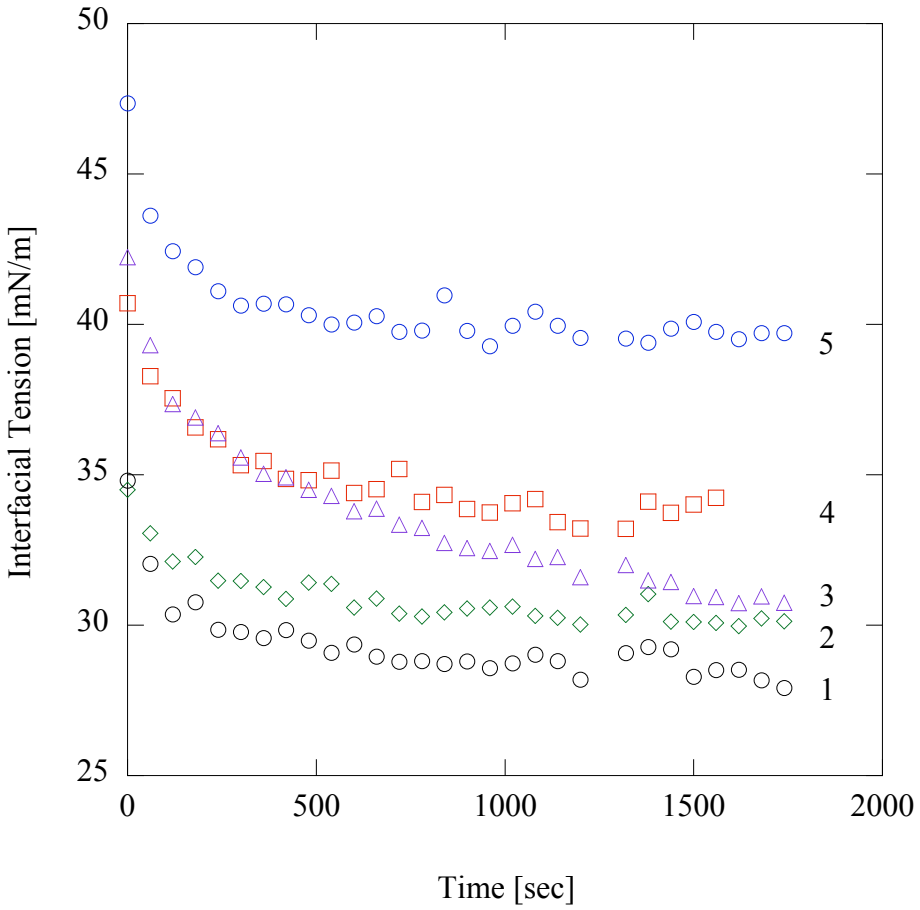

Figure 6.1: The interfacial tension of a water droplet in hexane with 4.4 ± 0.6 nm, n-dodecane-1-thiol capped gold nanoparticles at various concentrations: (1) 3.15×10^{16} particles/L, (2) 6.32×10^{15} particles/L, (3) 4.43×10^{15} particles/L, (4) 2.21×10^{15} particles/L and (5) 1.74×10^{15} particles/L.

The data obtained for the different types of nanoparticle suspensions were fitted by the Langmuir-Szyszkowski equation, which relates the interfacial tension to nanoparticle concentration in the bulk phase (See Equation 4.3) [93]. The parameters Γ_∞ and a_L, were obtained by fitting the Equation 4.3; using a nonlinear optimization

Table 6.1: Adsorption behaviour for 4.4 ± 0.6 nm n-dodecane-1-thiol capped gold nanoparticles at the hexane–water interface.

Nanoparticle concentration C [particle/L]	Equilibrium int. tension γ_∞[mN/m]	Diffusivity [m^2/s] D_0	D_∞
1.74×10^{15}	38.78	4.33×10^{-10}	3.93×10^{-11}
2.21×10^{15}	31.73	3.48×10^{-10}	1.73×10^{-11}
4.42×10^{15}	30.02	7.68×10^{-11}	1.44×10^{-11}
6.32×10^{15}	29.71	8.84×10^{-11}	5.05×10^{-13}
3.15×10^{16}	27.64	3.54×10^{-12}	1.50×10^{-13}

Table 6.2: Adsorption behaviour for 4.3 ± 0.7 nm n-hexane-1-thiol capped gold nanoparticles at the hexane–water interface.

Nanoparticle concentration C [particle/L]	Equilibrium int. tension γ_∞[mN/m]	Diffusivity [m^2/s] D_0	D_∞
1.92×10^{15}	37.92	3.51×10^{-10}	4.02×10^{-11}
4.00×10^{15}	37.61	3.14×10^{-10}	6.64×10^{-12}
5.49×10^{15}	36.46	7.48×10^{-11}	2.95×10^{-12}
2.75×10^{16}	34.03	4.51×10^{-12}	0.45×10^{-13}

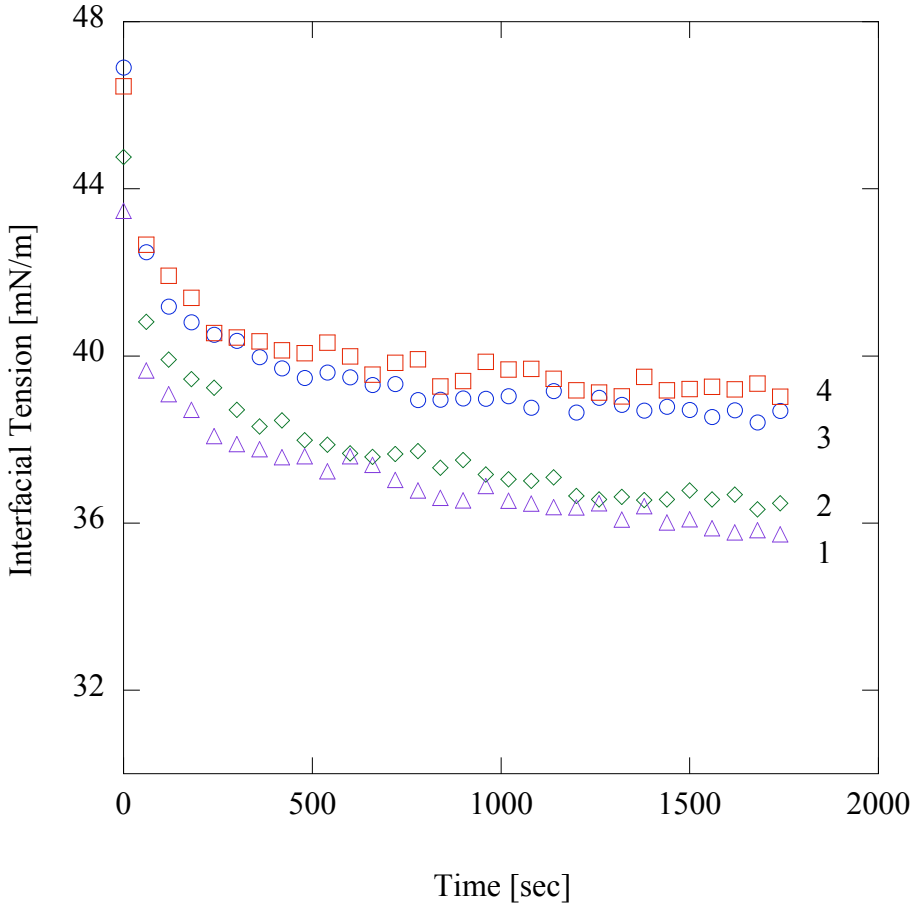

Figure 6.2: Interfacial tension of a water droplet in hexane with 4.3 ± 0.7 nm, *n*-hexane-1-thiol capped gold nanoparticles at various concentrations: (1) 2.75×10^{16} particles/L, (2) 5.49×10^{15} particles/L, (3) 4.00×10^{15} particles/L, and (4) 1.92×10^{15} particles/L.

scheme in MATLAB. These parameters were obtained by minimizing the sum of the square of errors between the experimental data and the predicted values. Using Equation 4.2, and the slope of the curve from the "equilibrium IFT vs concentration" graph, Γ_∞ was also estimated. The best fitting and estimated values for Γ_∞ from the experiment were almost the same.

6.1.1 Effects of Cap length and Capping Arrangements on the NPs Surface on Interfacial Tension

At the same bulk concentration, $4.3 \times 10^{15} \pm 7 \times 10^{13}$ particles/L,a significantly lower value of IFT is obtained for 4.4 nm *n*-dodecanthiol-1-thiol (30.02 vs 36.47) than 2.8 nm *n*-dodecane-1-thiol stabilized gold nanoparticles.These results again confirm that larger sized nanoparticles, decrease the IFT to a greater extent than smaller NPs. This can be seen from Table 6.1, and Table 5.2.

Although having almost the same size, and the same bulk concentration $(4.21 \pm 0.07) \times 10^{15}$ particles/L; the decrease in equilibrium IFT was found to be higher for 4.4 nm *n*-dodecane-1-thiol capped gold nanoparticles than 4.3 nm *n*-hexane-1-thiol capped gold nanoparticles. These results are shown in Table 6.1 and 6.2, and they indicate that the longer *n*-dodecane-1-thiol are more effective in reducing IFT than the shorter *n*-hexane-1-thiol. This result is in apparent contradiction with the finding (See Figure 5.6) for ~ 3 nm particles at a concentration of $(8.56 \pm 0.18) \times 10^{16}$ particles/L.

The obtained results can be analyzed with respect to the packing arrangement of ligands on the NPs surface. NPs are topologically equivalent or homeomorphic to spheres. The sulfur head groups of the ligands are tightly packed on the NP surface, and the tail groups ($-CH_3$) extend radially from the surface to the outer boundaries. The tail groups spacing of the adjacent ligands is larger than that of the head groups [108]. NPs capped with longer ligands take up more space between the adjacent tail ends than NPs with shorter ligands. Due to the longer molecular length, *n*-dodecane-1-thiol ligands are more flexible on the surface of AuNps than the shorter n-hexane-1-thiol ligands. This, in turn, increases the hydrophilic character of the *n*-dodecane-1-thiol capped gold nanoparticles compared to those capped with *n*-hexane-1-thiol.

This results in an increased surface activity of the n-dodecane-1-thiol capped gold nanoparticles compared to NPs of the same size but capped with n-hexane-1-thiol.

Reiterated from Chapter 5, 2.9 nm AuNPs capped with n-hexane-1-thiol are more surface active in reducing IFT than 2.8 nm AuNPs of same size capped with n-dodecane-1-thiol. Similarly sized ligands tend to spread with the same tilt angle on the NPs surface. Although having almost same size, the larger molecular length n-dodecane-1-thiol is more flexible than the shorter n-hexane-1-thiol on the NPs surface. However, the longer chains tend to cluster or lay along the NP surface, instead of splaying out uniformly over the NPs surface due to high curvature or poor packing on the NPs surface [109], [110],[108]. Thus, the shielding around the polar gold core reduces the surface activity of n-dodecane-1-thiol that of the shorter n-hexane-1-thiol. Consequently, at the same bulk concentration, a lower value of IFT is obtained using 2.9 nm n-hexane-1-thiol capped gold nanoparticles than using 2.8 nm n-dodecane-1-thiol capped gold nanoparticles. These results can be seen in Chapter 5, and also in work that has been published [97].

However, different adsorption behavior was observed for the smaller 2.9 nm n-hexane-1-thiol capped AuNPs and the larger 4.3 nm n-hexane-1-thiol capped AuNPs. The rate at which the IFT decreased was found to be higher for 2.9 nm n-hexane-1-thiol capped gold nanoparticles than that of 4.3 nm n-hexane-1-thiol capped gold nanoparticles at the same bulk concentration, $(4.16 \pm 0.1) \times 10^{15}$ particles/L.

For small NPs, the ligands tend to spread out more along the surface than on larger NPs; this means that the tilt angle of smaller NPs is greater than that of larger NPs. This leads to more space for their tail groups relative to their sulfur groups. The spacing between the tail groups decreases with an increase of NP diameter [111], [112]; whereas, the head group spacing remains unchanged as the size of the NP changes. The ligands are not ordered properly on small NPs; due to their high curvature [113], [110]. With an increase in NP size, the effect of curvature is reduced. The ligands are arranged more in a more orderly fashion on the NP surface as NP size increases. In the ordered phase, the ligands have the same tilt angle on the certain portions of the sphere [108], [112].

With the increase of the ratio of the radius of the NP to the length of the ligand, the polar core is more covered by the ordered ligands. This means that the tail groups

are more in contact with the water-hexane interface than that of the polar gold core. This, in turns, reduces the surface activity of 4.3 n-hexane-1-thiol compared to that of 2.9 nm n-hexane-1-thiol. As a result, at the same bulk concentration,$(4.16\pm0.1)\times10^{15}$ particles/L, a lower value of IFT is obtained using 2.9 nm n-hexane-1-thiol (31.70 vs 37.61) than using 4.3 nm n-hexane-1-thiol stabilized gold nanoparticles. This results can be seen in the Table 5.3 and Table 6.2.

From the aforementioned results, it is evident that the surface activity of the NP changes with the increase of the ratio of the radius of the NP to the length of the ligand. Therefore, the capping has a large effect on NP surface activity. These conclusions can also be confirmed by the results obtained by *Glaser et al.*[18]. The authors carried out a study using 10 nm gold nanoparticles stabilized with n-dodecane-1-thiol at the hexane-water interface [18]. They also observed that the larger the length of the capping agent, the larger the decrease in IFT [18]. They observed that at a bulk concentration of 7×10^{16} particles/L, the IFT drops to a value 35 mN/m. However, in this experiment, carried out at a bulk concentration of 3.65×10^{16} particles/L using 4.4 nm n-dodecane-1-thiol stabilized AuNPs, a significantly lower value of IFT was found. This showed that the surface activity of the AuNP changes with the increase of the ratio of the radius of the NP to the length of the ligand. *Ranatunga et al.* performed molecular dynamics simulations to characterize the behavior of surfactant funtionalized NPs, and also suggested that the coating has a profound effect on the interfacial activity of NPs. The functionalized ligands on the NPs surface are flexible; this permits particle deformation from an idealized spherical shape and results in a change in NPs activity [70]

6.1.2 Interaction Among the Non-mixed Nanoparticles at the Hexane–Water Interface.

In this section, data were analyzed to clarify that no interaction exists between non-mixed nanoparticles at the hexane–water interface. The data for 1.6 nm, 2.8 nm, 4.4 nm n-dodcanethiol capped AuNPs, and 2.9 nm, 4.3 nm n-hexanethiol capped AuNPs were analyzed in terms of the Frumkin models. The Frumkin adsorption isotherm and equation of state can be seen from Equation 4.13 and Equation 4.14, respectively. The obtained results show no interactions between the non-mixed nanoparticles at

the hexane–water interface. The parameters, Γ_∞, K and a_L were obtained to fit Equations 4.13 and 4.14 by using a nonlinear optimization scheme in MATLAB. The value of K is negative and very small positive number (< 1). Hence, the value K shows no evidence for favoring any interaction among the studied non-mixed nanoparticles [100],[101]. The best fit to the optimization procedure and the experimental data points for 1.6 nm, 2.8 nm *n*-dodecane-1-thiol capped AuNPs, and 2.9 nm *n*-hexane-1-thiol capped AuNPs were obtained. This can be seen in Figures 8.1, 8.2, and 8.3 in Appendix 8.2. The results indicate that interactions between unmixed nanopartices is insignificant. The obtained parameters from the Langmuir and the Frumkin models for synthesized AuNPs are shown in Table 6.3. The estimated adsorption parameters for AT-capped gold nanoparticles at the hexane–water interface are listed in Table 6.3. The adsorption parameters for 1.6 nm and 2.8 nm *n*-dodecane-1-thiol capped AuNPs, and 2.9 nm *n*-hexane-1-thiol capped AuNPs; are taken from Chapter 5. A maximum or nearly maximum coverage of nanoparticles at the interface was achieved at equilibrium for all of the nanoparticle concentrations that were tested (i.e., $\Gamma \cong \Gamma_{max}$).

Table 6.3: Adsorption constants obtained by an optimal fit for synthesized AuNPs under conditions shown in Table 3.2 and Table 3.3.

Capping mole.	Size [nm]	Model	Γ_∞ [mol/m^2]	Γ_{exp} [mol/m^2]	a_L [mol/m^3]	K
DT	1.6	L-M	1.27×10^{-6}	1.26×10^{-6}	1.15×10^{-7}	
		F-M	1.22×10^{-6}		3.49×10^{-6}	-7.29
DT	2.8	L-M	8.43×10^{-7}	9.19×10^{-7}	4.89×10^{-9}	
		F-M	8.30×10^{-7}		3.78×10^{-8}	-4.12
DT	4.4	L-M	5.99×10^{-7}	5.98×10^{-7}	5.87×10^{-12}	
		F-M	5.94×10^{-7}		5.82×10^{-13}	0.05
HT	2.9	L-M	7.82×10^{-7}	8.50×10^{-7}	2.38×10^{-10}	
		F-M	7.74×10^{-7}		1.52×10^{-10}	0.80
HT	4.3	L-M	5.92×10^{-7}	6.22×10^{-7}	5.78×10^{-10}	
		F-M	5.54×10^{-7}		2.94×10^{-10}	-1.11

Nanoparticles form self-assemble layers at the hexane–water interface.

To quantify the packing arrangements of nanoparticles at the hexane-water interface; the hydrodynamic diameter has to be precisely defined. The hydrodynamic diameter, d_H, is defined by $d_H = d_{TEM} + (2L)$, where d_{TEM} is the TEM measured core diameter of the particle, and L is the fully extended molecular length of the capping agent (attached to the particle). The molecular length is estimated by the formula $L = 0.12(n+1)$ nm, where n is the number of carbon atoms [108]. The estimated molecular lengths for hexanethiol (L_6) and dodecanthiol (L_{12}) are 0.86 nm and 1.56 nm. The value of d_H was estimated for all studied nanoparticles by following the method outlined by *Wuelfing et al.*[111]. *Wuelfing et al.* estimated the values d_H, for gold cores ($d \sim 1 - 5$) nm coated with self-assembled monolayers of alkhane-thiolate ligands. They stated that d_H values were in agreement with $d_{TEM} + (2L)$ values for the small core. However, for the larger core, d_H values were about a half monolayer shorter than $d_{TEM} + (2L)$. Adsorption density, Γ_∞, were estimated theoretically by taking into account the cap length, and also without consideration of the cap size. The estimated d_H and Γ_∞ values are shown in Table 6.4. Using Equation 4.9 and Equation 4.10, the minimum area occupied by the particles, and the adsorption energy at the hexane-water interface was estimated. This value is shown in Table 6.5. The low values of A_{min} indicate that the nanoparticles at the hexane–water interface formed tightly packed layers. The adsorption tendency is much higher for 4.4 nm n-dodecane-1-thiol gold particles than for 4.3 nm n-hexane-1-thiol capped nanoparticles, which is most likely caused by a significant difference in the values of free energy of adsorption for the two nanoparticle types. When the absolute value of ΔG_{ads} is high, a higher adsorption at the interface is obtained [95]; these results can be seen in Table 6.5. For 4.4 ± 0.6 nm n-dodecane-1-thiol capped particles, the theoretical maximum adsorption density is Γ_{squ} for a square arrangement of nanoparticles at the interface; and Γ_{hex} for a hexagonal (i.e., triangular) arrangement of nanoparticles at the interface can be seen in Table 6.4. The estimated value for $\Gamma_\infty = 5.99 \times 10^{-7}$ mol/m^2 is consistent with Γ_{hex}, indicating that the particles may be arranged in a hexagonal close packed arrangement at the interface. Similarly, for 4.3 ± 0.7 nm n-hexane-1-thiol capped particles, $\Gamma_\infty = 5.92 \times 10^{-7}$ mol/m^2 is consistent with the value Γ_{hex}; this means a close-packed hexagonal layers arrangement of the nanoparticles at the interface. *Dai et al.* observed the multiphase interactions and

Table 6.4: Estimated hydrodynamic particle diameter and theoretically estimated adsorption density for synthesized capped AuNPs under conditions shown in Table 3.2 and Table 3.3.

Capping molecule	Mol. length [nm]	d_{TEM} [nm]	d_h [nm]	Without cap		With cap	
				Γ_{squ} $\times 10^{-6}$ [mol/m^2]	Γ_{tri} $\times 10^{-6}$ [mol/m^2]	Γ_{squ} $\times 10^{-7}$ [mol/m^2]	Γ_{tri} $\times 10^{-7}$ [mol/m^2]
DT	$L_{12} = 1.56$	1.6	4.72	0.71	0.82	0.75	0.87
		($\pm$0.278)	($\pm$0.28)	($\pm$0.23)	($\pm$0.27)	($\pm$0.09)	($\pm$0.1)
DT	, ,	2.8	5.92	0.22	0.25	0.48	0.55
		($\pm$0.273)	($\pm$0.27)	($\pm$0.42)	($\pm$0.05)	($\pm$0.04)	($\pm$0.05)
DT	, ,	4.4	7.52	0.09	0.1	0.3	0.34
		($\pm$0.6)	($\pm$0.6)	($\pm$0.02)	($\pm$0.02)	($\pm$0.04)	($\pm$0.05)
HT	$L_6 = 0.84$	2.9	4.52	0.2	0.23	0.80	0.92
		($\pm$0.188)	($\pm$0.18)	($\pm$0.02)	($\pm$0.03)	($\pm$0.06)	($\pm$0.07)
HT	, ,	4.3	5.98	0.09	0.11	0.48	0.55
		($\pm$0.7)	($\pm$0.7)	($\pm$0.03)	($\pm$0.03)	($\pm$0.11)	($\pm$0.12)

Table 6.5: Adsorption parameter for synthesized AT-capped gold nanoparticles under conditions shown in Tables 3.2 and 3.3.

Capping mole.	Size [nm]	ΔG_{ads} [kJ/mol]	A_{min} [nm^2/particle]
DT	1.6	-39.5	1.32
DT	2.8	-47.0	1.97
DT	4.4	-64.0	2.77
HT	2.9	-54.8	2.12
HT	4.3	-52.0	2.80

self-assembled structure of nanoparticles at a trichloroethylene-water interface. They also found that 1-5 nm dodecanethiol-capped silver nanoparticles formed multilayers at the interface [114].

6.2 Nanoparticle Mixtures at the Hexane-Water Interface

For insignificant interactions among the nanoparticle, the Langmuir isotherm used for the single components can be generalized for two or multicomponent systems [102],[103]. The Langmuir isotherm for two component systems can be seen in Chapter 4. Using Equations 4.15, 4.16 and 4.17, the surface adsorption density for components A and B was estimated for NPs mixtures; values correspond to Γ_A and Γ_B [102],[103]. The parameters, Γ_{max}, $K_{L,A}$, and $K_{L,B}$, were obtained by fitting Equations 4.15, 4.16 and 4.17 using a nonlinear optimization scheme in MATLAB. The estimated values of Γ_A and Γ_B for all nanoparticle mixtures studied can be seen in Tables 6.6, 6.7 and 6.8.

As $\Gamma_{m,A} \neq \Gamma_{max}$, Equations 4.15, 4.16 and 4.17, cannot be used for studied nanoparticles mixtures. The obtained results indicate that there is significant surface interaction among nanoparticles in the mixtures. In light of this, the interaction parameters for mixtures of nanoparticles were estimated next.

6.2.1 Interfacial Properties and Nanoparticle–Nanoparticle Interaction During Adsorption From Nanoparticle Mixtures

In this section, the interfacial properties of three nanoparticle mixtures and respective nanoparticle-to-nanoparticle interactions at the hexane-water interface are quantitatively discussed. Using Equation 4.18 and Equation 4.19, the mole fraction of nanoparticles at the interface, X_1, and the interaction parameter, β, were estimated at the hexane-water interface. These parameters were estimated using interfacial tension isotherms that were obtained for each type of nanoparticle prior to mixing and data obtained for the mixed suspensions.

Table 6.6: Adsorption density for mixtures of 1.6 nm and 2.8 nm n-dodecane-1-thiol capped gold nanoparticles at the water–hexane interface.

Unmixed Conc. C [particle/L] 1.6 [nm]– 2.8[nm]	Mixture Con. C_t [particle/L]	Equilibrium IFT γ_∞ [mN/m]	Ads. density for NP1 Γ_A [mol/m^2]	Ads. density for NP2 Γ_B [mol/m^2]	Max. density Γ_{max} [mol/m^2]
$2.12 \times 10^{15} - 2.12 \times 10^{16}$	2.10×10^{15}	39.45	9.29×10^{-9}	6.89×10^{-7}	6.99×10^{-7}
$4.26 \times 10^{16} - 4.24 \times 10^{16}$	4.24×10^{16}	35.50	1.00×10^{-8}	6.88×10^{-7}	, ,
$1.06 \times 10^{17} - 8.48 \times 10^{16}$	9.46×10^{16}	35.46	1.00×10^{-8}	6.88×10^{-7}	, ,
$1.28 \times 10^{17} - 1.27 \times 10^{17}$	1.26×10^{17}	35.30	9.29×10^{-8}	6.89×10^{-7}	, ,
$1.28 \times 10^{17} - 2.12 \times 10^{16}$	6.14×10^{16}	37.53	5.31×10^{-8}	6.46×10^{-7}	, ,
$1.28 \times 10^{17} - 4.24 \times 10^{16}$	8.49×10^{16}	35.28	2.71×10^{-8}	6.71×10^{-7}	, ,

Table 6.7: Adsorption density for mixtures of 2.8 nm and 4.4 nm n-dodecane-1-thiol capped gold nanoparticles at the water–hexane interface.

Unmixed Conc. C [particle/L] 2.8 [nm]– 4.4[nm]	Mixture Con. C_t [particle/L]	Equilibrium IFT γ_∞ [mN/m]	Ads. density for NP1 Γ_A [mol/m^2]	Ads. density for NP2 Γ_B [mol/m^2]	Max. density Γ_{max} [mol/m^2]
$4.24 \times 10^{16} - 1.74 \times 10^{15}$	2.20×10^{16}	35.72	1.31×10^{-8}	4.51×10^{-7}	4.65×10^{-7}
$8.49 \times 10^{16} - 4.42 \times 10^{15}$	2.98×10^{16}	34.65	1.04×10^{-8}	4.54×10^{-7}	, ,
$8.49 \times 10^{16} - 2.21 \times 10^{15}$	4.35×10^{16}	39.77	1.75×10^{-8}	4.47×10^{-7}	..
$1.27 \times 10^{17} - 1.74 \times 10^{15}$	6.20×10^{16}	36.43	2.57×10^{-8}	4.39×10^{-7}	, ,

Table 6.8: Adsorption density for mixtures of 4.3 nm and 4.4 nm n-dodecane-1-thiol capped gold nanoparticles at the water–hexane interface.

Unmixed Conc. C [particle/L] 4.3 [nm]- 4.4[nm]	Mixture Con. C_t [particle/L]	Equilibrium IFT γ_∞ [mN/m]	Ads. density for NP1 Γ_A [mol/m^2]	Ads. density for NP2 Γ_B [mol/m^2]	Max. density Γ_{max} [mol/m^2]
$2.08 \times 10^{15} - 1.74 \times 10^{15}$	1.91×10^{15}	40.64	5.75×10^{-9}	3.99×10^{-7}	4.05×10^{-7}
$1.92 \times 10^{17} - 1.74 \times 10^{15}$	1.80×10^{15}	37.27	5.30×10^{-9}	3.99×10^{-7}	, ,
$5.49 \times 10^{15} - 1.74 \times 10^{15}$	4.24×10^{15}	41.18	4.02×10^{-8}	3.64×10^{-7}	, ,
$2.75 \times 10^{14} - 2.21 \times 10^{15}$	1.48×10^{16}	37.42	5.01×10^{-8}	3.54×10^{-7}	, ,
$2.75 \times 10^{16} - 4.42 \times 10^{15}$	1.98×10^{16}	37.25	4.02×10^{-8}	3.64×10^{-7}	, ,
$5.49 \times 10^{15} - 1.74 \times 10^{15}$	3.60×10^{15}	41.13	1.23×10^{-8}	3.92×10^{-7}	, ,
$5.49 \times 10^{17} - 6.32 \times 10^{15}$	5.70×10^{15}	36.39	1.51×10^{-8}	3.89×10^{-7}	, ,

Mixtures of 1.6 nm and 2.8 nm *n*-dodecane-1-thiol capped gold nanoparticles

Experiments were done to understand the interfacial properties of a mixture of 1.6 nm and 2.8 nm *n*-dodecane-thiol capped nanoparticles. The adsorption parameters for each type of nanoparticle can be seen in Tables 6.3 and 6.5. These values are taken from Chapter 5.

Figure 6.3 illustrates the interfacial tension isotherms at the hexane–water interface for two types of nanoparticles and an equimolar mixture of the two. Equilibrium IFT for two studied nanoparticle mixtures are shown in Table 6.9. Table 6.10 shows the interaction action parameter, β, for various mole fractions of the two types of nanoparticles in the bulk phase.

Figure 6.3 shows that 2.8 nm particles lowered the interfacial tension at the hexane-water interface much more effectively than 1.6 nm particles. This was expected, as the larger nanoparticles lead to a larger drop in the interfacial tension [1], [97]. The minimum area occupied by a particle at the interface (A_{min}) is 1.97 nm^2 for 2.8 nm nanoparticles, and 1.32 nm^2 for 1.6 nm particles. The estimated low value of A_{min} indicates that the hexane–water interface is tightly packed interface. The difference between the estimated ΔG_{ads} for the two types of nanoparticles can be seen in Table 6.5. Although the difference is not great, it still indicates a higher tendency for 2.8 nm nanoparticles to adsorb to the interface. The adsorption behaviour for mixtures of 1.6 nm and 2.8 nm *n*-dodecane-1-thiol capped gold nanoparticles can be seen in Table 6.9.

The estimated values of surface mole fraction, X_1, and β, for mixtures with different molar ratios of 1.6 nm and 2.8 nm particles are shown in Table 6.10. The table shows that the composition of nanoparticles at the interfacial layer is different from the composition of nanoparticles in the bulk hexane phase. Estimated values for β indicate that there is a repulsive interaction between the nanoparticles at the hexane–water interface. For equimolar mixtures, the values of X_1 are within the range of 0.51 to 0.66. The composition of nanoparticles at the interfacial layer cannot be predicted solely by the higher relative interfacial activities of the individual nanoparticles in the mixture. However, the interfacial area of non-equimolar mixtures is primarily occupied by nanoparticles with a higher activity (i.e., 2.8 nm). As the mole fraction

Table 6.9: Equilibrium IFT for mixtures of 1.6 nm and 2.8 nm n-dodecane-1-thiol capped gold nanoparticles at the water–hexane interface.

Unmixed concentration C [particle/L] 1.6 [nm]–2.8[nm]	Mixture concentration C_t [particle/L]	Equilibrium int. tension γ_∞[mN/m]	Mole Fraction α
$2.12 \times 10^{16} - 2.12 \times 10^{16}$	2.10×10^{16}	39.45	0.5
$4.26 \times 10^{16} - 4.24 \times 10^{16}$	4.24×10^{16}	35.50	0.5
$1.06 \times 10^{17} - 8.48 \times 10^{16}$	9.46×10^{16}	35.46	0.52
$1.28 \times 10^{17} - 1.27 \times 10^{17}$	1.26×10^{17}	35.30	0.5
$1.28 \times 10^{17} - 2.12 \times 10^{16}$	6.14×10^{16}	37.53	0.86
$1.28 \times 10^{17} - 4.24 \times 10^{16}$	8.49×10^{16}	35.28	0.75

Table 6.10: Interfacial mole fraction of 1.6 nm n-dodecane-1-thiol capped gold nanoparticles at the water–hexane interface and their interaction parameter.

Mole Fraction α	Surface Fraction X_1	Interaction Parameter β
0.5	0.51	8.77
0.5	0.52	6.88
0.52	0.51	9.85
0.5	0.54	8.53
0.86	0.43	11.80
0.75	0.47	10.30

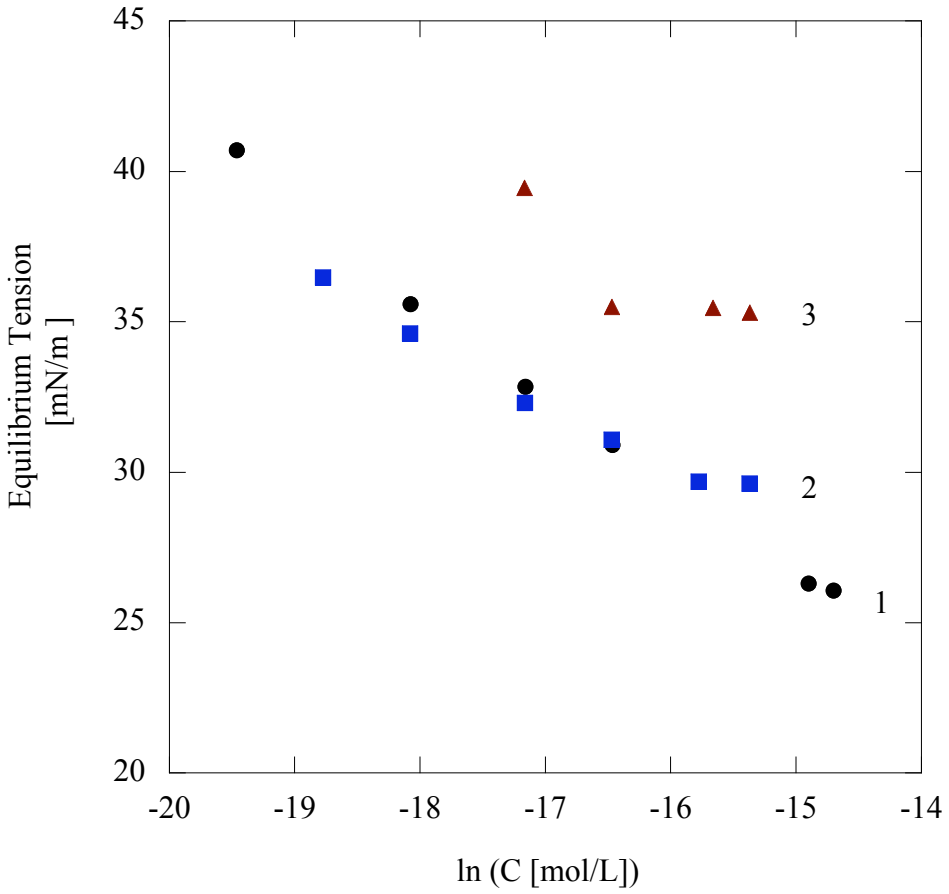

Figure 6.3: Extrapolated equilibrium interfacial tension of (1) 1.6 ± 0.28 nm, (2) 2.8 ± 0.27 nm *n*-dodecane-1-thiol capped gold nanoparticles and (3) their equimolar mixture

of 1.6 nm particles increases, fewer are found at the interface. There is a preference for the 2.8 nm particles to adsorb at the interface over the 1.6 nm particles, which indicates that higher activity nanoparticles are more prevalent at the interfacial layer. In effect, the presence of 1.6 nm particles at the interface is limited due to their lower activity when compared to the higher activity of the larger nanoparticles. It was found by *Lin et al.* [15], that larger nanoparticles are more stable at an interface than smaller particles. Hence, larger nanoparticles try to dominate at the hexane–water interface. The positive values that was estimated for β indicates a strong repulsion between the nanoparticles adsorbed at the interface. These results can be

seen in Table 6.9 and Table 6.10.

Mixtures of 2.8 nm and 4.4 nm *n*-dodecane-1-thiol capped gold nanoparticles.

This study was performed with a mixture of 2.8 nm and 4.4 nm *n*-dodecane-1-thiol nanoparticles. The adsorption behaviour for non-equimolar mixtures of nanoparticles was also studied. These are shown in Tables 6.11 and 6.12, respectively.

Table 6.11: Equilibrium IFT for mixtures of 2.8 nm and 4.4 nm *n*-dodecane-1-thiol capped gold nanoparticles at the water–hexane interface.

Unmixed Concentration C [particle/L] 2.8 [nm] – 4.4 [nm]	Mixture Concentration C_t [particle/L]	Equilibrium int. tension γ_∞[mN/m]	Mole Fraction α
$4.24 \times 10^{16} - 1.74 \times 10^{15}$	2.20×10^{16}	35.72	0.96
$8.49 \times 10^{16} - 4.42 \times 10^{15}$	2.98×10^{16}	34.65	0.95
$8.49 \times 10^{16} - 2.21 \times 10^{15}$	4.35×10^{16}	39.77	0.97
$1.27 \times 10^{17} - 1.74 \times 10^{15}$	6.38×10^{16}	35.22	0.98

Our findings show that the interfacial area was mainly occupied by the higher activity 4.4 nm particles. Hence, at the interface, the smaller particles were replaced by the larger particles [15].

6.2.2 Mixtures of 4.4 nm *n*-dodecane-1-thiol and 4.3 nm *n*-hexane-1-thiol capped gold nanoparticles.

The interfacial properties (i.e., equilibrium IFT, surface mole fraction, interaction parameter) of a mixture of same size but different ligand gold nanaoparticles were analyzed. The results obtained for non-equimolar mixtures of 4.4 nm *n*-dodecane-1-thiol and 4.3 nm *n*-hexane-1-thiol capped gold nanoparticles can be seen in Table 6.13 and Table 6.14.

Table 6.12: Interfacial mole fraction of 2.8 nm *n*-dodecane-1-thiol capped gold nanoparticles at the different concentrations.

Mole Fraction α	Surface Fraction X_1	Interaction Parameter β
0.96	0.54	7.38
0.95	0.47	7.06
0.97	0.44	15.0
0.98	0.49	8.95

Table 6.13: Equilibrium IFT for mixtures of 4.3 nm *n*-hexane-1-thiol and 4.4 nm *n*-dodecane-1-thiol capped gold nanoparticles at the water–hexane interface.

Unmixed Concentration C [particle/L] 4.3 [nm]–4.4[nm]	Mixture Concentration C_t [particle/L]	Equilibrium int. tension γ_∞[mN/m]	Mole Fraction α
$2.08 \times 10^{15} - 1.74 \times 10^{15}$	1.91×10^{15}	41.64	0.54
$1.92 \times 10^{17} - 1.74 \times 10^{15}$	1.80×10^{15}	37.27	0.52
$5.49 \times 10^{15} - 1.74 \times 10^{15}$	4.24×10^{15}	41.18	0.90
$2.75 \times 10^{14} - 2.21 \times 10^{15}$	1.48×10^{16}	37.42	0.92
$2.75 \times 10^{16} - 4.42 \times 10^{15}$	1.98×10^{16}	37.38	0.90
$5.49 \times 10^{15} - 1.74 \times 10^{15}$	3.60×10^{15}	41.13	0.76
$5.49 \times 10^{17} - 6.32 \times 10^{15}$	5.70×10^{15}	36.39	0.72

Table 6.14: Interfacial mole fraction of the 4.3 nm n-hexane-1-thiol capped gold nanoparticles and the molecular interaction parameter at the water–hexane interface.

Mole Fraction α	Surface Fraction X_1	Interaction Parameter β
0.54	0.63	8.64
0.52	0.68	4.03
0.90	0.50	10.1
0.92	0.53	10.8
0.90	0.57	11.3
0.76	0.55	10.9
0.72	0.78	4.56

The interfacial area was mainly occupied by 4.3 nm n-hexane-1-thiol capped nanoparticles. The longer chain length on the 4.4 nm n-dodecane-1-thiol capped particles may permit more van der Waals forces between the caps; resulting in a more stable interaction at the bulk phase. As a result, a more complex, intertwined, stable structure would result at the bulk phase, so there would be less concentration of n-dodecane-1-thiol gold nanoparticles adsorbed at the interface. The obtained IFT and β for non-equimolar mixtures of 4.3 nm n-hexane-1-thiol- and 4.4 nm n-dodecane-1-thiol capped gold nanoparticles are shown in Table 6.13 and Table 6.14. The molar concentration of 4.3 nm n-hexane-1-thiol capped nanoparticles was always higher than that for 4.4 nm nanoparticles. As a result, the interfacial area was mainly occupied by the lower activity particle, 4.3 nm n-hexane-1-thiol. The results show a repulsive interaction (i.e., β is positive) between nanoparticles adsorbed at the interface.

6.3 Summary

This study was performed with the aim to understand the interaction behaviour of mixtures of different sized and different ligand stablized gold nanoparticles at the hexane-water interface using pendant drop tensiometry. Using the NIBM theory that was developed for mixtures of surfactants, the interaction behaviour of alkanethiol-capped gold nanoparticles at the hexane–water interface was studied. The composition of the interfacial layer and the interaction parameter between two types of nanoparticles were then estimated using this theory. These results may prove useful in predicting the interfacial tension of nanoparticle mixtures and in determining the applicability of the NIBM theory to mixtures of nanoparticles. No interaction was observed between the unmixed studied nanoparticles. However, a significant interaction was found to be existed at the interface between NPs in a mixture. The composition of NPs at the interfacial layer is different from the composition of NPs in the bulk. It was observed that the most active nanoparticles concentrated at the interface. Regardless of the NP composition, all NP mixtures showed a repulsive interaction at the interface. The positive values of β indicate a repulsive interaction between the adsorbed nanoparticle types at the interface.

The next chapter illustrates the effects of temperature, pH and ionic strength of the aqueous phase on IFT at the liquid-liquid interface.

Chapter 7

Effects of Temperature, pH and Ionic Strength on the Adsorption of Nanoparticles at Liquid-Liquid Interfaces

This chapter describes the effects of temperature, ionic strength, and pH on the equilibrium and dynamic IFT of 4.4 nm gold nanopraticles capped with *n*-dodecanethiol at the liquid-liquid interfaces. To our knowledge, no other study has been done to characterize how pH, temperature and ionic strength affects the adsorption behavior of nanoparticles at oil–water interfaces. The results reported here showed that these factors significantly affect the tension of liquid–liquid interfaces with adsorbed gold nanoparticles.

7.1 Temperature Effect on the Adsorption Kinetics of *n*-Dodecane-1-Thiol Capped Gold Nanoparticles

The effect of temperature on the adsorption of 4.4 nm gold nanoparticles at the nonane-water interface was studied at two different bulk nanoparticle concentrations. Hexane was not suitable for temperature studies because of its high volatility at elevated temperatures. Measurements were carried out at pH =7.0 in the absence of NaCl. The middle point of acidic and basic conditions is pH=7.0; hence it was chosen to study the effect of temperature on adsorption kinetics of Au nanoparticles at liquid-liquid interfaces.The study was done in the time range 0 to 1500 sec. Results are summarized in Table 7.1 and Table 7.2 for low and high bulk nanoparticle concentrations, respectively. As shown in Figure 7.1, the equilibrium IFT increases as the temperature increases for both bulk nanoparticle concentrations. The dynamic IFT behavior of the gold nanoparticles as a function of temperature at nonane–water interface for the studied concentrations can be seen in Figure 7.2 and Figure 7.3.

Table 7.1: Effect of temperature on the adsorption behavior of *n*-dodecane-1-thiol capped gold nanoparticles at the nonane–water interface for low $(5.06 \pm 0.5) \times 10^{15}$ particle/L) bulk nanoparticle concentration.

Temperature	Equilibrium IFT	Diffusion Coefficient [m^2/s]			Adsorption Barrier
^oC	γ_∞ [mN/m]	D_{S-E} [m^2/s]	D_0 [m^2/s]	D_∞ [m^2/s]	ΔE [J]
26	35.17 ± 0.21	1.51×10^{-10}	1.22×10^{-10}	1.06×10^{-12}	1.95×10^{-20}
29	38.99 ± 0.3	1.61×10^{-10}	0.4×10^{-10}	1.39×10^{-12}	1.38×10^{-20}
30	41.14 ± 0.2	1.64×10^{-10}	0.38×10^{-10}	4.0×10^{-12}	0.92×10^{-20}
40	44.87 ± 0.17	1.95×10^{-10}	0.15×10^{-10}	12.3×10^{-12}	0.08×10^{-20}
43	43.45 ± 0.1	2.03×10^{-10}	0.34×10^{-10}	7.32×10^{-12}	0.63×10^{-20}

It was noticed that IFT reached almost a constant value after 40°C for low bulk nanoparticle concentrations, and around 38°C for high concentrations (See Figure 7.1). However, it was decided to continue the study up to 43°C. It was found that

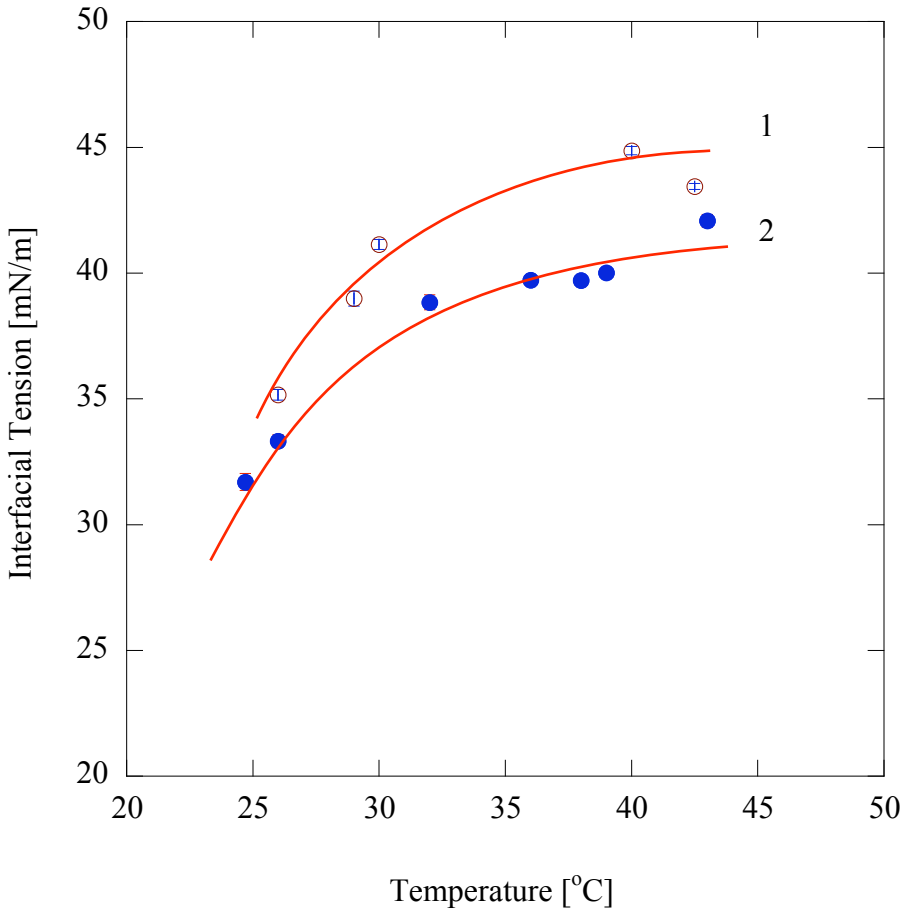

Figure 7.1: Water-nonane equilibrium interfacial tension as a function of temperature in the presence of Au nanoparticles capped with n-dodecane-1-thiol (1) at low $(5.06 \pm 0.5) \times 10^{15}$ particle/L and (2) at high $(1.2 \pm 0.1) \times 10^{16}$ particle/L bulk nanoparticle concentration. Lines are a guide to the eye.

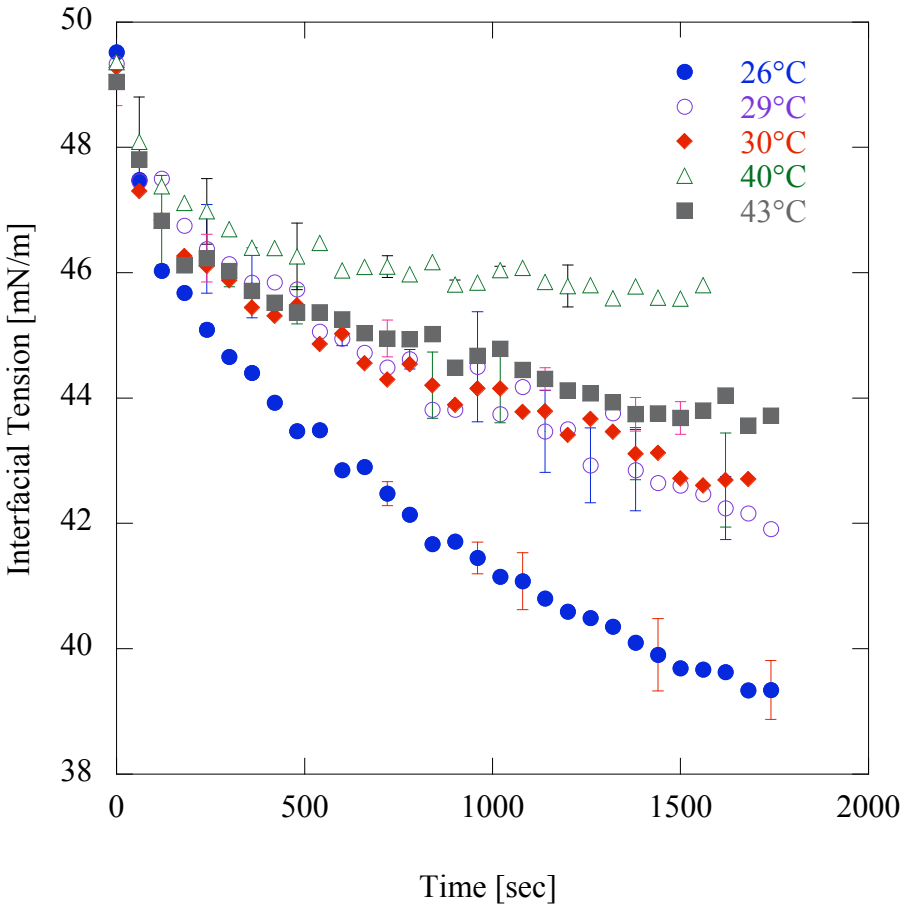

Figure 7.2: Water-nonane dynamic interfacial tension as a function of temperature in the presence of Au nanoparticles capped with n-dodecane-1-thiol at low $(5.06 \pm 0.5) \times 10^{15}$ particle/L bulk nanoparticle concentration.

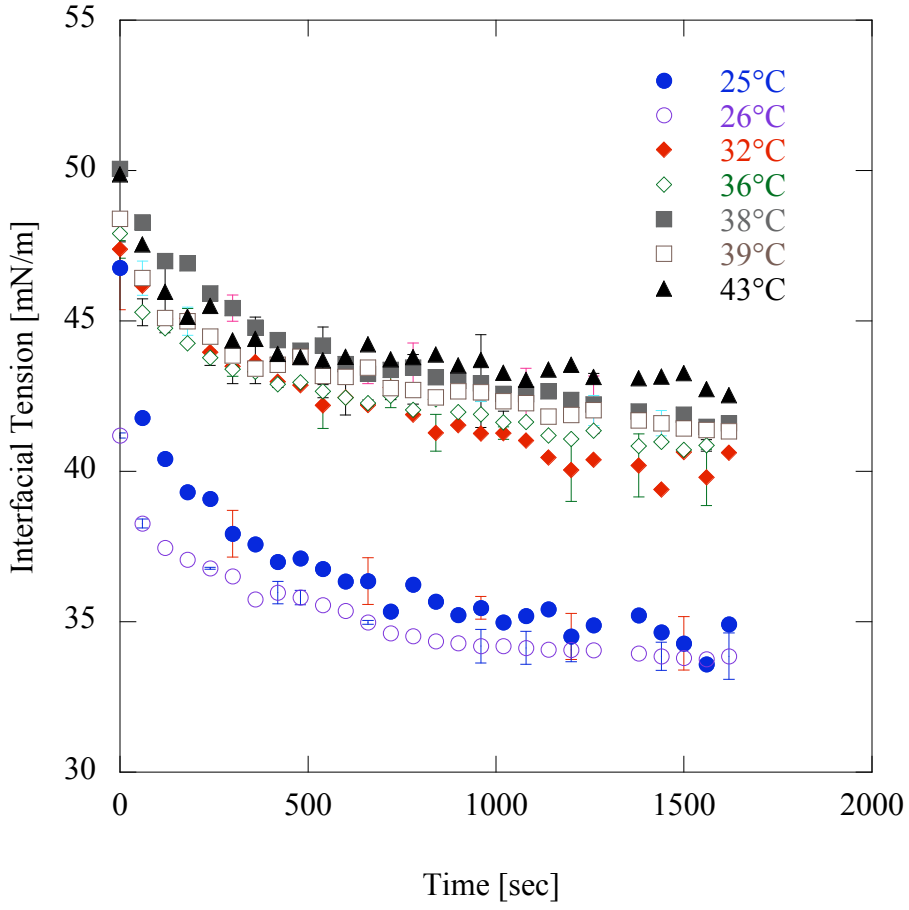

Figure 7.3: Water-nonane dynamic interfacial tension as a function of temperature in the presence of Au nanoparticles capped with *n*-dodecane-1-thiol at high $(1.2 \pm 0.1) \times 10^{16}$ particle/L) bulk nanoparticle concentration.

Table 7.2: Effect of temperature on the adsorption behavior of n-dodecane-1-thiol capped gold nanoparticles at the nonane–water interface for high $(1.2 \pm 0.1) \times 10^{16}$ particle/L) bulk nanoparticle concentration

Temperature	Equilibrium IFT	Diffusion Coefficient			Adsorption Barrier
^oC	γ_∞ [mN/m]	D_{S-E} [m^2/s]	D_0 [m^2/s]	D_∞ [m^2/s]	ΔE [J]
25	31.7 ± 0.34	1.52×10^{-10}	3.19×10^{-11}	4.84×10^{-13}	2.67×10^{-20}
26	33.33 ± 0.25	1.51×10^{-10}	—	—	—
32	38.84 ± 0.3	1.70×10^{-10}	1.95×10^{-11}	2.54×10^{-12}	1.82×10^{-20}
36	39.72 ± 0.2	1.82×10^{-10}	0.84×10^{-11}	1.25×10^{-12}	0.81×10^{-20}
38	39.71 ± 0.2	1.89×10^{-10}	2.28×10^{-11}	1.13×10^{-12}	1.29×10^{-20}
39	40.02 ± 0.15	1.95×10^{-10}	1.62×10^{-11}	1.83×10^{-12}	0.94×10^{-20}
43	42.08 ± 0.25	2.03×10^{-10}	1.67×10^{-11}	4.04×10^{-12}	0.61×10^{-20}

bulk concentration has a profound effect on adsorption kinetics of nanoparticles at the liquid-liquid interfaces [97]. Hence, for this work, the focus was given to explore the temperature effect on the adsorption kinetics of the nanoparticles for two bulk concentrations at liquid-liquid interfaces. Obtained results were not comparable to each other as bulk concentrations were different. The decrease in IFT is high for higher bulk concentration and low for lower bulk concentration. Results, shown in Table 7.1 and Table 7.2, were independent of each other. Therefore, temperature range inconsistency did not have any affect in understanding the temperature effect at two studied concentrations.

Using Equation 4.5 and Equation 4.7, the diffusion coefficient of the nanoparticles at the early times, D_0 and the late times D_∞ in the adsorption process were estimated for all observed temperatures. Accounting for the effect of temperature on the viscosity and the diffusion coefficient, the D_{S-E} value was estimated using Equation. 4.11 for the studied nanoparticles and can be found in Tables 7.1 and 7.2. It can be seen from Table 7.1, that at low bulk nanoparticle concentrations, the nanoparticles undergo almost free diffusion (i.e., $D_0 \simeq D_{S_E}$) at early times. At late times the diffusion coefficient, D_∞, decreases for all temperatures. For higher bulk nanoparticle concentrations, however, the particles did not exhibit free diffusion (i.e., $D_0 \neq D_{S_E}$)

at early times $D_\infty < D_0$ for all measured temperatures. A similar behaviour has been observed by *Kutuzov et al.* [1] for CdSe nanoparticles at the toluene–water interface for a constant temperature.

Taking the effective diffusivity equal to D_∞, the potential barrier to adsorption was calculated for the highest nanoparticle concentrations (1.2×10^{16} particles/L). At 25^oC and 43^oC, the estimated values of the potential barrier to adsorption, ΔE, are 2.67×10^{-20} J and 0.61×10^{-20} J, respectively. A similar behaviour was observed for the lower nanoparticle concentration suspensions (5.06×10^{15} particles/L). These results indicate that with an increase in temperature, the adsorption barrier decreases significantly for lower nanoparticle concentrations but remains almost constant at higher bulk nanoparticle concentrations. As temperature increases, the particles exhibit a near diffusion-controlled adsorption. Hence, the nanoparticles may diffuse from the interface back into the bulk phase. *Ye et al.*[34] and *Ataev*[44] have seen an increase in the IFT at oil–water interfaces (with and without added surfactants) as the temperature is raised. *Ye et al.* have argued that this behavior is due to the diffusion of surfactants from the interface into the oil phase. *Lutton et al.*[115] have argued that as the temperature increases the order of a crystalline monolayer of surfactant molecules adsorbed at the interface is lost. It is surmised that same effect may occur for nanoparticles adsorbed at liquid–liquid interfaces. Using Eq.4.2, the maximum adsorption density was estimated as $\Gamma_\infty = (8.52 \pm 0.39) \times 10^{-7}$mol/m^2 and $\Gamma_\infty = (6.05 \pm 1.29) \times 10^{-7}$mol/m^2 at the temperatures of 26^oC and 43^oC. The intrapolated value of maximum adsorption density was used for all of the other temperatures that were studied. Thus, as the temperature is increased, particle interfacial coverage decreases. At these temperatures, using Equation 4.9, the estimated area per particle, A_{min}, was found to be 1.94×10^{-18} m^2 and 2.74×10^{-18} m^2, respectively. Considering the area occupied by a single nanoparticle, it is obvious that fewer nanoparticles are necessary to saturate the interface at 43^oC than 26^oC, indicating that as temperature increases nanoparticles diffuse from the interface back into the bulk phase. The particles reached a maximum coverage at the temperature 26^oC and decreases as the temperature reached to 43^oC.

7.2 Effect of Ionic Strength on the Adsorption Kinetics of *n*-Dodecane-1-Thiol Capped Gold Nanoparticles

The effect of ionic strength was characterized by conducting experiments over a wide range of ionic strengths (NaCl concentrations from 0 to 0.5 M), at a constant pH of 7.0 in ambient atmosphere and a constant temperature of 297.65 K. The middle point of acidic and basic conditions is pH=7.0; hence it was chosen to study the effect of ionic strength on adsorption kinetics of Au nanoparticles at liquid-liquid interfaces. The study was done in the time range 0 to 1500 sec. The dynamic IFT behavior of the nanoparticles at constant bulk concentration and varying ionic strengths can be seen in Figure 7.5 and Figure 7.6. Obtained results were not comparable to each other as bulk concentrations were different. The reduction in IFT is high for higher bulk concentration and low for lower bulk concentration. Results, shown in Table 7.3 and Table 7.4, were independent of each other. Hence, inconsistency in NaCl concentrations did not have any affect in understanding the adsorption kinetics of nanoparticles at liquid-liquid interfaces. The equilibrium IFT values for two different bulk nanoparticle concentrations at different ionic strengths are shown in Figure 7.4. The effect of NaCl concentration on the dynamic IFT is not significant when the NaCl concentration is low. As the NaCl concentration is increased, the IFT decreases gradually for both of the nanoparticle concentrations that were considered.

It is known that colloidal Au made by chemical reduction develops a negative charge on the surface of the nanoparticle [116], [117], [118]. This charge is partially reduced by the capping ligand. Therefore, the synthesized gold nanoparticles must carry a slight negative charge. The negative charge introduces an electric double layer on the surface of gold nanoparticles at the interface. At very low NaCl concentrations ($\leqslant 0.005M$), the ions (Na^+ and Cl^-) in the bulk aqueous phase are stable and do not come close to the oil-water interface, so that the structure of water at the interface remains unperturbed [119]. As the NaCl concentration is increased (*e.g.* $\geqslant 0.005M$), ions come into closer contact with the oil–water interface. The reduction of the IFT upon adding NaCl is presumably due to a higher interaction between the gold nanoparticles and the aqueous solution. The sodium cation (Na^+)interacts

more readily with the partially negatively charged gold nanoparticles. The negative charge on the surface of gold nanoparticles are screened by the opposite charge of Na^+. This reduces the thickness of the double layer which in turn leads to a higher density of nanoparticles at the interface which reduces the IFT value. However, Cl^- are also present in the double-layer as counter ions and are assumed to also adsorb to the oil-water interface. *Tian et al.* [76] showed in a recent molecular dynamics simulation that there is possible adsorption of Cl^- ions at hydrophobic material–water interfaces. As the NaCl concentration increases, more nanoparticles are adsorbed to the interface due to their attraction to Na^+. More nanoparticles at the interface reduce the IFT [47]. This behavior was observed in our study for the higher bulk nanoparticle concentrations (see Table 7.3 and 7.4). Thus, salt reduces the IFT at the oil–water interface which indicates an increase in the number of particles at the interface as the ionic strength is increased.

Using Equation 4.5 and Equation 4.7, the diffusion coefficient of the nanoparticles at the earlier time, D_0, and the later time, D_∞, were estimated over a wide range of NaCl concentrations (i.e., NaCl= 0 M to 0.5 M).

Table 7.3: Effect of NaCl concentration on the adsorption behavior of *n*-dodecane-1-thiol capped gold nanoparticles at the hexane–water interface for low ($(1.7 \pm 0.04) \times 10^{15}$ particle/L) bulk nanoparticle concentration.

NaCl Con.	Equilibrium IFT	Diffusion Coefficient			Adsorption Barrier
[mol/L]	γ_∞ [mN/m]	D_{S-E} [m^2/s]	D_0 [m^2/s]	D_∞ [m^2/s]	ΔE [J]
0	38.78 ± 0.14	$3.36 \pm .46 \times 10^{-10}$	4.33×10^{-10}	3.93×10^{-11}	0.99×10^{-20}
0.005	37.42 ± 0.1	,,	7.10×10^{-10}	5.93×10^{-11}	1.02×10^{-20}
0.05	36.17 ± 0.14	,,	6.77×10^{-10}	4.45×10^{-11}	1.12×10^{-20}
0.1	35.09 ± 0.1	,,	3.50×10^{-10}	4.24×10^{-11}	1.09×10^{-20}
0.5	33.03 ± 0.24	,,	3.50×10^{-10}	3.27×10^{-11}	0.89×10^{-20}

Using Eq. 4.11 for the hexane–water system, D_{S-E} is estimated to be $3.36 \pm 0.46 \times 10^{-10}$ m^2/s (see Tables 7.3 and 7.4). For both bulk nanoparticle concentrations, the nanoparticles undergo almost free diffusion (i.e., $D_0 \simeq D_{S-E}$) at early times. At later times, the diffusion coefficient, D_∞, decreases for all of the NaCl concentrations

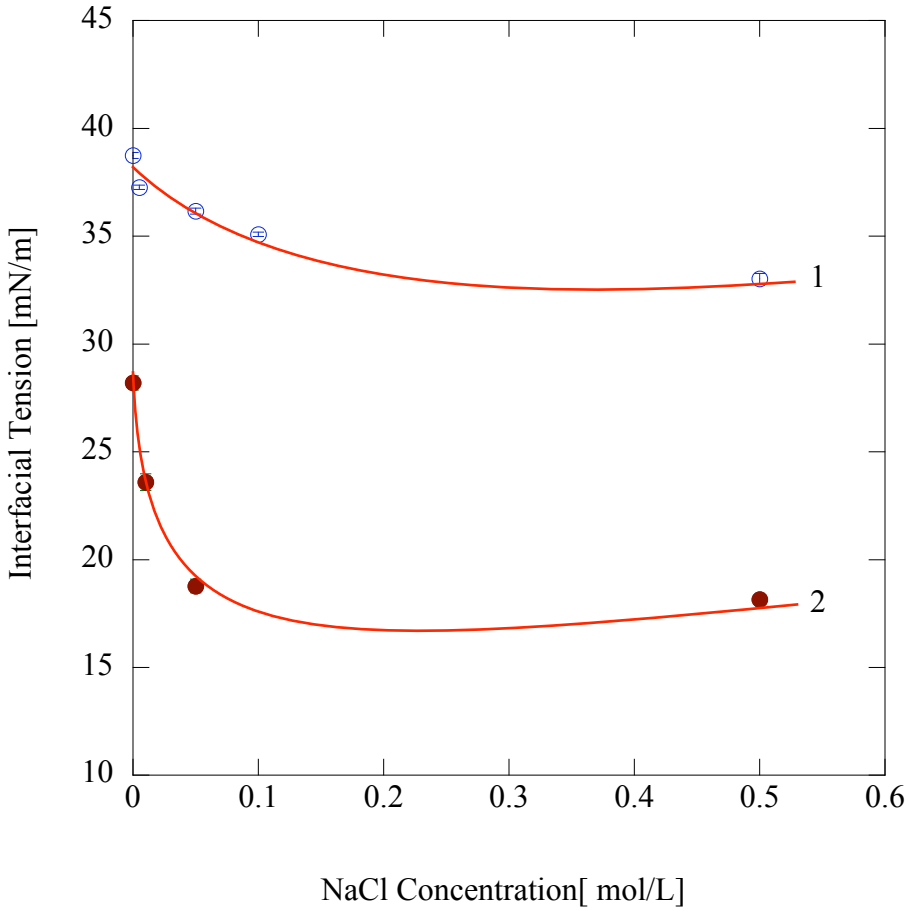

Figure 7.4: Water-hexane equilibrium interfacial tension as a function of NaCl concentration in the presence of Au nanoparticles capped with n-dodecane-1-thiol (1) at low $(1.7 \pm 0.04) \times 10^{15}$ particle/L and (2) at high $(6.3 \pm 0.04) \times 10^{15}$ particle/L bulk nanoparticle concentration. Lines are a guide to the eye.

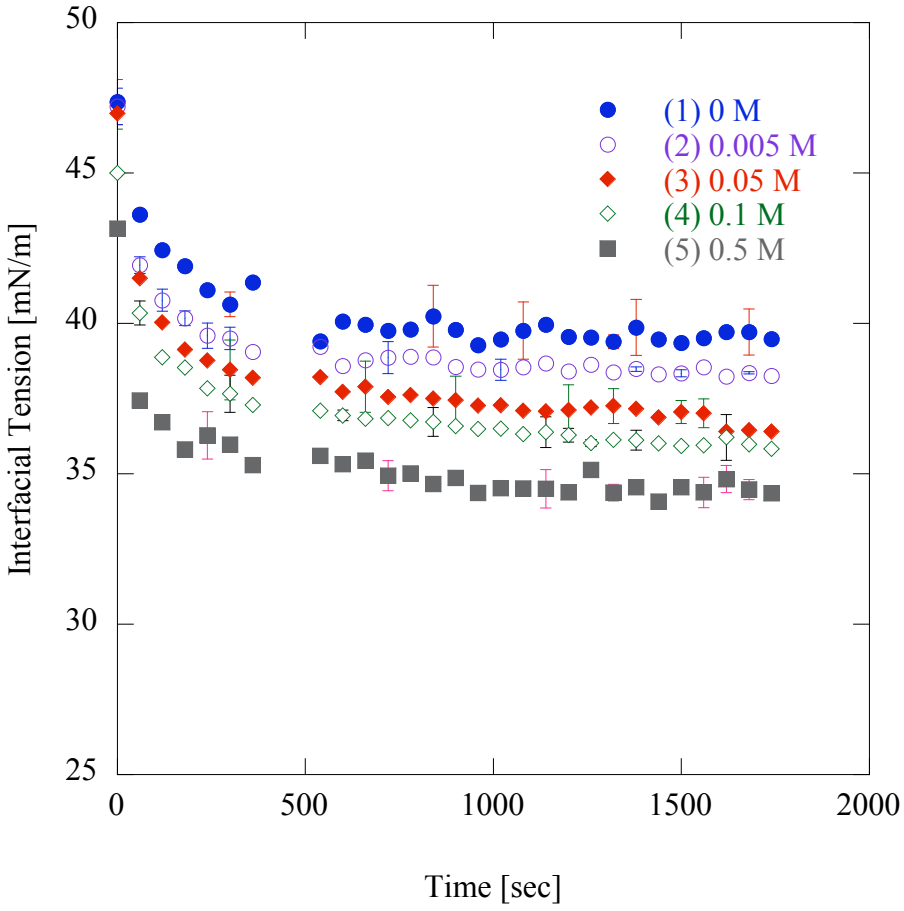

Figure 7.5: Water-hexane dynamic interfacial tension as a function of NaCl concentration (1) NaCl = 0 mol/L , (2) NaCl = 0.005 mol/L, (3) NaCl = 0.05 mol/L, (4) NaCl = 0.1 mol/L and (5) NaCl = 0.5 mol/L in the presence of Au nanoparticles capped with *n*-dodecane-1-thiol at low $(1.7 \pm 0.04) \times 10^{15}$ particle/L bulk nanoparticle concentration.

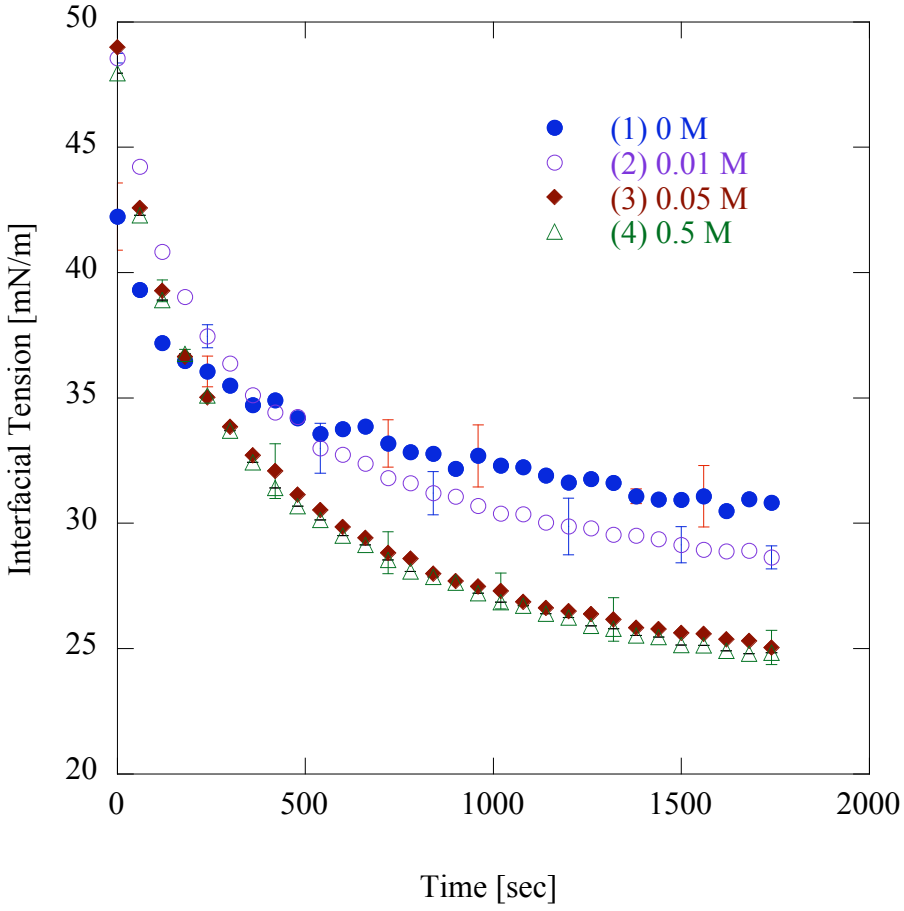

Figure 7.6: Water-hexane dynamic interfacial tension as a function of NaCl concentration (1) NaCl = 0 mol/L , (2) NaCl = 0.01 mol/L, (3) NaCl = 0.05 mol/L and (4) NaCl = 0.5 mol/L in the presence of Au nanoparticles capped with *n*-dodecane-1-thiol at high $(6.3 \pm 0.04) \times 10^{15}$ particle/L bulk nanoparticle concentration.

Table 7.4: Effect of NaCl concentration on the adsorption behavior of n-dodecane-1-thiol capped gold nanoparticles at the hexane–water interface for high $(6.3 \pm 0.04) \times 10^{15}$ particle/L) bulk nanoparticle concentration.

NaCl Con.	Equilibrium IFT	Diffusion Coefficient			Adsorption Barrier
mol/L	γ_∞ [mN/m]	D_{S-E} [m^2/s]	D_0 [m^2/s]	D_∞ [m^2/s]	ΔE [J]
0	28.20 ± 0.33	$3.36 \pm .46 \times 10^{-10}$	1.54×10^{-10}	3.19×10^{-13}	2.54×10^{-20}
0.01	23.6 ± 0.4	”	5.56×10^{-10}	1.14×10^{-13}	3.49×10^{-20}
0.05	18.78 ± 0.32	”	6.78×10^{-10}	0.78×10^{-13}	3.72×10^{-20}
0.5	18.16 ± 0.21	”	7.73×10^{-10}	0.73×10^{-13}	3.80×10^{-20}

,

that were studied. The potential barriers to adsorption, ΔE, were calculated by taking the effective diffusivity equal to D_∞. Without added NaCl and at a NaCl concentration of 0.5 M, the estimated values of ΔE was calculated for the highest nanoparticle bulk concentration $(6.3 \pm .04) \times 10^{15}$ particle/L)to be 2.54×10^{-20} J and 3.8×10^{-20} J, respectively. As the NaCl concentration was increased, the adsorption barrier likewise increased. However, for lower bulk concentrations, the barrier was almost constant.

7.3 Effect of pH on the Adsorption Kinetics of *n*-Dodecane-1-Thiol Capped Gold Nanoparticles

The effect of pH on adsorption was investigated over a range of pH without any added NaCl at a constant temperature of 297.65 K in an ambient atmosphere. The equilibrium IFT for low and high particle concentrations at various pH conditions can be seen in Tables 7.5 and 7.6. Obtained results were not comparable to each other as bulk concentrations were different. The reduction in IFT is high for higher bulk concentration and low for lower bulk concentration. Results, shown in Tables 7.5 and 7.6, were independent of each other. Hence, inconsistency in pH range did not have any affect in understanding the adsorption kinetics of nanoparticles at liquid-liquid interfaces. Due to less effective screening of the H^+ ion relative to Na^+, an extremely

large double layer is formed on the surface of the particles for acidic conditions. H^+ ions do not come as close to negative ions as metal ions do because of their smaller size [119] and it is expected that they maintain a greater distance from negative charges on gold nanoparticles than Na^+ would. This leads to little or no effect on the nanoparticles and the IFT remains almost the same when the pH is 7 or less. As the NaOH concentration is increased (i.e., pH >7), the IFT decreases due to the interaction of partially negatively charged gold nanoparticles with Na^+. The negative charges on the surface of gold nanoparticles are screened by Na^+, which reduces the thickness of the double layer. As the thickness of the double layer is reduced, more nanoparticles are attracted to the interface which lead to a reduction in the IFT. However, Cl^- can be present at the interface for the lower pH values that were studied, while OH^- can be present at higher pHs. It is surmised that these ions also adsorbed at the interface. *Tian et al.* [76] observed that it is possible for both Cl^- and OH^- ions to absorb at the interfaces between hydrophobic materials and water. This behavior was observed for the higher bulk nanoparticle concentration.

From Figure 7.7 to Figure 7.9, it is evident that at lower pH values (i.e.< 7), the IFT remained almost constant for both bulk nanoparticle concentrations. At higher pH values (i.e., > 7), the IFT decreases rapidly for both bulk nanoparticle concentrations. When the pH of the aqueous solution was reduced from 7 to 1.2, at the low nanoparticle concentration (1.7×10^{15} particle/L), the IFT increased by only 3.0 mN/m. An increase in the pH from 7 to 12.6 resulted in a decrease in the IFT by 15.65 mN/m. This behavior was also observed for higher nanoparticle concentrations, but with less of an affect. These results show that both the pH and the concentration of nanoparticles greatly influence the IFT value and, therefore, nanoparticle adsorption.

In Table 7.5 and Table 7.6, it can be seen that for both bulk nanoparticle concentrations, nanoparticles undergo almost free diffusion (i.e., $D_0 \simeq D_{S-E}$) at early times, while at later times, $D_\infty \ll D_0$ for all of the pH values that were considered. For pH= 1.2 and pH= 10.8, the estimated values for ΔE for the highest nanoparticle concentration ($6.3 \pm .04 \times 10^{15}$ particle/L), are 2.75×10^{-20} J and 3.47×10^{-20} J, respectively. As the pH was increased, the adsorption barrier also increased slightly for the higher bulk particle concentration, while the barrier remained almost constant for the lowest nanoparticle concentration that was studied.

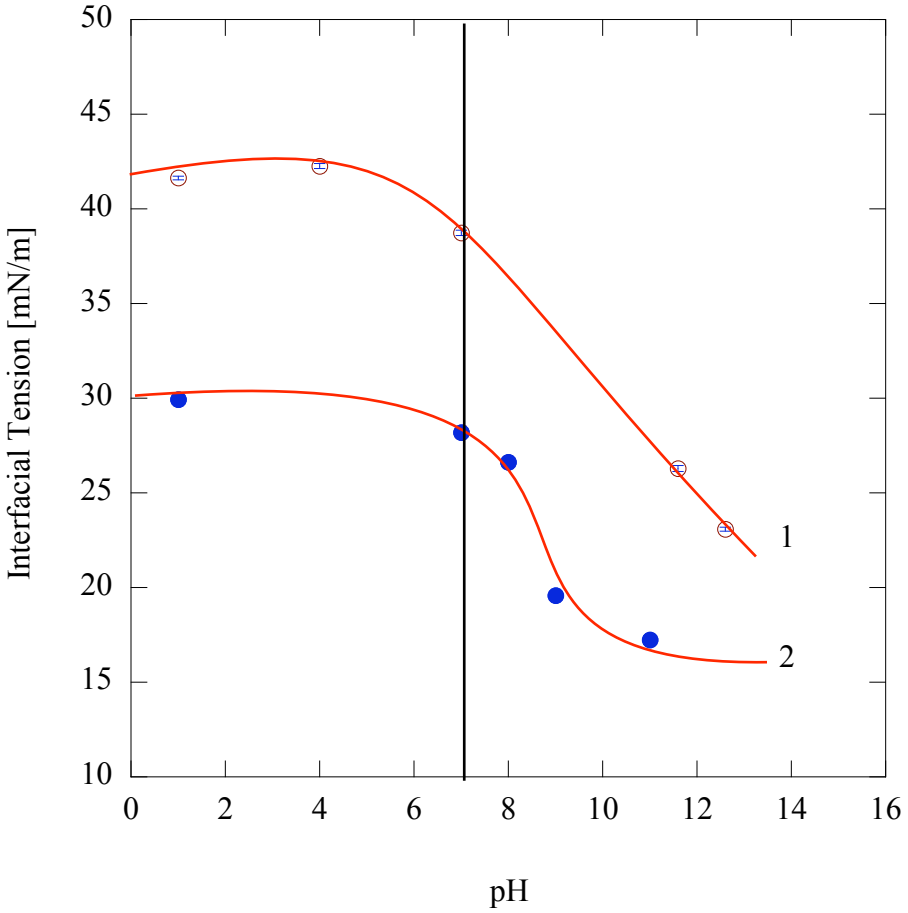

Figure 7.7: Water- hexane equilibrium interfacial tension as a function of pH in the presence of Au nanoparticles capped with n-dodecane-1-thiol (1) at low $(1.7 \pm 0.04) \times 10^{15}$ particle/L and (2) at high $(6.3 \pm 0.04) \times 10^{15}$ particle/L bulk nanoparticle concentration. Curves are added as a guide.

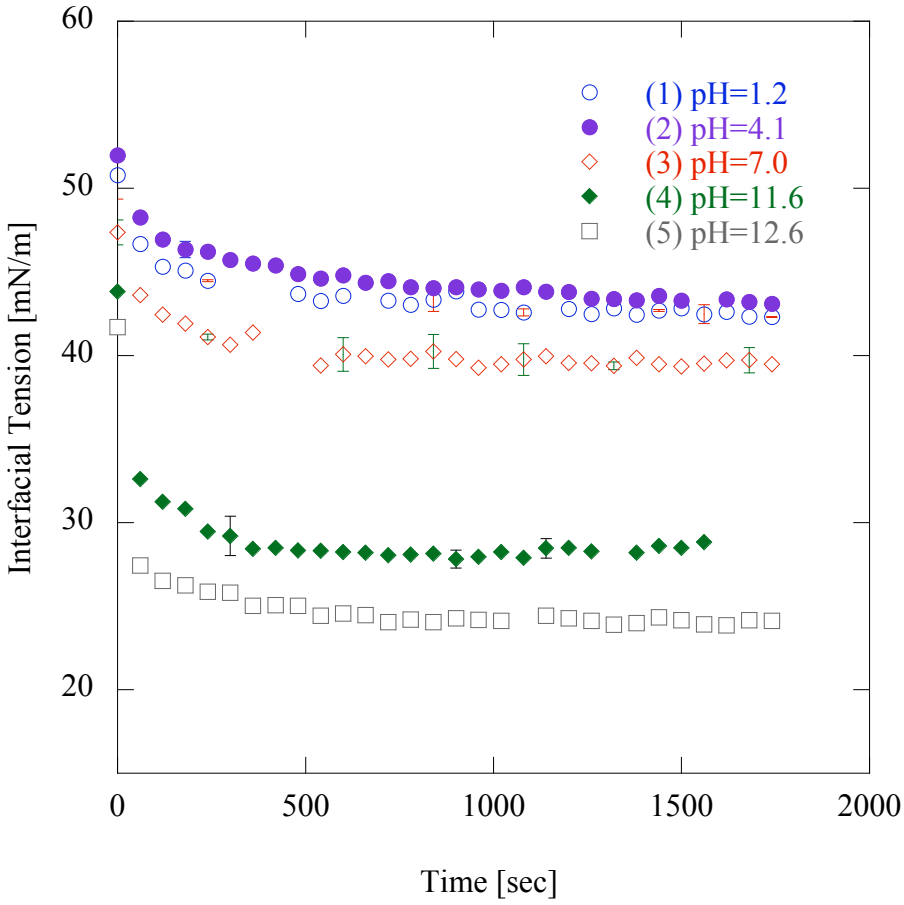

Figure 7.8: Water-hexane dynamic interfacial tension as a function of pH (1) pH= 1.2, (2) pH = 4.1, (3) pH = 7.0, (4) pH = 11.6 and (5) pH = 12.6 in the presence of Au nanoparticles capped with *n*-dodecane-1-thiol for low $(1.7 \pm 0.04) \times 10^{15}$ particle/L bulk nanoparticle concentration.

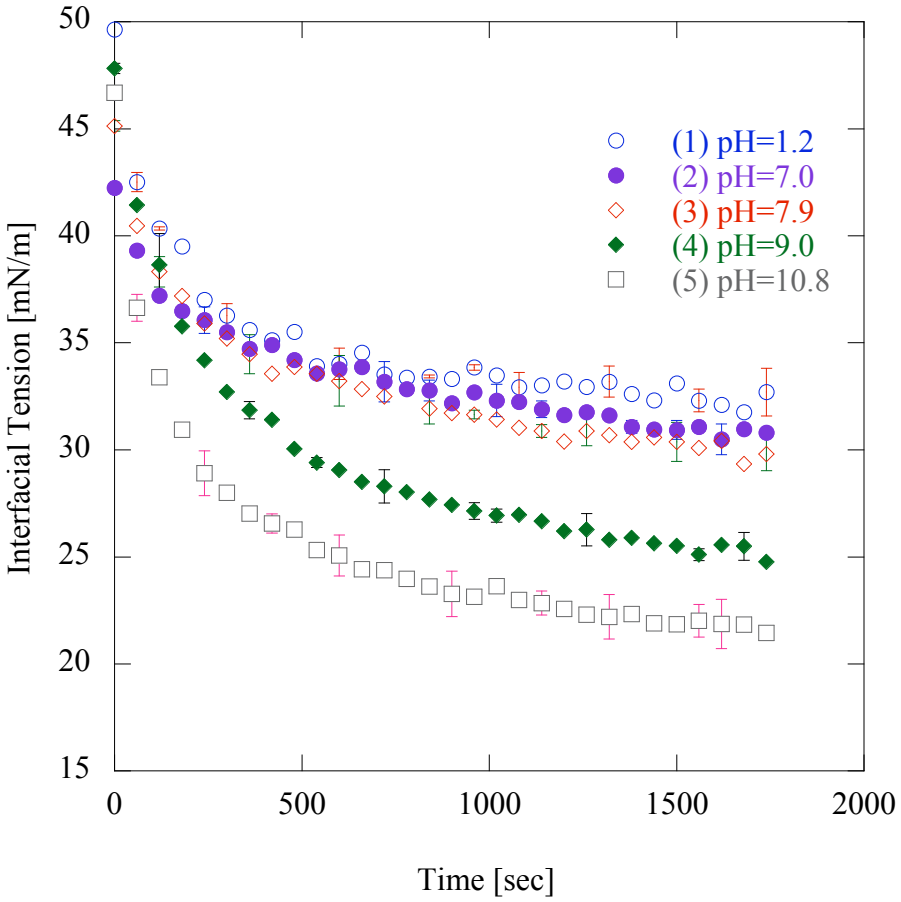

Figure 7.9: Water-hexane dynamic interfacial tension as a function of pH (1) pH = 1.2, (2) pH = 7.0, (3) pH = 7.9, (4) pH = 9.0 and (5) pH = 10.8 in the presence of Au nanoparticles capped with n-dodecane-1-thiol for high $(6.3 \pm 0.04) \times 10^{15}$ particle/L bulk nanoparticle concentration.

Table 7.5: Effect of pH on the adsorption behavior of *n*-dodecane-1-thiol capped gold nanoparticles at the hexane–water interface for low$(1.7 \pm 0.04) \times 10^{15}$ particle/L bulk nanoparticle concentration.

pH	Equilibrium IFT	Diffusion Coefficient			Adsorption Barrier
	γ_∞ [mN/m]	D_{S-E} [m^2/s]	D_0 [m^2/s]	D_∞ [m^2/s]	ΔE [J]
1.2	41.64 ± 0.1	$3.36 \pm .46 \times 10^{-10}$	3.28×10^{-10}	4.75×10^{-11}	0.79×10^{-20}
4.1	42.27 ± 0.13	,,	7.50×10^{-10}	2.75×10^{-11}	1.36×10^{-20}
7.0	38.74 ± 0.14	,,	4.33×10^{-10}	3.93×10^{-11}	0.99×10^{-20}
11.6	26.30 ± 0.16	,,	7.37×10^{-10}	2.86×10^{-11}	1.33×10^{-20}
12.6	23.09 ± 0.1	,,	4.41×10^{-10}	5.42×10^{-11}	0.86×10^{-20}

Table 7.6: Effect of pH on the adsorption behavior of *n*-dodecane-1-thiol capped gold nanoparticles at the hexane–water interface for high $(6.3 \pm 0.04) \times 10^{15}$ particle/L) bulk nanoparticle concentration.

pH	Equilibrium IFT	Diffusion Coefficient			Adsorption Barrier
	γ_∞ [mN/m]	D_{S-E} [m^2/s]	D_0 [m^2/s]	D_∞ [m^2/s]	ΔE [J]
1.2	29.93 ± 0.2	$3.36 \pm .46 \times 10^{-10}$	4.19×10^{-10}	5.12×10^{-13}	2.75×10^{-20}
7.0	28.20 ± 0.33	”	1.54×10^{-10}	3.19×10^{-13}	2.54×10^{-20}
7.9	26.63 ± 0.3	”	3.14×10^{-10}	2.52×10^{-13}	2.93×10^{-20}
9.0	19.59 ± 0.22	”	9.01×10^{-10}	1.04×10^{-13}	3.72×10^{-20}
10.8	17.24 ± 0.3	”	7.54×10^{-10}	1.62×10^{-13}	3.47×10^{-20}

7.4 Summary

This chapter describes the effects of temperature, ionic strength, and pH on the adsorption behavior of gold nanoparticles at the liquid–lquid interface was studied. All the factors found to have a profound affect on the adsorption behavior of nanoparticles at the oil–water interface. These findings may find use in applications of nanoparticles for encapsulation and catalysis.

The next chapter provides the summary of the thesis and the contributions to the research.

Chapter 8

Conclusions and Recommendations

8.1 Conclusions

This chapter concludes the thesis with a summary of contributions that the research presented in this thesis accomplished and a note on the future direction of research in this field.

This research has intensely focused on an investigation of the adsorption kinetics of alkhane-thiol capped gold nanoparticles at liquid-liquid interfaces. Alkhanethiol capped gold nanocrystals were synthesized to perform the experiments. By changing the thiol to gold ratio, different core sizes of alkhanethiolate protected gold nanoparticles were synthesized. Several techniques such as UV-Vis, HR-TEM, EDS and H-NMR were performed to characterize the particles. Prior to this study, the adsorption kinetics of gold NPs was poorly understood, despite the fact that adsorption is a prerequisite for self-assembly into useful supra-colloidal structures. During the literature survey, reports were found that demonstrated changing interfacial tension correlated with changes in NP bulk concentration, particle size, temperature, ionic strength and pH. This thesis focuses on understanding the effects of these variables on, adsorption kinetics at liquid-liquid interfaces. IFT measurements of gold-capped nanoparticles at liquid-liquid interfaces were performed by pendant drop experiments using ADSA.
The following list summarizes the research objectives of this thesis:

Objective I: To investigate the adsorption kinetics of different sized n-dodecanethiol and n-hexanethiol capped gold nanoparticles at the liquid -liquid interface. The following factors were studied with respect to their effects on the interfacial tension at a hexane-water interface:

- The effect of NP bulk concentration.
- The effect of NP size.
- The effect of capping agent.

Objective II: To determine the interaction parameter representative of the interfacial properties of mixtures of NPs. These experiments were performed by estimating the interaction parameters at hexane-water interfaces. The following variables were explored

- mixtures of differently size NPs.
- mixtures of differently capped NPs.

Objective III: To determine the effects of temperature, ionic strength and pH on the IFT and adsorption behaviour of AuNPs at the liquid-liquid interface. The following factors were studied with respect to their effects on the interfacial tension at the nonane-water and hexane-water interface:

- The effect of temperature.
- The effect of ionic strength.
- The effect of pH.

Throughout the whole research work, the effects of these parameters were studied in order to understand the adsorption kinetics of the capped gold nanoparticles at liquid-liquid interfaces.

The results obtained in this research work are summarized as follows:

1. With an aim to improve the understanding of self-assembly of ligand-stabilized nanoparticles at liquid-liquid interfaces, we studied, by pendant drop tensiometry, the kinetics of alkanethiol-stabilized gold nanoparticles at the hexane-water interface. From the time evolution of the interfacial tension at the early ($t \longrightarrow 0$) and late ($t \longrightarrow \infty$) stages of adsorption we could infer a switch, with increasing interfacial coverage, from diffusion-controlled kinetics to interaction-controlled kinetics.

2. The potential barrier for nanoparticle adsorption to the hexane-water interface was estimated from the diffusion constants of the late stages of adsorption and found equal to approximately $10k_BT$, for gold nanoparticles of different size stabilized with different ligands (n-dodecane-1-thiol and n-hexane-1-thiol).
3. For constant bulk concentration and nanoparticle size, it was additionally found that adsorption of nanoparticles stabilized with shorter alkanethiol ligands leads to a lower equilibrium interfacial tension.
4. The goal was to understand the interaction behavior of mixtures of different size and different ligand-stablized gold nanoparticles at the liquid-lquid interface by pendant drop tensiometry.The composition of the mixed adsorbed monolayer at the hexane-water interface is completely different from the bulk hexane phase. Although high interfacial activities of the individual nanoparticles formed a densely populated interface, they lost the tendency to adsorb more in mixed systems.
5. The positive values of β indicate the repulsive interaction between the adsorbed nanoparticles in the mixed monolayer. The estimated interfacial composition and repulsive interaction in the mixed monolayer are highly dependent on the bulk mole fraction, α.
6. Possible formation of association complexes and the interaction between the nanoparticles can explain this behavior. The interfacial isotherms obtained for the individual nanoparticles and their mixture show no synergism in interfacial tension reduction. These findings may be contribute to the design of nanoparticle formulations of controlled tension alkane-thiol capped gold nanoparticles at liquid-liquid interface or interfacial compositions with the minimal amounts of NPs used.
7. Temperature was found to have a profound affect on the adsorption behavior of nanoparticles at the oil–water interface. The IFT was found to increase for both low and high bulk nanoparticle concentrations as the temperature was raised.
8. On the other hand, the IFT was found to decrease as the ionic strength and pH of the aqueous phase was increased. It is surmised that an increase in the ionic strength and pH of the aqueous phase, leads to more nanoparticles adsorbing at the interface between the fluids. These findings improve our understanding

of nanoparticle adsorption at liquid-liquid interfaces and may contribute to developing applications for gold nanoparticles (e.g., encapsulation and catalysis).

8.2 Recommendations and Future work

The results obtained in this work may be improved upon by exploring the following suggestions and recommendations:

- The solvent chain-length has an effect on IFT. The larger the chain length, the higher the IFT drop. Investigations should be done using different solvents to clarify the effect of hydrocarbon chain length on IFT.
- It is known that Janus particles are more effective at decreasing the IFT than homogenous nanoparticles. It may be worthwhile to modify the capped gold nanoparticles for use as Janus particles, despite the fact that Janus particle synthesis requires significant effort. Janus particles exhibit enhanced stability compared to homogenous nanoparticles. The use of gold-capped Janus particles could reduce the thermal fluctuations in the self-assembly experiments.
- The NP surface ligands are responsible for its stability, controlled interfacial self-assembly, and interfacial properties at the interface. It is necessary to better quantify the role that surface ligands play on NP interaction at the interface. Further experiments using gold-NPs capped with different ligands, different terminal groups, and different ligand chain lengths would be beneficial.

  It has been shown that the binding energy of the NPs at the liquid-liquid interface can be controlled by selecting appropriate surface ligands.
- The research presented in this thesis was performed by using the pendant drop technique. The images of the drop were taken at a frequency of one image per minute. The images were then processed and fitted to the Laplace equation to give the IFT over time. As the studied particles are very surface active, it is suggested that images of the drop should be taken at a frequency of one image per millisecond or one image per second. This will improve understanding of the adsorption kinetics of the capped gold nanoparticles at the liquid-liquid interfaces more precisely; especially at earlier stages.

- The stability of nanoparticles at the fluid interfaces is strongly dependent on particle geometry because this affects the free energy of the NPs. This study may be extended to different shapes of capped gold nanoparticles. This will improve the understanding of self-assembly of non-spherical nanoparticles at the interface. At present, the study of interfacial self-assembly of non-spherical NPs is a major challenge.
- Further investigations may involve studying the reversibility of the interfacial attachment of the particles at the liquid-liquid interface. These experiments could open the possibility of further developing the encapsulation technique at the liquid-liquid interface.
- It is known that pressure has an effect on IFT. A study may be conducted to determine the effect of pressure on IFT at the interfaces. The temperature chamber may be modified for such experiments.
- Experiments performed using different types of salts could be done to improve the understanding the effect of ionic strength on IFT at the interfaces.

By incorporating the above suggestions, future studies may help to better understand the adsorption kinetics of capped nanoparticles at liquid-liquid interfaces. More knowledge may help to improve the potential of these NPs for use in applications including encapsulation, controlled self-assembly, size selective adsorption, and biocatalysis at liquid-liquid interfaces.

Appendix

List of Publications

The research presented in this thesis originated the following publications:

1. Sultana Ferdous and Marios. A. Ioannidis and Dale Henneke, "Adsorption kinetics of alkhanethiol-capped gold nanoparticles at the hexane-water interface," Published in *Journal of Nanoparticle Research*, DOI 10.1007/s11051-011-0565-y.
2. Sultana Ferdous and Marios. A. Ioannidis and Dale Henneke, "Effects of temperature, pH and ionic strength on the adsorption of nanoparticles at liquid-liquid interfaces," Accepted in *Journal of Nanoparticle Research*. [Revised manuscript]
3. Sultana Ferdous and Marios. A. Ioannidis and Dale Henneke, "Interaction behaviour during adsorption of mixtures of alkhanethiol capped gold nanoparticles at the hexane-water interface," Ready to submit in *Journal of Nanoparticle Research*.

Some Experimental Analysis

- The best fit to the Frumkin model discussed in Chapter 6 (See Section 6.1) are shown below:
- Figure 8.4 shows the interfacial tension at the water-hexane interface discussed in Chapter 4 (See Section 4.3).

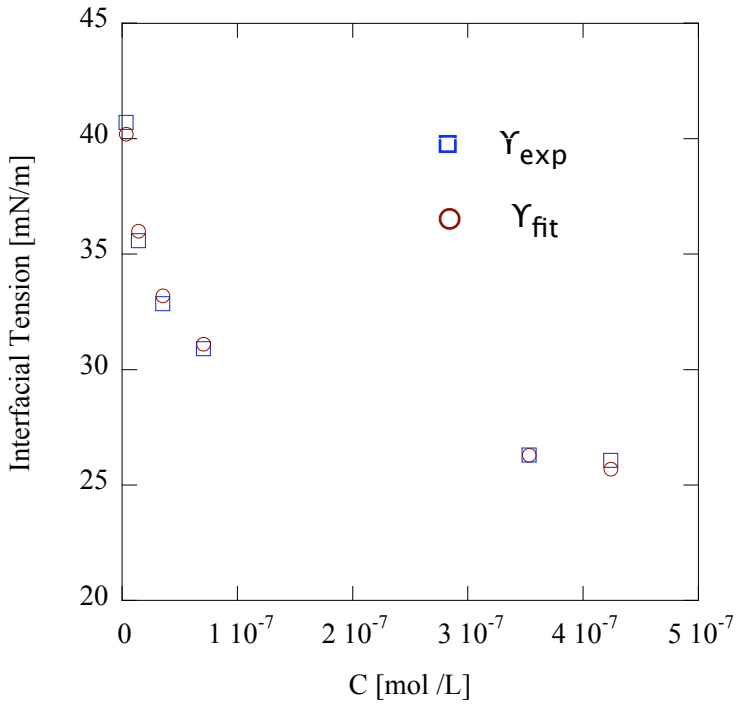

Figure 8.1: The best fit obtained from Frumkin isotherem using the optimization procedure and the experimental points for 1.6 nm n-dodecane-1-thiol capped gold nanoparticles.

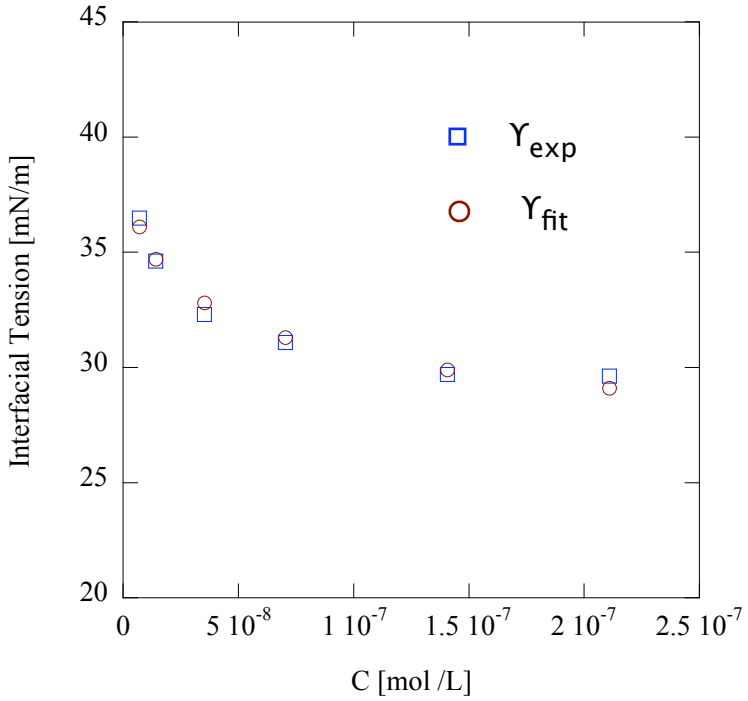

Figure 8.2: The best fit obtained from Frumkin isotherem using the optimization procedure and the experimental points for 2.8 nm n-dodecane-1-thiol capped gold nanoparticles.

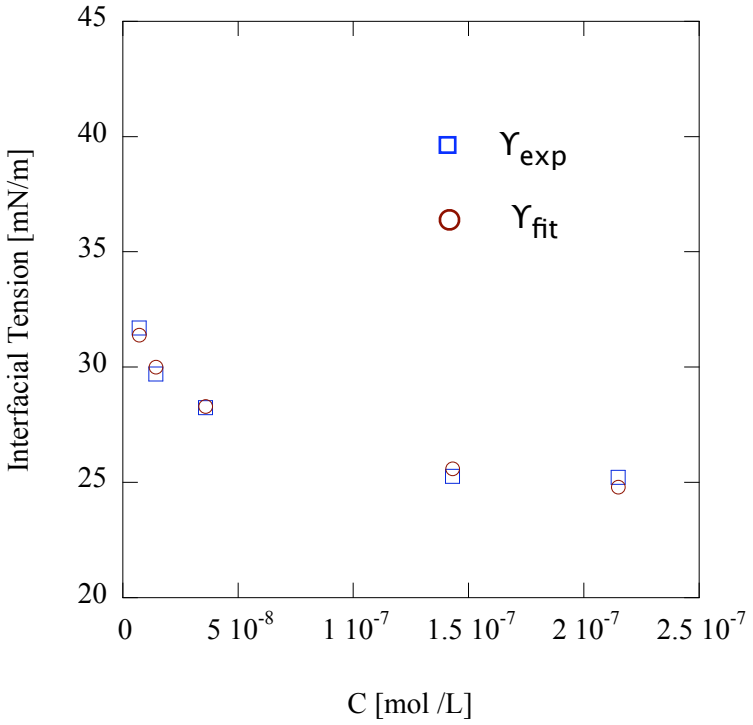

Figure 8.3: The best fit obtained from Frumkin isotherem using the optimization procedure and the experimental points for 2.9 nm n-hexane-1-thiol capped gold nanoparticles.

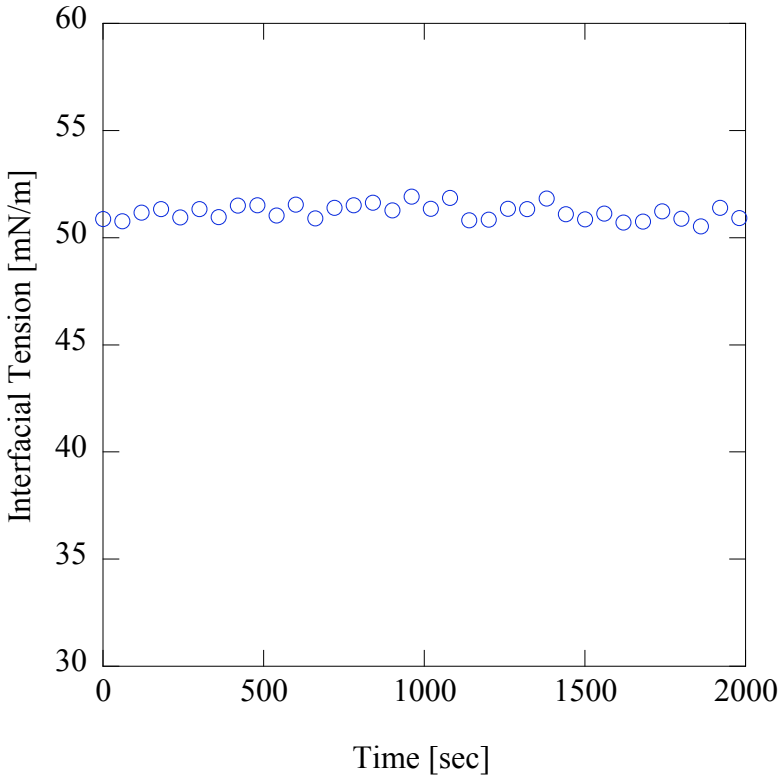

Figure 8.4: Interfacial tension at a pure water-hexane interface.

Bibliography

[1] S. Kutuzov, J. He, R. Tangirala, T. Emrick, T. P. Russel, and A. Boeker, "On the kinetics of nanoparticle self-assembly at liquid/liquid interfaces," *Phys. Chem. Chem. Phys.*, vol. 9, pp. 6351–6358, November 2007. iii, xvi, 3, 4, 24, 27, 28, 29, 30, 80, 92, 96, 98, 99, 115, 128

[2] H. Ma, M. Luo, and L. L. Dai, "Influences of surfactant and nanoparticle assembly on effective interfacial tensions," *Phys. Chem. Chem. Phys*, vol. 10, pp. 2207–2213, February 2008. 1, 25, 26

[3] Z. Mao, H. Xu, and D. Wang, "Molecular mimetic self-assembly of colloidal particles," *Adv. Funct. Mater*, vol. 20, pp. 1053–1074, 2010. 1, 9, 24

[4] L. Isa, E. Amstad, M. Textor, and E. Reimhult, "Self-assembly of iron oxide-poly(ethyleneglycol) core -shell nanoparticles at liquid-liquid interfaces," *Chimia*, vol. 64, no. 3, pp. 145–149, 2010. xv, 1, 3, 4, 8, 9

[5] R. Krishnaswamy and A. K. Sood, "Growth, self-assembly and dynamics of nano-scale films at fluid interfaces," *J. Mater. Chem*, vol. 20, pp. 3539–3552, 2010. 1, 3

[6] B. P. Binks and P. D. I. Fletcher, "Particles adsorbed at the oil-water interface: A theoretical comparison between spheres of uniform wettability and janus particles," *Langmuir*, vol. 17, pp. 4708–4710, 2001. 2, 46

[7] A. Boeker, J. He, T. Emrick, and T. P. Russell, "Self-assembly of nanoparticles at interfaces," *Soft Matter*, vol. 3, pp. 1231–1248, 2007. xv, 2, 3, 8, 20

[8] K. Du, E. Glogowski, T. Emrick, T. P. Russell, and A. D. Dinsmore, "Adsorption energy of nano- and microparticles at liquid-liquid interfaces," *Langmuir*, vol. 26, no. 15, pp. 12518–12522, 2010. 2, 20, 33, 34

[9] B. P. Binks and T. S. Horozov, *Colloidal particles at liquid interfaces*. Cambridge University Press, Cambridge, 2006. 2, 9

[10] P. Pieranski, "Two-dimensional interfacial colloidal crystals," *Phys. Rev. Lett.*, vol. 45, no. 7, pp. 569–572, 1980. 2

[11] R. Aveyard and J. H. Clint, "Particle wettability and line tension," *J. Chem. Soc., Faraday Trans*, vol. 92, no. 1, pp. 85–89, 1996. 2, 20, 23, 24

[12] D. L. Cheung and S. A. F. Bon, "Interaction of nanoparticles with ideal liquid-liquid interfaces," *Physical Review Letters*, vol. 102, pp. 066103–066107, 2009. 2, 20

[13] F. Bresme and M. Oettel, "Nanoparticles at fluid interfaces," *J. Phys.: Condens.Matter*, vol. 19, pp. 413101–413134, 2007. xvii, 2, 46

[14] B. P. Binks, "Particles as surfactants–similarities and differences," *Current Opinion in Colloid and Interface Science*, vol. 7, pp. 21–41, 2002. 2, 3, 9, 24

[15] Y. Lin, H. Skaff, T. Emrick, A. Dinsmore, and T. Russell, "Nanoparticle assembly and transport at liquid-liquid interfaces," *Science*, vol. 299, pp. 226–229, 2003. xv, 2, 3, 18, 20, 21, 117, 118

[16] D. Patra, F. Ozdemir, O. Miranda, B. Samanta, A. Sanyal, and V. M. Rotello, "Formation and size tuning of colloidal microcapsules via host-guest molecular recognition at the liquid-liquid interface," *Langmuir*, vol. 25, no. 24, pp. 13852–13854, 2009. 3

[17] S. Crossley, J. Faria, M. Shen, and D. E. Resasco, "Solid nanoparticles that catalyze biofuel upgrade reactions at the water/oil interface," *Science*, vol. 327, pp. 68–72, 2010. 3

[18] N. Glaser, D. J. Adams, A. Boeker, and G. Krausch, "Janus particles at liquid-liquid interfaces," *Langmuir*, vol. 22, pp. 5227–5229, 2006. xvii, 3, 4, 46, 47, 48, 108

[19] A. F. H. Ward and L.Tordai, "Time-dependence of boundary tensions of solutions i. the role of diffusion in time-effects," *J. Chem. Phys*, vol. 14, pp. 453–461, 1946. 3, 79

[20] L. Liggieri, F. Ravera, and A. Passerone, "A diffusion-based approach to mixed adsorption kinetics," *Colloids and Surfaces A: Physicochemical and Engineering Aspects*, vol. 114, pp. 351–359, 1996. 3, 80, 98

[21] J. Eastoe, J. S. Dalton, P. G. A. Rogueda, E. R. Crooks, A. R. Pitt, and E. A. Simister, "Dynamic surface tensions of nonionic surfactant solutions," *J. Colloid. Interface. Sci*, vol. 188, pp. 423–430, 1997. 4, 29, 30, 100

[22] J. Zhou, J. Ralston, R. Sedev, and D. A. Beattie, "Functionalized gold nanoparticles : Synthesis, structure and colloid stability," *J. Colloid and Interface Science*, vol. 331, no. 2, pp. 251–262, 2009. 4, 12

[23] J. R. Campanelli and X. Wang, "Dynamic interfacial tension of surfactant mixtures at the liquid-liquid interfaces," *Journal of Colloid and Interface Science*, vol. 213, pp. 340–351, 1999. 4

[24] T. Gurkov, T. Horozov, I. Ivanov, and R. Borwankar, "Composition of mixed adsorption layers of non-ionic surfactants on oil/water interfaces," *Colloids and Surfaces A: Physicochemical and Engineering Aspects*, vol. 87, pp. 81–92, 1994. 4

[25] V. Fainerman and R. Miller, "Dynamic surface tensions of surfactant mixtures at the water-air interface," *Colloids and Surfaces A: Physicochemical and Engineering Aspects*, vol. 97, pp. 65–82, 1995. 4

[26] M. J. Rosen and X. Hua, "Surface concentrations and molecular interactions in binary mixtures of surfactants," *J. Colloid and Interface Science*, vol. 86, no. 1, pp. 164–172, 1982. 4

[27] B. Y. Zhu and M. J. Rosen, "Synergism in binary mixtures of surfactants iv. effectiveness of surface tension reduction," *J. Colloid and Interface Science*, vol. 99, no. 2, pp. 435–442, 1984. 4

[28] J. K. Angarska, K. D. Tachev, and N. D. Denkov, "Composition of mixed adsorption layers and micelles in solutions of sodium dodecyl sulfate and dodecyl acid diethanol amide," *Colloids and Surfaces A: Physicochem. Eng. Aspects*, vol. 233, pp. 193–201, 2004. 4

[29] M. J. Rosen and D. S. Murphy, "Synergism in binary mixtures of surfactants v. two-phase liquid-liquid systems at low surfactant concentrations," *J. Colloid and Interface Science*, vol. 110, no. 1, pp. 224–236, 1986. 4

[30] X. Hua and M. J. Rosen, "Synergism in binary mixtures of surfactants i. theoretical analysis," *J. Colloid and Interface Science*, vol. 90, no. 1, pp. 212–219, 1982. 4

[31] P. Mukerjee and C. C. Chan, "Effects of high salt concentrations on the micellization of octyl glucoside: salting-out of monomers and electrolyte effects on the micelle-water interfacial tension," *Langmuir*, vol. 18, pp. 5375–5381, 2002. 5

[32] M. Gradzielski, "Effect of the cosurfactant structure on the bending elasticity in nonionic oil-in-water microemulsions," *Langmuir*, vol. 14, pp. 6037–6044, 1998. 5

[33] R. Aveyard, B. P. Binks, J. Chen, J. Esquena, and P. D. I. Fletcher, "Surface and colloid chemistry of systems containing pure sugar surfactant," *Langmuir*, vol. 14, pp. 4699–4709, 1998. 5

[34] Z. Ye, F. Zhang, L. Han, P. Luo, J. Yang, and H. Chen, "The effect of temperature on the interfacial tension between crude oil and gemini surfactant solution," *Colloids and Surfaces A: Physicochem. Eng. Aspects*, vol. 322, pp. 138–141, 2008. 5, 31, 128

[35] B. B. Sauer, Y. L. Chen, G. Zografi, and H. Yu, "Surface light scattering studies of dipalmitoylphosphatidylcholine monolayers at the air/water and heptane/water interfaces," *Langmuir*, vol. 4, pp. 111–117, 1988. 5

[36] R. S. Mohamed, A. C. S. Ramos, and W. Loh, "Aggregation behavior of two asphaltenic fractions in aromatic," *Energy Fuels*, vol. 13, pp. 323–327, 1999. 5

[37] A. Shioi, H. Kumagai, Y. Sugiura, and Y. Kitayama, "Oscillation of interfacial tension and spontaneous interfacial flow at a water/oil interface composed of di(2-ethylhexyl)phosphoric acid," *Langmuir*, vol. 18, pp. 5516–5522, 2002. 5

[38] R. Aveyard, B. P. Binks, and P. D. I. Fletcher, "Interfacial tensions and aggregate structure in $C_{12}E_5$/oil/water microemulsion systems," *Langmuir*, vol. 5, no. 5, pp. 1210–1217, 1989. 5

[39] J. Rudin, C. Bernard, and D. T. Wasan, "Effect of added surfactant on interfacial tension and spontaneous emulsification in alkali/acidic oil systems," *Ind. Eng. Chem. Res*, vol. 33, pp. 1150–1158, 1994. 5

[40] S. H. Shin and D. S. Kim, "Studies on the interfacial characterization of o/w emulsion for the optimization of its treatment," *Environ. Sci. Technol*, vol. 35, pp. 3040–3047, 2001. 5

[41] J. Saien and S. Akbari, "Interfacial tension of toluene + water + sodium dodecyl sulfate from (20^o to 50^o)c and ph between 4 and 9," *J. Chem. Eng. Data*, vol. 51, pp. 1832–1835, 2006. 5

[42] A. Miquilena, V. Coll, A. Borges, J. Melendez, and S. Zeppieri, "Influence of drop growth rate and size on the interfacial tension of triton X-100 solutions as a function of pressure and temperature," *Int. J. Thermophys*, vol. 31, pp. 2416–2424, 2010. 5, 31

[43] T. Sottmann and R. Strey, "Ultralow interfacial tensions in water-n-alkane-surfactant systems," *J. Chem. Phys*, vol. 106, no. 20, pp. 8606–8615, 1997. 5, 31

[44] G. M. Ataev, "Anomalous temperature dependence of interfacial tension in water-hydrocarbon mixtures," *Russian Journal of Physical Chemistry A*, vol. 81, no. 12, pp. 2094–2095, 2007. 5, 31, 128

[45] L. Han, Z. Ye, H. Chen, and P. Luo, "The interfacial tension between cationic gemini surfactant solution and crude oil," *J. Surfact Deterg*, vol. 12, pp. 185–190, 2009. 5

[46] A. G. Gaonkar, "Effects of salt, temperature, and surfactants on the interfacial tension behavior of a vegetable oil/water system," *Journal of Colloid and Interface Science*, vol. 149, no. 1, pp. 256–260, 1992. xvi, 6, 37, 38, 39, 40

[47] S. Simovic and C. A. Prestidge, "Adsorption of hydrophobic silica nanoparticles at the PDMS droplet-water interface," *Langmuir*, vol. 19, pp. 8364–8370, 2003. 6, 43, 130

[48] S. Simovic and C. A. Prestidge, "Hydrophilic silica nanoparticles at the PDMS droplet-water interface," *Langmuir*, vol. 19, pp. 3785–3792, 2003. 6, 37

[49] F. K. G. Santos, E. L. B. Neto, M. C. P. A. . Moura, T. N. C. Dantas, and A. A. D. Neto, "Molecular behavior of ionic and nonionic surfactants in saline medium," *Colloids and Surfaces A: Physicochem. Eng. Aspects*, vol. 333, pp. 156–162, 2009. 6

[50] Y. Li, X. He, X. Cao, G. Zhao, X.Tian, and X. Cui, "Molecular behavior and synergistic effects between sodium dodecylbenzene sulfonate and triton X-100 at oil/water interface," *Journal of Colloid and Interface Science*, vol. 307, pp. 215–220, 2007. 6

[51] F. Ravera, E. Santini, G. Loglio, M. Ferrari, and L. Liggieri, "Effect of nanoparticles on the interfacial properties of liquid/liquid and liquid/air surface layers," *J. Phys. Chem. B*, vol. 110, pp. 19543–19551, 2006. 7, 26

[52] Z. Niu, J. He, T. P. Russell, and Q. Wang, "Synthesis of nano/microstructures at fluid interfaces," *Angrew. Chem. Int. Ed.*, vol. 49, pp. 10052–10066, 2010. xv, 8

[53] R. J. K. U. Ranatunga, C. T. Nguyen, B. A. Wilson, W. Shinoda, and S. O. Nielsen, "Molecular dynamics study of nanoparticles and non-ionic surfactant at an oil water interface," *Soft Matter*, vol. 7, pp. 6942–6952, 2011. xv, 8, 26, 27

[54] R. Aveyard, J. H. Clint, and T. S. Horozov, "Aspects of the stabilisation of emulsions by solid particles: Effects of line tension and monolayer curvature energy," *Phys. Chem. Chem. Phys.*, vol. 5, pp. 2398–2409, 2003. 9, 10, 24

[55] D. Wang, H. Duan, and H. Moehwald, "The water/oil interface: the emerging horizon for self-assembly of nanoparticles," *Soft Matter*, vol. 1, pp. 412–416, 2005. xv, 10, 24, 25, 36

[56] F. Reincke, W. K. Kegel, H. Zhang, M. Nolte, D. Wang, D. Vanmaekelbergh, and H. Moehwald, "Understanding the self-assembly of charged nanoparticles at the water/oil interface," *Phys. Chem. Chem. Phys.*, vol. 8, pp. 3828–3835, 2006. xvi, xvii, 10, 23, 39, 41, 42, 43

[57] R. J. Good and M. V. Ostrovsky, "Mass transfer and dynamic liquid-liquid interfacial tension," *J. Colloid and Interface Science*, vol. 106, no. 1, pp. 122–130, 1985. 11, 19

[58] W. H. Binder, "Supramolecular assembly of nanoparticles at liquid-liquid interfaces," *Angew. Chem. Int. Ed.*, vol. 44, pp. 5172–5175, 2005. 11

[59] A. Goebel and K. Lunkenheimer, "Interfacial tension of the water/n-alkane interface," *Langmuir*, vol. 13, no. 2, pp. 369–372, 1997. xvii, 11, 43, 44, 45, 83, 84

[60] P. V. Baptista, M. K-Montewka, J. P-Oles, G. Doria, and R. Franco, "Gold-nanoparticle-probebased assay for rapid and direct detection of mycobacterium tuberculosis dna in clinical samples," *Clinical Chemistry*, vol. 52, no. 7, pp. 1433–1434, 2006. 12

[61] A. S. Thakor, J. Jokerst, C. Zavaleta, T. F. Massoud, and S. S. Gambhir, "Gold nanoparticles: A revival in precious metal administration to patients," *Nano Lett.*, vol. 11, no. 10, pp. 4029–4036, 2011. 12

[62] P. Ghosh, G. Han, M. De, C. K. Kim, and V. M. Rotello, "Gold nanoparticles in delivery applications," *Advanced drug delivery reviews*, vol. 60, no. 7, pp. 1307–1315, 2008. 12

[63] D. Patra, "Colloidal microcapsules: surface engineering of nanoparticles for interfacial assembly," 2011. xv, 19

[64] Y. Lin, A. Boeker, H. Skaff, D. Cookson, A. D. Dinsmore, T. Emrick, and T. P. Russell, "Nanoparticle assembly at fluid interfaces: structure and dynamics," *Langmuir*, vol. 21, pp. 191–194, September 2005. 22

[65] S. Komura, Y. Hirose, and Y. Nonomura, "Adsorption of colloidal particles to curved interfaces," *J. Chem. Phys.*, vol. 124, pp. 241104–4, 2006. 23

[66] R. Aveyard and J. H. Clint, "Liquid droplets and solid particles at surfactant solution interfaces," *J. Chem. Soc. Faraday Trans.*, vol. 91, no. 17, pp. 2681–2697, 1995. 24

[67] S. Zeppieri, J. Rodriguez, and A. L. L. de Ramos, "Interfacial tension of alkane + water systems," *J. Chem. Eng. Data*, vol. 46, no. 5, pp. 1086–1088, 2001. xvi, 31, 32

[68] K. Motomura, H. Iyota, M. Aratono, M. Yamanaka, and R. Matuura, "Thermodynamic consideration of the pressure dependence of interfacial tension," *J. Colloid and Interface Science*, vol. 93, no. 1, pp. 264–269, 1983. xvi, 31, 33, 34

[69] H. Duan, D. Wang, D. G. Kurth, and H. Moehwald, "Directing self-assembly of nanoparticles at water/oil interfaces," *Angew. Chem. Int. Ed.*, vol. 43, pp. 5639–5642, 2004. xvi, 32, 35

[70] R. J. K. U. Ranatunga, R. J. B. Kalescky, C.-C. Chiu, and S. O. Nielsen, "Molecular dynamics simulations of surfactant functionalized nanoparticles in

the vicinity of an oil water interface," *J. Phys. Chem. C*, vol. 114, pp. 12151–12157, 2010. xvi, 34, 35, 36, 100, 108

[71] E. Glogowski, J. He, T. P. Russell, and T. Emrick, "Mixed monolayer coverage on gold nanoparticles for interfacial stabilization of immiscible fluids," *Chem. Commun.*, vol. 32, pp. 4050–4052, 2005. 35

[72] K. G. Marinova, R. G. Alargova, N. D. Denkov, O. D. Velve, D. N. Petsev, I. B. Ivanov, and R. P. Borwankar, "Charging of oil-water interfaces due to spontaneous adsorption of hydroxyl ions," *Langmuir*, vol. 12, no. 8, pp. 2045–2051, 1996. 40

[73] W. Dickinson, "The effect of pH upon the electrophoretic mobility of emulsion of certain hydrocarbons and aliphatic halides," *Trans. Faraday Soc*, vol. 37, pp. 140–148, 1941. 40

[74] A. Göabler, M. Wegener, A. R. Paschedag, and M. Kraume, "The effect of pH on experimental and simulation results of transient drop size distributions in stirred liquid-liquid dispersions," *Chem. Eng. Sci*, vol. 61, pp. 3018–3024, 2006. 40

[75] S. Maab, A. Gabler, A. R. Paschedag, and M. Kraume, "Proceedings of international conference on multiphase flow, ICMF, Leipzig, Germany," *Martin-Luther- University Hale-Wittenberg: Germany*, pp. 321–327, 2007. 40

[76] C. S. Tian and Y. R. Shen, "Structure and charging of hydrophobic material/water interfaces studied by phase-sensitive sum-frequency vibrational spectroscopy," *PNAS*, vol. 106, no. 36, pp. 15148–15153, 2009. 40, 130, 135

[77] F. Bresme and J. Faraudo, "Orientational transitions of anisotropic nanoparticles at liquid-liquid interfaces," *J. Phys.: Condens. Matter.*, vol. 19, no. 37, pp. 375110–375122, 2007. 45, 46

[78] A. D. Dinsmore, M. F. Hsu, M. G. Nikolaides, M. Marquez, A. R. Bausch, and D. A. Weitz, "Colloidosomes: Selectively permeable capsules composed of colloidal particles," *Science*, vol. 298, pp. 1006–1009, 2002. 46

[79] B. Samanta, D. Patra, C. Subramani, Y. Ofir, G. Yesilbag, A. Sanyal, and V. M. Rotello, "Stable magnetic colloidosomes via click-mediated crosslinking of nanoparticles at water-oil interfaces," *Small*, vol. 5, no. 6, pp. 685–688, 2009. 46

[80] B. Derjaguin and L. Landau *Acta Physico-Chim*, vol. 14, p. 633, 1941. 49

[81] E. J. W. Verwey and J. T. G. Overbeek, "Theory of the stability of lyophobic colloids, elsevier: Amsterdam," 1948. 49

[82] "Zeta potential An Introduction in 30 minutes," 2000. 49

[83] K. L.-. Smith, A. Jackson, and D. C. Pozzo, "SANS and SAXS analysis of charged nanoparticle adsorption at oil-water interfaces," *Langmuir*, vol. 28, no. 5, pp. 2493–2501, 2012. 49

[84] O. I. del Rio and A. W. Neumann, "Axisymmetris drop shape analysis: Computational methods for the measurement of interfacial properties from the shape and dimensions of pendant and sessile drops," *J. Colloid and Interface Science*, vol. 196, pp. 136–147, 1997. 50, 51

[85] D. Y. Kwok, L. K. Cheung, C. B. Park, and A. W. Neumann, "Study on the surface tensions of polymer melts using axisymmetric drop shape analysis," *Poly. Eng. and Sci*, vol. 38, no. 5, pp. 757–764, 1998. 50, 51, 56

[86] M. Hoorfar and A. W. Neumann, "Axisymmetris drop shape analysis (adsa) for the determination of surface tension and contact angle," *J. Adhesion*, vol. 80, pp. 727–743, 2004. 51, 56

[87] M. Hoorfar, M. A. Kurz, and A. W. Neumann, "Evaluation of the surface tension measurement of axisymmetric drop shape analysis (ADSA) using a single parameter," *Colloids and Surfaces A: Physicochemical and Engineering Aspects*, vol. 260, no. 1-3, pp. 277–285, 2005. 51, 56

[88] M. Brust, M. Walker, D. Bethell, D. J.Schiffrin, and R.Whyman, "Synthesis of thiol-derivatized gold nanoparticles in a two-phase liquid-liquid system," *J. Chem. Soc., Chem. Commun*, pp. 801–802, 1994. 56, 69

[89] M. J. Hostetler, J. E. Wingate, C. J. Zhong, J. E. Harris, R. W. Vachet, M. R. Clark, J. D. Londono, S. J.Green, J. J.Stokes, G. D. Wignall, G. G. L, M. D. Porter, N. D.Evans, and R. W. Murray, "Alkanethiolate gold cluster molecules with core diameters from 1.5 to 5.2 nm: Core and monolayer properties as a function of core size," *Langmuir*, vol. 14, pp. 17–30, 1998. 56, 57, 64, 66, 69

[90] S.-H. Chen, D.-C. Wang, G.-Y. Chen, and C.-L. Jan, "Size control of the self-assembly gold nanoparticles," *Journal of Medical and Biological Engineering*, vol. 26, no. 3, pp. 137–142, 2006. 62

[91] X. Liang, Z.-J. Wang, and C.-J. Liu, "Size-controlled synthesis of colloidal gold nanoparticles at room temperature under the influence of glow discharge," *Nanoscale Research Letters*, vol. 5, pp. 124–129, 2010. 63

[92] M. M. Alvarez, J. T. Khoury, T. G. Schaaff, M. N. Shafigullin, I. Vezmar, and R. L. Whetten, "Optical adsorption spectra of nanocrystal gold molecules," *J. Phys. Chem. B*, vol. 101, pp. 3706 – 3712, 1997. 64

[93] B. V. Szyskowski, "Experimentelle studien über kapillare eigenschaften der asserigen losungen von fettsauren," *Z. Phys. Chem.*, vol. 64, pp. 385–414, 1908. 79, 103

[94] V. B. Fainerman, A. V. Makievski, and R.Miller, "The analysis of dynamic surface tension of sodium alkyl sulphate solutions, based on asymptotic equations of adsorption kinetic theory," *Colloids and Surfaces A: Physicochemical and Engineering Aspects*, vol. 87, pp. 61–75, 1994. 79, 102

[95] J. Saien and S. Akbari, "Interfacial tension of hydrocarbon + different ph aqueous phase systems in the presence of triton X-100," *Ind. Eng. Chem. Res*, vol. 49, pp. 3228–3235, 2010. 79, 82, 101, 110

[96] K. Radzio and K. Prochaska, "Interfacial activity of trioctyloamine in hydrocarbon/water systems with nonorganic electrolytes," *J. Colloid and Interface Science*, vol. 233, pp. 211–218, 2001. 79

[97] S. Ferdous, M. A. Ioannidis, and D. Henneke, "Adsorption kinetics of alkanethiol-capped gold nanoparticles at the hexane-water interface," *J. Nanoparticle Research*, vol. 13, no. 12, pp. 6579–6589, 2011. 80, 107, 115, 127

[98] E. L. Cussler, *Diffusion Mass transfer in fluid systems.* 2009. 80

[99] R. Pan, J. Green, and C. Maldarelli, "Theory and experiment on the measurement of kinetic rate constants for surfactant exchange at an air/water interface," *Journal of Colloid and Interface Science*, vol. 205, pp. 213–230, 1998. 81

[100] C. D. Taylor, D. S. Valkovska, and C. D. Bain, "A simple and rapid method for the determination of the surface equations of state and adsorption isotherms for efficient surfactants," *Phys. Chem. Chem. Phys.*, vol. 5, pp. 4885–4891, 2003. 81, 109

[101] H.-C. Chang, C.-T. Hsu, and S.-Y. Lin, "Adsorption kinetics of $C_{10}E_8$ at air-water interface," *Langmuir*, vol. 14, pp. 2476–2484, 2003. 81, 109

[102] H.-C. Chang and E. I. Franses, "Adsorption dynamics of surfactants at the air/water interface: a critical review of mathematical models, data and mechanisms," *Colloids and Surfaces A: Physical and Engineering Aspects*, vol. 100, pp. 1–45, 2005. 81, 112

[103] P. Joos, *Dynamic surface phenomena*. No. ISBN 90-6764-300-9, VSP BV, 1999. 81, 112

[104] K. Sharma, C. Rodgers, R. M. Palepu, and A. Rakshit, "Studies of mixed surfactant solutions of cationic dimeric (gemini) surfactant with nonionic surfactant $C_{12}E_6$ in aqueous medium," *Journal of Colloid and Interface Science*, vol. 268, pp. 482–488, 2003. 82, 101

[105] M. J. Rosen and Q. Zhou, "Surfactant-surfactant interactions in mixed monolayer and mixed micelle formation," *Langmuir*, vol. 17, pp. 3532–3537, 2001. 82, 101

[106] K. Prochaska and K. Staszak, "Adsorption at the liquid/liquid interface in mixed systems with hydrophobic extractants and modifiers 1. study of equilibrium interfacial tension at the hydrocarbon/water interface in binary mixed systems," *J. Colloid and Interface Science*, vol. 285, pp. 1–8, 2005. 82, 101

[107] Y.-K. Park, S.-H. Yoo, and S. Park, "Assembly of highly ordered nanoparticle monolayers at a water/hexane interface," *Langmuir*, vol. 23, pp. 10505–10510, 2007. 100

[108] A. M. Jackson, Y. Hu, P. J. Silva, and F. Stellacci, "From homoligand- to mixed-ligand- monolayer protected metal nanoparticles: A scanning tunelling microscopy investigation," *J. Am. Chem. Soc.*, vol. 128, no. 34, pp. 11135–11149, 2006. 106, 107, 110

[109] J. M. R-Lopez, L. J. Giovanetti, F. G. Requejo, S. R. Isaacs, Y. S. Shon, and M. Salmeron, "Molecular conformation changes in alkylthiol ligands as a function of size in gold nanoparticles: X-ray absorption studies," *Physical Review B*, vol. 74, pp. 073410–4, 2006. 107

[110] M. J. Hostetler, J. J. Stokes, and R. W. Murray, "Infrared spectroscopy of three-dimensional self-assembled monolayers: N-alkanethiolate monolayers on gold cluster compounds," *Langmuir*, vol. 12, pp. 3604–3612, 1996. 107

[111] W. P. Wuelfing, A. C. Templeton, J. F. Hicks, and R. W. Murray, "Taylor dispersion measurements of monolayer protected clusters: A physicochemical determination of nanoparticle size," *Anal. Chem.*, vol. 71, pp. 4069–4074, September 1999. 107, 110

[112] P. K. Ghorai and S. C. Glotzer, "Molecular dynamics simulation study of self-assembled monolayers of alkanethiol surfactants on spherical gold nanoparticles," *J. Phys. Chem. C*, vol. 111, no. 43, pp. 15857–15862, 2007. 107

[113] J. He, P. Kanjanaboos, N. L. Frazer, A. Weis, X.-M. Lin, and H. M. Jaeger, "Fabrication and mechanical properties of large-scale freestanding nanoparticle membranes," *Small*, vol. 6, no. 13, pp. 1449–1456, 2010. 107

[114] L. L. Dai, R. Sharma, and C. y. Wu, "Self-assembled structure of nanoparticles at a liquid-liquid interface," *Langmuir*, vol. 21, pp. 2641–2643, 2005. 112

[115] E. S. Lutton, C. E. Stauffer, J. B. Martin, and A. J. Fehl, "Solid and liquid monomolecular film at oil/h_2o interfaces," *Journal of colloid and interface science*, vol. 30, no. 3, pp. 283–290, 1969. 128

[116] M. D. Malinsky, K. L. Kelly, G. C. Schatz, and R. P. V. Duyne, "Chain length dependence and sensing capabilities of the localized surface plasmon resonance of silver nanoparticles chemically modified with alkanethiol self-assembled monolayers," *J. American Chemical Society*, vol. 123, no. 7, pp. 1471–1482, 2001. 129

[117] N. K. Chaki, P. Singh, C. V. Dharmadhikari, and K. P. Vijayamohanan, "Single-electron charging features of larger, dodecanethiol-protected gold nanoclusters: electrochemical and scanning tunneling microscopy studies," *Langmuir*, vol. 20, no. 23, pp. 10208–10217, 2004. 129

[118] B. M. Quinn, P. Liljeroth, V. Ruiz, T. Laaksonen, and K. Kontturi, "Electrochemical resolution of 15 oxidation states for monolayer protected gold nanoparticles," *J. Am. Chem. Soc*, vol. 125, no. 22, pp. 6644–6645, 2003. 129

[119] M. J. Shultz, C. Schnitzer, D. Simonelli, and S. Baldelli, "Sum frequency generation spectroscopy of the aqueous interface: ionic and soluble molecular so-

lutions," *Int. Reviews in Physical Chemistry*, vol. 19, no. 1, pp. 123–153, 2000. 129, 135